SPATIAL AND TEMPORAL PATTERNS OF ANTIMICROBIAL ACTION AGAINST *STAPHYLOCOCCUS EPIDERMIDIS* BIOFILMS

by

William Marshall Davison

A dissertation submitted in partial fulfillment
of the requirements for the degree

of

Doctor of Philosophy

in

Engineering

MONTANA STATE UNIVERSITY
Bozeman, Montana

February 2008

©COPYRIGHT

by

William Marshall Davison

2008

All Rights Reserved

APPROVAL

of a dissertation submitted by

William Marshall Davison

This dissertation has been read by each member of the dissertation committee and has been found to be satisfactory regarding content, English usage, format, citation, bibliographic style, and consistency, and is ready for submission to the Division of Graduate Education.

Dr. Philip S. Stewart
Committee Chair

Approved for the Department of Chemical and Biological Engineering

Dr. Ronald W. Larsen
Department Head

Approved for the Division of Graduate Education

Dr. Carl A. Fox
Vice Provost

STATEMENT OF PERMISSION TO USE

In presenting this dissertation in partial fulfillment of the requirements for a doctoral degree at Montana State University, I agree that the Library shall make it available to borrowers under rules of the Library. I further agree that copying of this dissertation is allowable only for scholarly purposes, consistent with "fair use" as prescribed in the U.S. Copyright Law. Requests for extensive copying or reproduction of this dissertation should be referred to ProQuest Information and Learning, 300 North Zeeb Road, Ann Arbor, Michigan 48106, to whom I have granted "the exclusive right to reproduce and distribute my dissertation in and from microform along with the non-exclusive right to reproduce and distribute my abstract in any format in whole or in part."

William Marshall Davison

February 2008

ACKNOWLEDGEMENTS

My research project would not have been successful without the help of many talented individuals who helped me throughout my time in the CBE and at MSU. Phil Stewart has been the best advisor and mentor I have ever had, helping me sift, distill, and communicate complex information to diverse audiences. I strive to emulate his even-keel, never judgmental or condescending demeanor as I enter the workforce. The members of my Graduate Committee have been great sources for information: Joe Seymour, Ross Carlson, and Warren Jones. Betsey Pitts has been instrumental in my growth as a researcher. Her genius problem solving skills amaze me, and she always has fun when she is working – a combination I hope to carry with me into the Real World. Peg Dirckx was a great resource in the CBE who pays more attention to detail in one day than most do in their lifetime. Her willingness to help CBE'ers with presentations, publications, and professionalism is unmatched, and ensures that any work possessing the CBE name is of the highest quality. John Neuman is an unsung hero in the CBE whose work is often unappreciated and overlooked. Thank you, John! Thanks to Isaac Klapper and Raaja Raajan Angathevar Veluchamy who helped me with the modeling portion of this dissertation. This project was funded by the W. M. Keck Foundation.

I received yet more support outside the walls of the CBE, without which I would have failed miserably. My wife, Wendy, is the most amazing person I have ever known and has offered unwavering encouragement during my time in Graduate School. I have learned as much from her as I have in the classroom and laboratory. Finally, I would like to thank my mom, siblings, and extended family for their support along this journey.

TABLE OF CONTENTS

1. INTRODUCTION 1

Staphylococcus epidermidis 1
Biofilm 2
Antimicrobial Efficacy Against Biofilms 4
Protective Mechanism: Slow Penetration 5
Protective Mechanism: Tolerant Subpopulation 6
Visualizing Antimicrobial Action in Biofilms 8
Mathematical Biofilm Modeling 9
Objectives of this Dissertation 11

2. BACKGROUND 14

Microscopic Visualization of Biofilms 14
Confocal Scanning Laser Microscopy 14
Fluorophores 15
Calcein-AM 15
Cyanoditolyl Tetrazolium Chloride (CTC) 17
Antimicrobial Agents 18
Quaternary Ammonium Compound 18
Chlorine 19
Glutaraldehyde 20
Nisin 21

3. MATERIALS AND METHODOLOGY 22

Bacteria and Media 22
Stains and Dyes 22
Calcein-AM 22
5-Cyano-2, 3-di-4-tolyl-tetrazolium Chloride 23
Antimicrobial Agents Used for Treatment 23
Barquat 23
Chlorine 24
Glutaraldehyde 24
Nisin 24
Planktonic Bacterial Analysis: Flow Cytometry 25
Planktonic Viability Testing 26
Chlorine Residual Measurements 27
Viability after CAM Staining 28
Biofilm Reactor Analysis 29
Image Analysis 31

TABLE OF CONTENTS - CONTINUED

Mathematical Biofilm Modeling with Matlab®.....32

4. RESULTS 36

Planktonic Bacteria.....36
Flow Cytometry.....36
Viability Testing.....57
Biofilm.....59
Mathematical Modeling of Antimicrobial Diffusion.....79

5. DISCUSSION 85

6. CONCLUSIONS.....99

Considerations for Future Work.....101

REFERENCES……..…….....104

LIST OF TABLES

Table Page

3-1. Molecular weights and diffusion coefficients in water at 25°C.....34

4-1. Flow cytometry data for unstained control experiments (n = 18). 36

4-2. Flow cytometry data for 1 h CAM staining of planktonic bacteria.(n = 18)..38

4-3. Flow cytometry data for 1 h PBS wash of planktonic bacteria. (n = 18).....39

4-4. Flow cytometer data for 1 h PBS control treatment. (n = 3).....41

4-5. Flow cytometry data for 1 h treatment with Barquat. (n = 3) 42

4-6. Flow cytometry data for 1 h treatment with 50 mg/L chlorine. (n = 3).....45

4-7. Flow cytometry data for 1 h treatment with 10 mg/L chlorine. (n = 3).....47

4-8. Total and free chlorine residual during 1 h treatment of planktonic cells with 10 mg/L chlorine. 48

4-9. Flow cytometry data for 1 h treatment with glutaraldehyde. (n = 3).....49

4-10. Flow cytometry data for 1 h treatment with nisin. (n = 3) 51

4-11. Comparison of antimicrobial treatments as analyzed with flow cytometry. 54

4-12. Average CAM fluorescence loss at different regions in biofilm clusters after 1 h treatment. 78

4-13. Values for t_{50}, changes in area coverage, and percent CTC staining after 1 h treatment.....79

4-14. Average CAM fluorescence loss at different regions in corner biofilms after 1 h treatment.....79

4-15. Values for t_{50} (at a depth of 120 μm) and distance the edge of the corner biofilm retracted during treatment. Negative numbers in the Δ edge column are indicative of biofilm shrinkage or retraction toward the wall. 79

LIST OF TABLES - CONTINUED

Table Page

4-16. Comparison between t_{50} (measured fluorescence loss time) and α_{50} (predicted biocide diffusion time) values at the periphery of biofilm clusters. D_e is the effective diffusion coefficient in biofilm at 23°C. 84

4-17. Comparison between t_{50} (measured fluorescence loss time) and α_{50} (predicted biocide diffusion time) values at the medial region of biofilm clusters. D_e is the effective diffusion coefficient in biofilm at 23°C. 84

4-18. Comparison between t_{50} (measured fluorescence loss time) and α_{50} (predicted biocide diffusion time) values at the center of biofilm clusters. D_e is the effective diffusion coefficient in biofilm at 23°C. 84

LIST OF FIGURES

Figure Page

2-1.Chemical structure of Calcein-AM. 16

2-2. Chemical structure of CTC. 18

2-3. Molecular structure of Barquat® MB-80. 19

2-4. Molecular structure of glutaraldehyde. 20

2-5. Molecular structure of nisin. 21

3-1. Glass capillary biofilm reactor. 30

4-1. Representative flow cytometry histograms of unstained control. Time is in minutes. 37

4-2. Representative flow cytometer histograms for 1 h CAM staining phase. Time is in minutes. 39

4-3. Representative flow cytometer histograms for 1 h PBS wash phase. Time is in minutes. 40

4-4. Representative flow cytometry histogram data for 1 h PBS control treatment. The first panel shows the final time point of the PBS wash period, immediately prior to the control treatment. Time is in minutes. 43

4-5. Representative flow cytometer histogram data for 1 h Barquat treatment. The top left panel shows the final time point of the PBS wash phase, immediately prior to Barquat treatment. Time is in minutes. 44

4-6. Representative histogram data for 1 h treatment with 50 mg/L chlorine. The top left panel shows the final time point of the PBS wash phase, immediately prior to treatment with 50 mg/L chlorine. Time is in minutes. 46

4-7. Total chlorine standard curve. 48

LIST OF FIGURES - CONTINUED

Figure Page

4-8. Representative histograms of 1 h treatment with 10 mg/L chlorine. The top left panel shows the final time point of the PBS wash phase, immediately prior to treatment with 10 mg/L chlorine. Time is in minutes. 50

4-9. Representative histogram data for 1 h glutaraldehyde treatment. The top left panel shows the final time point of the PBS wash phase, immediately prior to glutaraldehyde treatment. Time is in minutes. 52

4-10. Representative histogram data for 1 h treatment with nisin. The top left panel shows the fluorescence intensity at the end of the PBS wash phase, immediately prior to nisin treatment. Time is in minutes. ...53

4-11. Relative change in mean FITC intensity during antimicrobial treatment. ...54

4-12. FSC vs. SSC scatter plots from the final time point of the representative experiment for each antimicrobial treatment. Red dots represent cells that have lost their fluorescence. Green dots are cells that fluoresce green. Time is in minutes. 56

4-13. Comparison between log reduction in events/mL (flow cytometer) and CFU/mL (plate counts) after 1 h biocide treatment. The heavy black lines represent the detection limit for the chlorine and nisin treatments...58

4-14. CAM staining 1 h time series. The first and last images are transmission-mode images, showing biofilm in grey and bulk fluid in white. All other images are fluorescence images, showing CAM staining. 61

4-15. Time series images from 1 h PBS wash phase. The first image is in transmission-mode, showing biofilm in grey and bulk fluid in white. Fluorescence images show the retention of CAM in the biofilm. The last picture is a combined image showing the biomass in grey and fluorescence in green. 62

4-16. Biofilm cluster before and after 1 h PBS control treatment. Transmission-mode images show biofilm in black and bulk fluid in white, and fluorescence images were overlayed which showed the presence of CAM staining. 63

LIST OF FIGURES - CONTINUED

Figure Page

4-17. Relative fluorescence loss during 1 h PBS control treatment. 64

4-18. Relative fluorescence loss in biofilm clusters during 1 h Barquat treatment for a typical experiment.....65

4-19. Fluorescence loss and biofilm erosion during 1 h Barquat treatment. The final image is the transmission-mode image overlayed with the green fluorescence image in order to show both biomass and the presence of CAM staining after treatment. 66

4-20. Relative fluorescence loss during 1 h treatment with 50 mg/L chlorine.....68

4-21. Fluorescence loss and biofilm erosion during 1 h treatment with 50 mg/L chlorine. The final image is the transmission-mode image overlayed with the fluorescence image to show both biomass and CAM fluorescence. 69

4-22. Relative fluorescence loss during 1 h treatment with 10 mg/L chlorine.....71

4-23. Fluorescence loss and biomass erosion during 1 h treatment with 10 mg/L chlorine. The last panel shows both transmission-mode and fluorescence images, overlayed, in order to show both biomass and CAM fluorescence. 72

4-24. Relative fluorescence loss during 1 h glutaraldehyde treatment. 73

4-25. Fluorescence loss and biomass erosion during 1 h glutaraldehyde treatment. The final image shows both transmission-mode and fluorescence images, overlayed, in order to display both biomass and CAM fluorescence. 75

4-26. Relative fluorescence loss in isolated clusters during 1 h nisin treatment. ..76

4-27. Relative fluorescence loss in corner biofilm during 1 h nisin treatment.....76

4-28. Fluorescence loss and biomass erosion during 1 h nisin treatment. The final image shows both transmission-mode and fluorescence images, overlayed, in order to display both biomass and CAM fluorescence. 77

LIST OF FIGURES - CONTINUED

Figure Page

4-29. PBS control biofilm before (A) and after (B) CTC staining. 78

4-30. Average CTC staining expressed as percentage CTC intensity, relative to PBS control. 78

4-31. Non-reactive diffusion of Barquat into different regions of a model biofilm cluster. 81

4-32. Non-reactive diffusion of 50 mg/L chlorine into different regions of a model biofilm cluster.....82

4-33. Non-reactive diffusion of 10 mg/L chlorine into different regions of a model biofilm cluster.....82

4-34. Non-reactive diffusion of glutaraldehyde into model cluster.....83

4-35. Non-reactive diffusion of nisin into model cluster. 83

ABSTRACT

This study investigated the spatio-temporal patterns of antimicrobial action against *Staphylococcus epidermidis* planktonic and biofilm bacteria. Bacteria were stained with a fluorogenic esterase substrate, Calcein-AM, which allowed for the visualization of cells that possessed intact cell membranes. Four different antimicrobial agents were tested for their effect upon cell viability as associated with membrane integrity. The four biocides were Barquat®, glutaraldehyde, chlorine, and nisin.

Planktonic bacteria were analyzed with flow cytometry, observing fluorescence loss during 1 h antimicrobial treatment. Treatment with Barquat resulted in initial fluorescence loss, which increased during the treatment period to levels which were present prior to the introduction of biocide, along with a decrease in cell density. Treatments with glutaraldehyde and chlorine resulted in increased average fluorescence intensity for the cell population, accompanied by decreased cell density for chlorine and increased cell density for glutaraldehyde. Nisin treatment resulted in a decrease in CAM fluorescence with an increase in cell density. Viable cell plate counts showed average log reductions in CFU/mL of 3.61, 3.83, 4.12, 4.26, and 4.67 for Barquat, glutaraldehyde, high and low concentrations of chlorine, and nisin treatments, respectively. There was no apparent correlation between plate counts and flow cytometry data.

Biofilm bacteria were analyzed with time-lapse confocal scanning laser microscopy, observing fluorescence loss during biocide treatment. Biofilms treated with Barquat lost an average of 91.5% of their initial fluorescence, and clusters decreased in areal coverage by 9%. Fluorescence loss during Barquat treatment suggested the presence of a tolerant subpopulation of bacteria in the interior regions of the biofilm. Glutaraldehyde treatment reduced the average fluorescence by 16%, and cluster area did not change. There was CTC staining after glutaraldehyde treatment only. The high and low concentrations of chlorine treatment showed averages of 100% and 79% reductions in CAM staining, with liquefaction of biomass causing erosion events which reduced areal coverage by 90% and 43%, respectively. Nisin treatment reduced CAM staining by an average of 100%, while shrinking the cluster area by 8%. Corner biofilms showed qualitative differences during treatment than isolated clusters.

Mathematically-predicted biocide diffusion times were much faster than experimentally observed fluorescence loss in biofilms.

CHAPTER 1

INTRODUCTION

Staphylococcus epidermidis

Staphylococcus epidermidis is a species of gram-positive cocci-shaped (spherical) bacteria and is a subspecies of the coagulase-negative staphylococci (CNS). CNS species are widely distributed over the surface of the human body and comprise the majority of the commensal bacterial microbiota (107). Among the CNS, *S. epidermidis* is the most common species associated with infection in humans. Although *S. epidermidis* was considered rather innocuous in the past, it is now considered an opportunistic pathogen which attacks those with compromised immune defenses and it has become the most important cause of nosocomial (hospital-acquired) infections (176).

The most important nosocomial infections caused by *S. epidermidis* are those associated with the attachment of the bacteria to foreign bodies implanted or indwelling in the human body (176). The most common of these infections include those associated with prosthetic cardiac valves (16) (46) (62) (99) (141), cerebrospinal fluid shunts (21) (67) (134) (135), orthopedic appliances (110) (183) (184) (185), intravascular catheters (7) (15), and other bloodstream infections (12) (119) (132). *S. epidermidis* is most often the primary infective agent in compromised hosts, such as immunocompromised patients (AIDS patients, patients under immuno-suppressive chemotherapy, and premature newborns). The portal of entry into the human body in all of these patients is usually an intravenous catheter (50) (164). Surface-associated *S. epidermidis* infections on

indwelling catheters or implanted prosthetic devices are complicated by the ability of these bacteria to form biofilms, which is discussed in more detail below, which frequently leads to the removal and reinsertion of the devices (71). Biofilm formation on medical implants has even led to the characterization of a new infectious disease called chronic polymer-associated infection (59) (175).

Biofilm

Biofilms are defined as matrix-enclosed bacterial populations which are attached to each other and/or to surfaces or interfaces. This definition includes microbial aggregates and floccules and also adherent populations within the pore spaces of porous media (35). The attachment of bacteria to surfaces, and thus biofilm, was first described in 1936 (200), and its universal distribution among varying environments was observed in 1978 (34). Bacterial communities are most often associated with both biotic and abiotic surfaces, and when surface associated, they are termed biofilms (37) (38) (101) (158). As bacteria grow in a biofilm, they encase themselves with excreted extracellular polymeric substances (EPS) consisting of polysaccharides, DNA, proteins, and other cellular byproducts. This EPS matrix allows bacteria to form heterogeneous structures and community-type environments (36).

Bacterial biofilms can exist in any environment where a surface and water exist. They have been implicated in many industrial, environmental, and medical environments including heat exchanger fouling, drinking water distribution pipe fouling, occluding porous media, medical prosthetic implant infections, and dental caries. Biofilms differ

significantly from their free-floating (planktonic) counterparts both genotypically (genetically) and phenotypically (functionally). It has been shown that when biofilms attach to surfaces and adopt a sessile growth state, they express different genes which makes them phenotypically different from their planktonic form (131). Intercellular communication between bacteria, termed quorum sensing, has been shown to occur during the formation of biofilms and is vital to the survival of bacterial biofilm populations (82).

Biofilms were once thought to be mats or "lawns" of microbial growth with flat geometries. Research has shown that biofilm communities sometimes form very heterogeneous structures with fluid channels interconnecting larger clusters of microorganisms. This heterogeneity is thought to aid in nutrient and waste transport to, from, and into biofilm clusters. Individual bacterial species often produce differing biofilm structures, depending upon growth conditions. The accepted biofilm growth cycle occurs with these steps: 1) initial attachment, 2) EPS production, 3) early development of biofilm architecture, 4) maturation, and 5) dispersion of cells (162). Although biofilms possess complex heterogeneous structural architecture which aids in nutrient transport to individual clusters, nutrient limitation still exists in these communities. Nutrient limitation on the interior of biofilm clusters, at depths of approximately 50 microns, has been shown mathematically (123) and experimentally (18) (42) (181). Also, it has been shown that in these same microenvironments on the interior of biofilm clusters, metabolic activity is decreased (120) (145) (177) (181).

Antimicrobial Efficacy Against Biofilms

Biofilm bacteria possess many different characteristics than their free-floating (planktonic) counterparts; one of these being an increased tolerance to antibiotics or other antimicrobial treatments. This increased resistance to conventional killing methods in biofilms is well-documented (94) (97) (152). Antimicrobial control of biofilm bacteria is a very important issue since biofilms are detrimental in industrial and medical applications, ranging from heat exchangers and drinking water, to artificial prostheses infections and cystic fibrosis. Much is known about the genetic and molecular basis of antibiotic resistance in bacteria, but these protective mechanisms do not appear to be at the root of the reduced antimicrobial susceptibility in biofilms (150).

It has been shown that disaggregated biofilm bacteria which are dispersed into suspension and subsequently challenged with an antimicrobial agent recover their susceptibility to that agent, suggesting that the increased protection from killing by the biofilm mode of growth is reversible (5) (6) (182). This rapid increase in susceptibility upon dispersion from a biofilm suggests an adaptive resistance mechanism rather than a heritable genetic alteration. Several different mechanisms of biofilm resistance have been proposed, including slow or incomplete antimicrobial penetration into biofilms, and a dormant persister state of some subpopulation of cells within the biofilm (150). In this study, these two hypothetical protective mechanisms will be tested in parallel with other hypotheses of antimicrobial resistance in biofilms.

Protective Mechanism: Slow Penetration

As biofilm bacteria grow, the biofilm EPS matrix may offer a protective barrier to antibiotic or antimicrobial penetration. This barrier would retard or inhibit the diffusion of larger antimicrobial molecules through the matrix, disallowing access to microbial cells. If the antimicrobial does not have access to the target cells, it follows that the biocide cannot act upon the bacteria.

Biofilms are primarily composed of water, and solutes can easily diffuse in the biofilm matrix. Research has been done experimentally showing that antibiotics and antibiotic-sized molecules can penetrate through a biofilm matrix (177) (198) (199). Mathematical estimations of penetration times for different sized molecules into biofilms have also been calculated. Effective diffusion coefficients of solutes in biofilms, with molecular weights ranging from 100 to 1000, have been shown to be approximately 40 percent of their respective diffusion coefficients in pure water (149) (151). Antibiotic diffusion coefficients have also been determined in polysaccharide or glycoprotein gels and the results are corroborative, ranging from 36 to 76 percent of their respective values in pure water (27) (57). In most of the experiments that demonstrate effective antibiotic penetration, the test microorganism survived (5) (39) (51). Therefore, other mechanisms of protection besides incomplete penetration must be present in biofilms.

The primary mode of transport within biofilm cell clusters is diffusion (160) (41). Often coupled with diffusion is the reactivity of the biocide with the organic material present in the biofilm. This reaction-diffusion interaction may provide insight into diffusion limitation of biocides into biofilm, and has been analyzed mathematically (148)

(157). Chemical sorption of antibiotics or other antimicrobial agents to EPS components may explain slow diffusion into biofilms as well (90) (148). Methods have been developed to monitor penetration of certain antimicrobial agents into biofilm, however these monitoring systems are generally invasive, requiring direct, destructive sampling during experimentation. The proposed research in this project will use a noninvasive, direct-visualization technique to correlate the penetration of biocides into biofilms.

Protective Mechanism: Tolerant Subpopulation

A second protective mechanism proposed by researchers suggests the presence of a small subpopulation of cells within biofilm that is less susceptible to antimicrobial attack. These cells may be in a different growth phase than other bacteria, may reside in a microenvironment which offers increased protection from antimicrobial attack, or may be in a type of hibernation state. It has been shown that physiological heterogeneity exists in the diverse, complex structure that most biofilms possess. One hypothesis suggests that diversity within bacterial biofilm populations provides "insurance effects" to help guarantee the survival of the population as a whole (17). Studies in other biological systems have shown that functionally distinct subpopulations within a community can produce insurance effects, especially during periods of increased environmental stress (100) (193) (167).

Within biofilm, the bacterial population possesses growth rates ranging from exponential growth to metabolically stagnant (20) (163). Researchers have directly visualized patterns of varying bacterial growth and activity in biofilms using fluorescent probes (180) (192) and genetic reporters (145). Slow-growing or stationary phase cells

are present within biofilm due to chemical concentration gradients (145). Along with varied growth states within biofilm, concentration gradients of certain metabolic nutrients are present. These gradients in concentration of vital metabolic substrates and products suggest cellular energetic heterogeneity in biofilm (187). All of these factors suggest that slow growth of some subpopulation of cells is no doubt present within biofilm and may be one piece of the antimicrobial tolerance puzzle, since many antibiotics are most or only effective when bacteria are actively growing (55) (170).

Biofilms possess an increased tolerance to many different antimicrobial agents. Antibiotics, chemical disinfectants, and sterilizing agents all show retarded action against biofilm bacteria when compared to their planktonic counterparts. One possible explanation of this decreased susceptibility to such a broad spectrum of antimicrobial attack is the existence of a subpopulation of cells in biofilm which are dormant, spore-like "persister" cells (142) (152). Persisters are cells that neither grow nor die in the presence of bactericidal agents, and therefore are essentially invulnerable to antimicrobial attack (95). Persister cells also offer one explanation to the recalcitrance of biofilm after antimicrobial attack. When protected cells are isolated and re-cultured, the resulting culture is no more tolerant to antimicrobial treatment than an average culture, suggesting that they are not fully dormant, but are still viable (105).

It has been shown that the presence of resistant cells within a biofilm is a function of the growth state of the cells (81). Persisters could exist in a biofilm if the majority of a population was killed by treatment, while some small fraction of cells was unaffected and remained viable. Data consistent with the persister hypothesis would show

measurements of biphasic biofilm killing in which the majority of the population is rapidly killed while a fraction of the population is killed more slowly (150). These data have been shown to exist, supporting the hypothesis of persisters (19) (58). This persister hypothesis also offers the only explanation for the fact that bacteria can display reduced susceptibility even in very thin biofilms (30) (40). These cells could potentially persevere and resuscitate when conditions are more favorable for regrowth.

Besides slow growth, there may be other sources of resistance within biofilms that are related to a less susceptible subpopulation of cells: chemical concentration gradients leading to slow growth may also contribute to a decrease in antimicrobial effectiveness within biofilm; variations in pH can negatively impact the efficacy of antibiotics (122) (174); the action of some antibiotics is dependent on the availability of oxygen (165); and the complex and heterogeneous biofilm structure is correlated with lower oxygen concentrations (42). These results show that both pH and oxygen concentration gradients are present within the biofilm matrix, creating isolated microenvironments which may lead to resistant subpopulations of cells.

Visualizing Antimicrobial Action in Biofilms

Current technologies in microscopy allow for images to be captured over the course of time. This time-lapse microscopy has allowed biofilm researchers to observe many phenomena associated with biofilm attachment, growth and development, and detachment. Researchers have tracked cellular migration over time and related it to biofilm development in *Pseudomonas aeruginosa* (85). The bulk fluid flow around

heterogeneous biofilm structures has been displayed with this technology (160), as well as the viscoelastic properties and flow of biofilm itself (84) (159). Others have watched the diffusive penetration of certain solutes into biofilms (77) (121). Temporal patterns of gene expression in biofilm have also been recorded (120) (194), as well as planktonic-like cellular motility and mobility within hollow biofilm clusters (74) (168).

Very few studies have been performed which display the real-time action of antimicrobial agents against biofilms. These studies utilized time-lapse microscopy, but the techniques were detrimental to the specimens, and were generally followed by staining or plating (13) (60) (79). The methods offer much information, but fall short of illustrating the spatial and transient patterns of antimicrobial action against biofilms because they do not allow for the direct observation of a single spot over the course of time.

A portion of this project was devoted to the development of a technique which allows for the non-invasive, direct observation of spatio-temporal patterns of antimicrobial action against *in situ* biofilms.

Mathematical Biofilm Modeling

Mathematical computer models of biofilm phenomena can be useful tools that help predict biofilm behavior or attempt to mimic laboratory results. The first computer models for biofilm research were developed in 1963. They were relatively simple and were designed to investigate substrate utilization in fixed film wastewater treatment systems (8). In 1974, Atkinson and Davies modeled substrate concentration gradients in

biofilms, particularly those that resulted from bacterial growth (9) . This modeling effort resulted in an analytical solution to the classic reaction-diffusion problem.

Biofilm models have become increasingly complex, as the understanding of biofilm phenomena has developed. The first work which modeled transient, dynamic biofilm behavior investigated species interaction in mixed species biofilms, as well as growth, decay, attachment, and detachment of bacteria to surfaces (83) (178) (179). These works led others to model and predict biofilm phenomena that were observed experimentally. Models were employed to investigate decreased penetration of antibiotics into biofilms, physiological resistance to antimicrobial attack due to slow growth rates, and the potential existence of a damaged cell state in biofilms which may help explain the reduced susceptibility of biofilms to antimicrobial agents (123) (147) (155). Other models have been used to investigate biofilm formation (78), quorum sensing (47) (73) (106), and pH effects in biofilms (44) (53).

Modeling biofilms became more advanced with the application of cellular automata rules imposed upon biofilm systems, in which a grid of "cells" is in one of a finite number of states. The discrete nature of cellular automata models allowed researchers to implement the structural heterogeneity that biofilms possess instead of assuming that all biofilms are flat slabs of microbial communities (32) (65) (186). Picioreanu et al. advanced the capabilities of the multi-dimensional cellular automata model by imposing discrete characteristics only to bacteria, polymers, and other solids, while solving the liquid nutrient field using differential equations (113) (114) (115).

This discrete-differential cellular automata model was further advanced by adapting an individual-based simulator to model each bacterium as an individual entity which is capable of free movement not restricted to the traditional cellular automata matrix (87) (88) (89). This advanced model has been used to describe such behaviors as detachment (25) (73) (189), reduced susceptibility of biofilms to antimicrobial treatment (24), and motility (112).

Cellular automata and discrete-differential models are not the only advanced models which are present in biofilm research today. Others have developed computer programs to describe viscoelastic properties of biofilm (3), biofilm growth (2) (4) (48), and biomass-fluid flow interactions (31) (45) (116) (169). These models, along with experimental laboratory results, will offer more insight into the challenges associated with biofilms.

Objectives of this Dissertation

This research project investigated the spatial and time-related effects of antimicrobial biocide treatment against *S. epidermidis* bacteria. The first objective was to develop a technique which allowed for the non-invasive, real-time visualization of antimicrobial action against *in situ* biofilms. A fluorogenic esterase substrate, Calcein-AM, was utilized to interrogate bacterial cell membrane integrity before, during, and after antimicrobial treatment. Cells were stained with Calcein-AM prior to antimicrobial treatment, and the retention or loss of cell-associated fluorescence throughout the treatment period offered insight into the state of the bacterial cell membrane.

This technique was then applied to analyze the spatio-temporal patterns of antimicrobial action for four different biocides. The biocides used for this project were Barquat (a quaternary ammonium disinfectant), chlorine (a reactive disinfectant), glutaraldehyde (a fixative agent and sterilant), and nisin (an antimicrobial peptide).

Planktonic bacteria were evaluated in two ways: 1) flow cytometry analysis provided real-time information about the cell population during treatment and 2) plate counts before and after treatment gave viability data for each treatment. Biofilms were observed using time-lapse confocal scanning laser microscopy, which provided real-time spatio-temporal patterns of antimicrobial action within biofilms. The digital images captured from each biofilm experiment were analyzed with image analysis software which allowed for the generation of numerical data from the images. The techniques used in this project to investigate real-time antimicrobial-induced cell membrane permeabilization were novel, and provide fundamental knowledge to the field of biofilm microbiology.

A mathematical computer model was created in order to conduct a comparative study between theoretical diffusion calculations and experimental observations during the antimicrobial treatment of biofilms. Often, model simulations offer insight into the incredibly complex, heterogeneous biofilm phenomena.

This report is organized into six main chapters. The first two chapters include introductory historical information and background knowledge necessary for the understanding and relevance of this work. Chapter 3 lays out the resources and laboratory procedures employed during this project. Chapter 4 describes the results from

the experimental procedures and modeling efforts. The fifth chapter summarizes the outcomes of the experimental procedures, offers insight into their significance, and displays how prior work may support the proposed hypotheses. The final chapter provides concise conclusions and also offers ideas toward expanding upon this research project.

CHAPTER 2

BACKGROUND

Microscopic Visualization of Biofilms

The structure of biofilms has been analyzed visually using many microscopic techniques, including the use of light microscopy to examine wet mounts (86) (111), and of scanning and electron microscopy techniques (33) (93). While light microscopy offers insight into the three-dimensionality of biofilm structure, its drawbacks lie in the fact that there is out-of-focus haze in every field of view due to the light scattering of material which is not in the focal plane. Electron microscopy is very invasive and often results in artifacts due to sample preparation. It has been reported that biofilm preparation for electron microscopic analysis can induce morphological changes (dehydration, embedding, and disruption), leading to 50% shrinkage during fixation. Also, time course analysis of biofilm development or monitoring would prove to be extremely difficult (92). Confocal scanning laser microscopy (CSLM) offers distinct advantages for non-invasive, *in situ* monitoring of hydrated biofilm samples.

Confocal Scanning Laser Microscopy

Confocal microscopy was invented in 1955 (103) and has allowed researchers to perform point-by-point illumination of specimens, collecting only some of the reflected light, and virtually eliminating the unwanted scattered light that obscures an image when the entire specimen is illuminated at the same time (136). The light returning from the

illuminated specimen passes through a pinhole, filtering out any light that was not directly in the focal plane. Thus, only the points in the specimen which are directly in the focal plane are collected, and sent to photomultiplier tube detectors (PMTs). For visualization of this data, the detectors are connected to a computer, which builds the images one pixel at a time. For a 512 x 512-pixel image this is generally done at a frame rate of 0.1-30 Hz (136).

Confocal microscopes can be configured in order to capture images in the x-y plane, the x-z plane, and the y-z plane. These images can be reconstructed to give researchers an idea of the three-dimensional structure of the specimen. Confocal images can also be collected for a certain plane over the course of an allotted amount of time. This is often called time-lapse microscopy, or the collecting of a "time series." Depending on the resolution of the images collected, the elapsed time between collected images can be as little as 1 second. This project utilized time series images over the course of 1 h, taken every 30 sec.

Fluorophores

Calcein-AM

Fluorogenic esterase substrates have been used extensively to determine cell membrane integrity and to test for cell viability in bacterial populations (10) (43) (127). The acetoxymethyl (AM) ester derivatives of fluorescent markers constitute a widely useful group of these probes. Calcein-AM (CAM) (Invitrogen, C-3100MP) is one of

these compounds. CAM has a molecular weight of 994.87 and its chemical formula is $C_{46}H_{46}N_2O_{23}$. The structure of CAM can be seen in Figure 2-1.

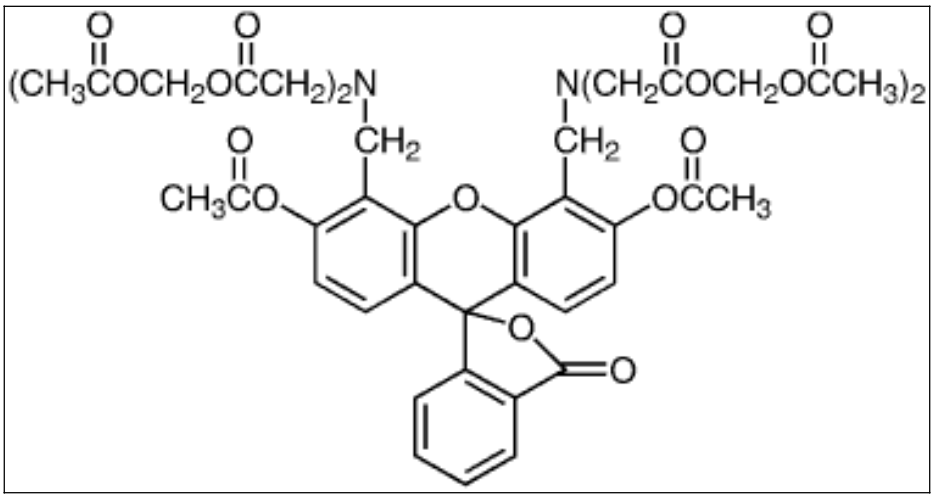


Figure 2-1.Chemical structure of Calcein-AM.

The uncharged CAM can passively diffuse across a bacterial cell membrane, and it is a fluorogenic esterase substrate. Once inside the cell, the AM linkages are cleaved by nonspecific cellular esterase enzymes and the calcein molecule becomes charged, causing it to remain inside any cell with an intact membrane. Along with becoming charged after the hydrolysis of the esters, the calcein molecule becomes fluorescent and is easily visualized using long-wave UV excitation (488 nm). The peak absorption wavelength for CAM is 494 nm, and the emission peak is 514 nm, making it readily excited when a 488 nm laser is used (75). CAM is a preferred stain in dye retention tests (138). This technique allows for direct visualization of bacterial cells with intact cell membranes via CSLM.

Cyanoditolyl Tetrazolium Chloride (CTC)

Redox dyes have the ability to change color depending upon their oxidative state. To be useful in CSLM microscopy studies, a redox dye would have to be fluorescent in only one oxidation state – ideally, the reduced state. Also, the stain should be water insoluble once reduced. The redox dye 5-Cyano-2, 3-di-4-tolyl-tetrazolium chloride (CTC) (Polysciences, Inc., Warrington, PA) has met these criteria and the reduced form, with formazan (CTF), is intensely fluorescent (137) (143) (144).

CTC is a monotetrazolium redox dye which produces a fluorescent formazan (CTF) when it is chemically or biologically reduced. The molecular weight of CTC is 311.8, its chemical formula is $C_{16}H_{14}ClN_5$, and its structure can be seen in Figure 2-2. The CTF is deposited intracellularly as fluorescent red crystals. Until recently, CTC had only been employed as a cellular redox indicator of respiratory (i.e., electron transport) activity in cytochemical experiments with Ehrlich ascites tumor cells (137) (143) (144). One study describes the first application of CTC for microscopic visualization of actively respiring bacteria in native and nutrient-modified environmental samples and in bacterial biofilms formed on microscope slides (124). Other, more recent studies have show the effectiveness of CTC as an indicator of respiratory activity in many different biofilms (72) (133) after subjected to an antimicrobial challenge (72) (154) (191) (197). This compound is a vital redox dye and is easily detected intracellularly because of its bright red fluorescence when illuminated by long-wave UV light (488 nm). Moreover, the fluorescent nature of the compound greatly facilitates its use in studying actively respiring bacteria in biofilms.

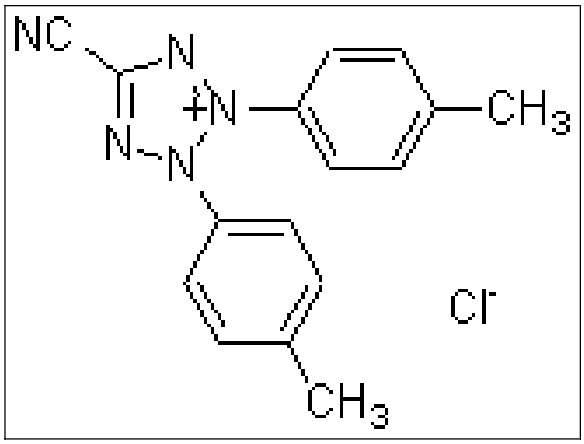


Figure 2-2. Chemical structure of CTC.

Antimicrobial Agents

The use of disinfecting and antimicrobial agents against biofilms has been well documented and highly variable with respect to the types of agents tested. This project focused on the efficacy of four different types of antimicrobial agents against *S. epidermidis* planktonic cultures and biofilms. The quaternary ammonium compound Barquat® MB-80 (Lonza, Inc.), chlorine, glutaraldehyde, and the antimicrobial peptide nisin were all tested for this project.

Quaternary Ammonium Compound

Quaternary ammonium compounds (benzalkonium chloride) (QACs) are cationic surfactants commonly used in disinfecting agents and industrial cleaning supplies. They are categorized by the length of their C-chains (22) and are non-specific bactericides. When used in surface disinfectants, sanitizers, and/or certain types of water treatment formulations, these QACs have been found to possess superior biocidal action against a broad spectrum of microbes. The hydrophobic properties of QACs change with length of

C-chains. These compounds act against microbial communities in a way which alters the hydrophobic properties of individual bacterial cells and/or the properties of the EPS matrix of biofilms. Alterations in biofilm hydrophobicity could alter the attachment of the bacteria to the surface or other cells. Positively-charged QACs may be electrostatically attracted to the negatively-charged bacteria and EPS matrix components.

The QAC used in this research project, Barquat® MB-80, has a mean molecular weight of 357 (153). Its chemical formula is n-Alkyl (C_{14}-50%, C_{12}-40%, C_{16}-10%) dimethyl benzyl ammonium chloride, with the stock solution containing 80% active ingredient. A depiction of the molecular structure is shown below in Figure 2-3.

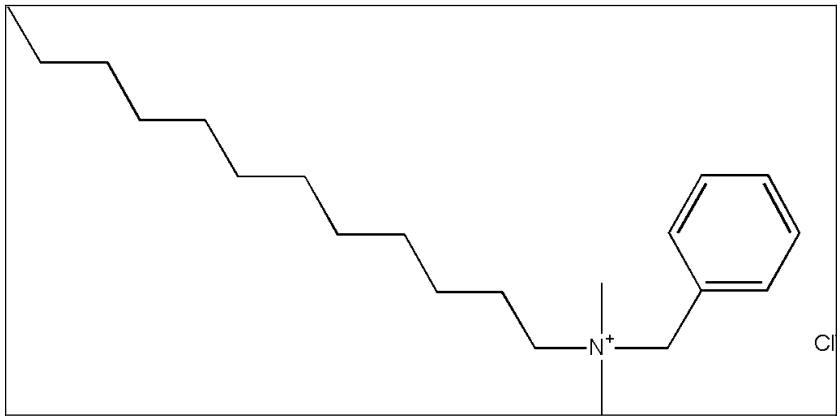


Figure 2-3. Molecular structure of Barquat® MB-80.

Chlorine

The use of chlorine has many industrial applications, especially for the disinfection of municipal drinking water. It is also utilized in other industrial settings as a biocide. These applications include disinfection of cooling water towers, swimming pools, paper mills, food processing plants (28). Aqueous hypochlorite solutions are used in dentistry to aid in the disinfection of tooth surfaces during invasive procedures like

root canals. At neutral pH, water chemistry dictates the presence of equal amounts of hypochlorous acid and hypoclorite ion. The hypochlorite/hypochlorous acid solution (hereafter referred to as "chlorine") is a highly reactive aqueous solution which reacts readily with (oxidizes) organic material.

Two different concentrations of chlorine were tested in this research project. The "high" concentration refers to 50 mg L^{-1} and the "low" concentration refers to 10 mg L^{-1}.

Glutaraldehyde

Glutaraldehyde is a bactericidal chemical disinfecting agent, and at high concentrations is considered a sterilizing agent. It is effective against both gram positive and gram negative microbes. In microbiology, glutaraldehyde is often used as a fixative agent for microbial cultures. Glutaraldehyde works as a biocide by denaturing and cross-linking cellular proteins, thus halting any metabolic processes associated with enzyme activity and effectively killing the microbes. It has a molecular weight of 100.1, its chemical formula is $C_5H_8O_2$, and its molecular structure is shown in Figure 2-4.

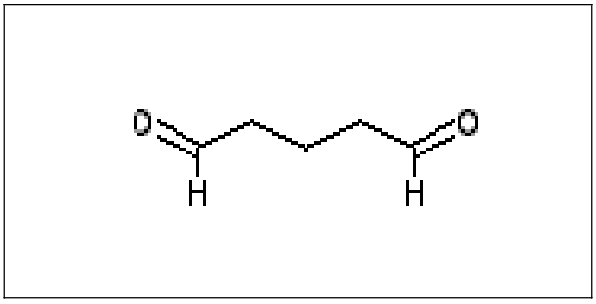


Figure 2-4. Molecular structure of glutaraldehyde.

Nisin

Antimicrobial peptides (bacteriocins) represent ancient host defense effector molecules present in organisms across the evolutionary spectrum (195). Lantibiotics are antimicrobial peptides which are derived from bacteria, one of which is nisin. Nisin is produced by *Lactococcus lactis subsp lactis* strains and is commonly used in the food industry to prevent food spoilage by organisms such as *Listeria spp*. It is a cationic, class 1 lantibiotic which is highly active against gram positive bacteria (49) (76), and active against some gram negative bacteria (146). The mature nisin structure is only 34 amino acids long and contains 5 rings, with a molecular weight of 3354 (140). The molecular structure of nisin can be seen in Figure 2-5.

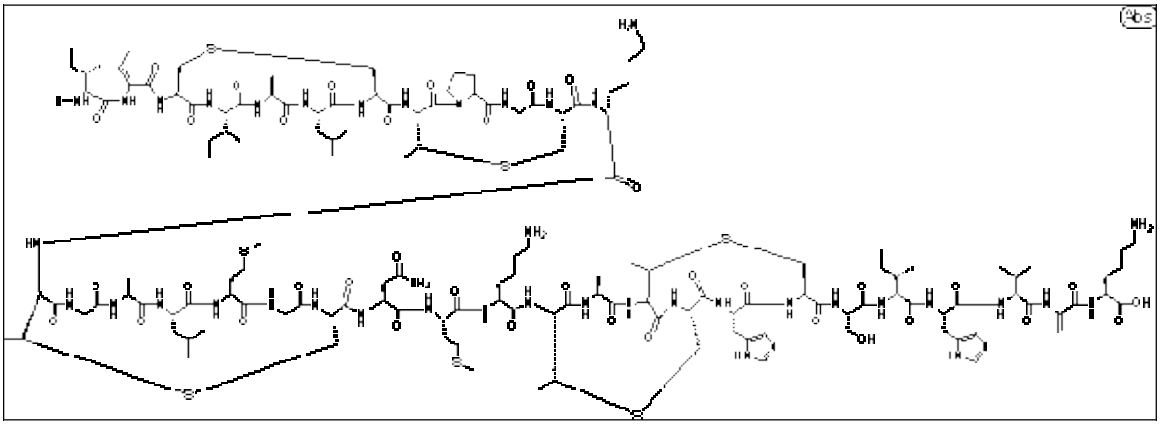


Figure 2-5. Molecular structure of nisin.

The primary target of nisin, as with most antimicrobial peptides, is the bacterial cell membrane. It is thought that nisin interferes with the cellular energy supply by creating pores in the membrane and dissipating its chemiosmotic potential (126).

CHAPTER 3

MATERIALS AND METHODOLOGY

Bacteria and Media

Staphylococcus epidermidis strain RP62A (ATCC #35984) was grown overnight in full-strength tryptic soy broth (TSB) at 37^{o}C in a shaking incubator. This "overnight culture" was used as an inoculum for the growth of capillary biofilms. For planktonic experiments, the overnight culture was subcultured 1:10 into fresh TSB, re-incubated, and allowed to reach exponential growth phase (approximately 2-3 hr) prior to a second 1:10 dilution into sterile phosphate-buffered saline (PBS) for staining and further analysis. PBS is an aqueous solution containing 2 μM $MgCl_2$ and 0.31 μM KH_2PO_4, with a pH of 7.2 ± 0.2.

Stains and Dyes

Calcein-AM

CAM, in individual vials containing 50 μg, was dissolved in 100 μl of dimethyl sulfoxide (DMSO) to make a stock solution. This stock solution was diluted by adding 20 μl into 1 mL of filter sterilized PBS for a working concentration of 9.85 μM CAM. Both planktonic and capillary biofilm bacteria were statically stained with CAM for 1 h.

5-Cyano-2, 3-di-4-tolyl-tetrazolium Chloride

Respiratory activity in biofilms treated with antimicrobial agents was analyzed using CTC. The extracellular presence of phosphate was decreased by flowing sterile water through the capillary for 30 min prior to CTC staining, since the presence of phosphate has been shown to affect CTC reduction (118) (139). A mass of 0.01 g of CTC powder was dissolved in 25 mL of filter-sterilized, deionized (DI) water for a final concentration of 0.04% CTC (0.013 mM) and the solution was used immediately after preparation. Aluminum foil was wrapped around the container of the CTC solution to reduce the exposure to exterior lighting.

Prior to staining the biofilm with CTC, the capillary tubing was rinsed with DI water to remove any residual phosphate, a component of the buffer. The CTC solution was pumped through the capillary for 10-15 min, 3 times, over the total staining period of 2 h. This intermittent flow ensured that the biofilm bacteria would be exposed to a higher concentration of CTC when compared to static staining, while keeping the overall cost of the experimentation to a minimum. After the 2 h staining period, the biofilm was visualized with CSLM.

Antimicrobial Agents Used for Treatment

Barquat

A balance was used to measure 625 mg of the quaternary ammonium compound n-Alkyl (C_{14}-50%, C_{12}-40%, C_{16}-10%) dimethylbenzylammonium chloride, called Barquat® MB-80 (Lonza, Fair Lawn, NJ), into a vial. The Barquat was diluted by

adding 100 mL of sterile PBS to make a stock solution of 5 g/L. This stock solution was further diluted 1:100 in sterile PBS to reach the final working concentration of 50 mg/L (0.140 mM) Barquat.

Chlorine

A concentrated, reagent grade sodium hypochlorite (NaOCl) solution containing 10-13% available chlorine (Sigma, St. Louis, MO) was diluted into filter sterilized PBS to attain a working concentration of 10 mg/L (0.28 mM) chlorine or 50 mg/L (1.41 mM) chlorine, depending upon the treatment (high or low concentration, respectively). The pH of the treatment solution was 7.2 ± 0.3, and at this pH the solution contained equal proportions of hypochlorous acid and hypochlorite ion.

Glutaraldehyde

A reagent grade solution of 50% (w/w) glutaraldehyde (Fisher Scientific) was diluted by adding 885 µl to 100 mL sterile PBS to make a stock solution of 5 g L^{-1}. This stock solution was further diluted 1:100 to a working concentration of 50 mg L^{-1} (0.50 mM) glutaraldehyde.

Nisin

A powder containing 2.5% (w/w) nisin (Sigma-Aldrich) was diluted by adding 0.5 g powder to 5 mL sterile PBS. This stock solution was diluted further into sterile PBS for a final working concentration of 50 mg L^{-1} (14.9 µM) nisin.

Planktonic Bacterial Analysis: Flow Cytometry

An overnight culture of *S. epidermidis* bacteria was grown in Tryptic Soy Broth (TSB), subcultured 1:10 into fresh, 37°C TSB, and then incubated for an additional 2-3 h which allowed the culture to reach exponential-phase ($OD_{600} = 0.050 \pm 0.005$). The exponential-phase bacteria were diluted 1:10 into filter sterilized PBS for CAM staining and subsequent analysis. Cells were stained for 1 hr by adding 9.85 μM Calcein-AM (CAM) in phosphate-buffered saline (PBS) solution. Samples were further diluted 1:10 in filter sterilized PBS, and placed in special test tubes with filter caps (Falcon). These test tubes were placed on the flow cytometer for analysis. Measurements were collected at t = 0, 20, 40, and 60 min of CAM staining. Staining progress and rates were measured using a BD FACSAria™ Cell Sorter flow cytometer (Becton-Dickinson, USA).

All data collected during flow cytometry experiments is in the form of green fluorescence intensity of cells within the planktonic population. The particular protocol applied uses FITC (fluorescein isothiocyanate) as the standard green fluorescent dye. An arbitrary threshold was established using an unstained control of *S. epidermidis* in order to separate stained cells from unstained cells, with this value equal to 300 on the FITC (green fluorescence) intensity scale. An internal threshold was set at 500 on the Side Scatter Channel (SSC), which is protocol for bacterial analysis on this flow cytometer. The number of total events recorded at each time step was 5000, and the output was in the form of histograms.

Following CAM staining, the planktonic cells were centrifuged at 4600 g for 4 min, the supernatant removed, and the cells were resuspended in sterile PBS in order to

remove any CAM in the bulk fluid. This was analogous to the PBS wash period for biofilm experiments. Samples were taken during this PBS "wash" phase of the experiment (at t = 0, 20, 40, 60 min) in order to determine whether cells retain the fluorescent calcein. An antimicrobial agent was then added to the cell suspension and fluorescence loss was tracked with the flow cytometer in order to determine changes in cellular permeability. During the antimicrobial treatment phase, samples were analyzed at t = 0, 5, 10, 15, 20, 40, 60 min.

Often during the course of an experiment, the sample flow rate was adjusted. This flow rate varied from 1.0-11.0, which corresponds to a volumetric flow rate of 10-120 μL/min. By recording the flow rate and total time necessary to collect 5000 events, the bacterial cell density (in events/mL) was calculated.

Planktonic Viability Testing

Planktonic cell viability was tested concurrently during flow cytometry analysis. Serial dilutions were performed on the planktonic cultures for both an untreated control sample and a biocide treated sample. These serial dilutions were taken immediately before and after the 1 h treatment period, and the dilutions were enumerated using the drop-plate method on tryptic soy agar (TSA) plates (64). In order to eliminate the presence of residual biocide after the treatment period, a 1 mL sample of both the untreated control and biocide-treated cell suspensions were filtered onto polycarbonate membranes which had a 0.22 μm pore size. The filtered samples were rinsed with 5 mL of DI water, and the cells were resuspended in 1 mL PBS by vortexing for 1 min. The

cells which were removed from the filters were serially diluted and enumerated using the drop-plate method. Efficacy of the 1 h biocide treatment was established by using log reductions.

Chlorine Residual Measurements

The concentration of residual total and free chlorine was measured in triplicate to determine the chlorine demand associated with planktonic bacterial cells. The planktonic cultures were prepared as if they were to be analyzed using flow cytometry, by diluting the cells from an exponential-phase culture 1:10 in sterile PBS. This diluted culture was centrifuged at 4600g for 4 min, the supernatant removed, and the cells were resuspended in sterile PBS. Concentrations of 10 and 50 mg/L chlorine were added to the cell suspension, and chlorine residuals were measured at t = 0, 15, 30, 45, and 60 min.

Total chlorine measurements were performed spectrophotometrically using a Spectronic Genesis 5 spectrophotometer. A pillow (packet) of DPD Total Chlorine Reagent for 5 mL Samples (Hach) was poured into an empty vial. At each time point, 5 mL of the diluted cell suspension was added to the vial which contained the DPD powder and the solution was vortexed for about 30 sec to ensure good mixing. Approximately 1 mL of the mixture was placed into a cuvette and the absorbance was measured at 515 nm (ABS_{515}). The ABS_{515} was compared to a chlorine standard curve and diluted if necessary in order to ensure the measured value fell within the linear range of the standard curve. If a dilution was necessary, the true total chlorine concentration was back-calculated by simple multiplication. The “blank” for these experiments which was

used as a relative comparison for any absorbance values was the dilute cell suspension without the addition of chlorine, but with the other reagents (e.g., DPD).

Free chlorine residual concentration measurements were performed spectrophotometrically using a LaMotte DC1100 free chlorine detector. Here, 10 mL of the diluted cell suspension was placed into a special cuvette-like vial which fit precisely into the detector. Exactly 5 drops (about 0.25 mL) of each DPD 1A and DPD 1B solutions were added to the vial and the vial was placed into the detector. The detector had a digital read-out which displayed free chlorine concentration in parts-per-million (ppm), equivalent to mg/L.

Viability after CAM Staining

The effect of CAM staining on planktonic cell viability was tested by plate counts before and after a 1 h CAM staining period. Planktonic cells were prepared for CAM staining in the same fashion as for flow cytometry experiments. A sample was taken from the cell suspension before and after 1 h CAM staining. Each sample was filtered onto a polycarbonate membrane which had a 0.22 μm pore size and rinsed with PBS to remove any extracellular CAM (fluorescent or non-fluorescent) that may have been present. The membranes were then vortexed for 1 min in PBS to suspend the cells in solution. The cell suspension was serially diluted and drop-plated on TSA plates. Colony forming units (CFU) were enumerated after 18-22 h of incubation at 37^{o}C.

Biofilm Reactor Analysis

The glass capillary biofilm reactor was used for growing *S. epidermidis* biofilms under continuous flow, using techniques similar to those previously published (121) (181). This reactor is a glass tube with a square cross-section (I.D. = 0.9mm) and wall thickness of 0.17mm, allowing for easy observation under a microscope when attached to the microscope stage with a capillary holder (Biosurface Technologies, Bozeman, MT). A turbid overnight culture of *S. epidermidis* grown in tryptic soy broth (TSB) served as the inoculum for the capillary biofilm experiments. The inoculum was statically incubated in the reactor for 4 hr at 37^{o}C, allowing time for the bacteria to attach to the capillary walls. After the initial attachment period, 1/10 strength TSB was pumped through the capillary at a rate of 1 mL/min for 24 hr at 37^{o}C, which approximated the hydrodynamic conditions typically present in a central venous catheter (54) (125). Figure 3-1 shows a picture of this reactor system.

The hydrodynamic conditions within the biofilm reactor were calculated using the flow rate and reactor dimensions as previously published (161). The average flow velocity at 37^{o}C during the biofilm development was 2.06 cm/sec, the Reynolds number (Re) was 27, and the shear stress (at the center line of the flow cell) was 0.127 N/m^2. During the PBS washing and treatment periods (described below), the reactor was at room temperature, 23^{o}C. At this temperature, the hydrodynamic reactor conditions changed slightly, with a Reynolds number of 20 and a wall shear stress of 0.171 N/m^2. The increase in shear stress is attributed to the decrease in Re (resulting in an increased friction factor) and an increase in the density of water with the lower temperature.

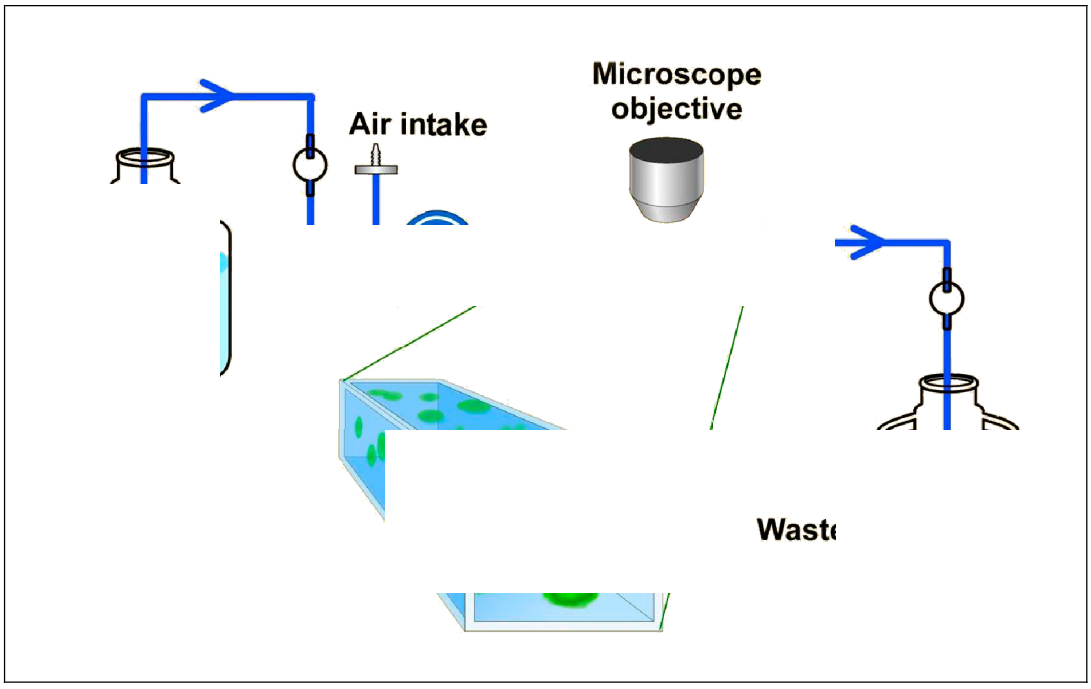


Figure 3-1. Glass capillary biofilm reactor.

The 24 hr biofilm was statically stained with CAM for 1 hr by injecting 9.85 μM CAM to fill the glass tube, and the spatio-temporal patterns of staining in isolated biofilm clusters was observed using a Leica TCS-SP2 AOBS Confocal Scanning Laser Microscope (CSLM). After the staining period, the biofilm was "washed" by pumping sterile PBS through the capillary at a rate of 1 mL/min to observe the retention of cell-associated fluorescent calcein. Following the wash period, an antimicrobial agent was pumped through the capillary at the same flow rate, and the spatio-temporal patterns of loss of fluorescence were observed with the CSLM. These rates of fluorescence loss allowed for measurement of diffusivity of different antimicrobial agents. Images were recorded every 30 seconds for a total of 1 hour for each phase: CAM staining, PBS wash, and antimicrobial treatment.

Following the 1 hr antimicrobial treatment period, CTC was introduced to the capillary flow cell, intermittently, for 2 h. Images were captured to record any respiratory activity in the biofilm, depicted by the presence of red fluorescence originating from the reduced CTC.

Image Analysis

Digital images captured using the CSLM were analyzed using MetaMorph, a quantitative image analysis program. The average green fluorescence intensity was measured at different locations within each selected biofilm cluster. Average intensity measurements were collected from the periphery, the center, and at an intermediate location within biofilm clusters termed the "medial" region. The regions at the periphery and medial areas of biofilm clusters were square regions with dimensions 8.79 x 8.79 μm, while the single center region had dimensions 17.58 x 17.58 μm. Therefore, the total area analyzed at the periphery, medial, and center of each cluster was equal. For corner biofilms, three regions at each of the different depths located at the periphery, and at depths of 60 and 120μm were analyzed. Changes in intensity were normalized by dividing by the initial intensity at the beginning of each 1 hr time series of antimicrobial treatment. This normalized intensity (I/Io) was used to compare relative loss of fluorescence during 1 h biocide treatment periods.

Changes in cluster morphology during antimicrobial treatment were also analyzed using this software. A freeform polygon was traced around the edge of the transmission-mode image of the cluster prior to antimicrobial treatment. A threshold was applied to

the images, which designated how much biofilm (dark pixels) covered the area enclosed by the freeform polygon region. For each image in the 1 h time series, and for each antimicrobial treatment, the percentage of the freeform polygon region covered by biomass was recorded. Data collected from the image analysis was easily exported and manipulated in the spreadsheet program Microsoft® Excel.

Mathematical Biofilm Modeling with Matlab®

Matlab®, a computer software package used for numerical analysis, was used to generate data which was subsequently compared to laboratory results from the biofilm experiments. Penetration of nonreacting agents into biofilm can be estimated using simple mathematical techniques. For an antimicrobial agent to be nonreacting, it is assumed that no reaction or sorption phenomena take place in the biofilm. The transient diffusion of a nonreacting antimicrobial agent into a sphere of biofilm (or a hemisphere of biofilm attached to a surface) in response to a step increase in the bulk fluid concentration of the agent can be described by the diffusion equation in spherical coordinates as seen in Equation 1.

$$\frac{\partial C}{\partial t} = D_e \left\{ \frac{1}{r^2} \frac{\partial}{\partial r} \left(r^2 \frac{\partial C}{\partial r} \right) + \frac{1}{r^2 \sin\theta} \frac{\partial}{\partial \theta} \left(\sin\theta \frac{\partial C}{\partial \theta} \right) + \frac{1}{r^2 \sin^2\theta} \frac{\partial^2 C}{\partial \phi^2} \right\} \qquad (1)$$

where C is the concentration of biocide, t is time, D_e is an effective diffusion coefficient for the biocide in the biofilm, and r is a spatial coordinate indicating radial position in the biofilm. If the initial and boundary conditions are such that the concentration of biocide

in the hemisphere of biofilm is dependent only on radial position and time, the equation is simplified to Equation 2.

$$\frac{\partial C}{\partial t} = D_e\left(\frac{\partial^2 C}{\partial r^2} + \frac{2}{r}\frac{\partial C}{\partial r}\right) \tag{2}$$

$$\text{at } r = R, C = C_0 \text{ for all } t > 0 \tag{3}$$

$$\text{at } r = 0, \frac{\partial C}{\partial r} = 0 \text{ for all } t > 0 \tag{4}$$

$$\text{at } t \le 0, C = 0 \text{ for all } 0 \le r \le R \tag{5}$$

Equation 2 is a form of Fick's Second Law of Diffusion in spherical coordinates, representing an unsteady mass balance on the antimicrobial agent. The left-hand side of Equation 2 represents the local change in concentration of the antimicrobial agent, while the right-hand side represents the net change in concentration due to diffusive transport. Equations 3 and 4 are boundary conditions ensuring constant concentration of the agent at the bulk fluid-biofilm interface and a no-flux condition at the substratum, respectively. Equation 5 is an initial condition that specifies no antimicrobial is present in the biofilm at time zero. A similar analysis for different biofilm geometry has been published previously (156).

The variable D_e is an effective diffusion coefficient in the biofilm. The value of D_e is generally smaller than the aqueous diffusion coefficient for the same solute in pure water, D_{aq}, due to the presence of biomass and extracellular material in the EPS matrix. Experimental measurements of the ratio of D_e/D_{aq} have been reviewed and guidelines and

formulae are presented for estimations of D_e/D_{aq} (149). This ratio depends upon the size of the molecule as well as its electrostatic charge. For this research, D_e/D_{aq} values will be 0.6 (chlorine) and 0.2 (Barquat, glutaraldehyde, and nisin). Values for aqueous diffusion coefficients are given in Table 3-1

Table 3-1. Molecular weights and diffusion coefficients in water at 25°C.

Solute	[g mol^{-1}] MW	[cm^2 sec^{-1}] D_{aq} x 10^6
Hypochlorous acid[a]	50.1	19.0
Glutaraldehyde[b]	100.1	9.32
Barquat[b]	357	4.27
Nisin[c]	3354	1.90

[a]Comparison to ion mobilities of Cl^-, ClO_3^-, and ClO_4^- (70)
[b](153)
[c]Polson method (117) (171)

The exact solution to Eqs (2) through (5) is

$$\frac{C}{C_0} = 1 + \frac{2R}{\pi r}\sum_{n=1}^{\infty}\frac{(-1)^n}{n}\sin\frac{n\pi r}{R}e^{-\frac{D_e n^2\pi^2 t}{R^2}} \tag{6}$$

where r is radial position and R is the radius of the cluster. This equation can be reproduced graphically (23). The degree to which the antimicrobial penetrates the biofilm depends on the parameter, β, which is

$$\beta = \frac{D_e t}{R^2} \tag{7}$$

The time it takes for a given antimicrobial to diffuse into the biofilm can be calculated in several different ways using the above equations. A new parameter, t_{50}, has

been developed for this research, and represents the time it takes for a 50% decrease in fluorescence at the center of a cluster during an antimicrobial treatment period (experimental approach). Another parameter, α_{50}, represents the time it takes for the antimicrobial concentration in the center of the biofilm cluster to reach 50% of the bulk fluid concentration (mathematically-predicted approach). This parameter is analogous to one calculated by Stewart (151). At time α_{50}, the parameter β has been calculated to be 0.139. Therefore, experimental results and mathematical predictions can be compared for each antimicrobial agent.

For each 1 h biocide treatment, α_{50} and t_{50} values can be compared for each region within a biofilm cluster. For the diffusive biocide penetration calculations, α_{50} values were calculated for radial positions of r/R = 0.9, 0.5, and 0.1 for the periphery, medial, and center regions of the model cluster, respectively.

CHAPTER 4

RESULTS

Planktonic Bacteria

Flow Cytometry

Triplicate experiments for each antimicrobial used against planktonic bacteria were analyzed using flow cytometry. An unstained control experiment was analyzed in parallel with each experiment in order to verify that the cytometer was working properly. For eighteen unstained control experiments, the mean FITC intensity value for the entire bacterial population was recorded at t = 0, 60, 120, and 180 min. Also at these time points, the percentage of the bacterial cells (events) which registered green fluorescence intensity greater than the arbitrary threshold of 300 on the FITC scale (% Green) was recorded. The values for the unstained control experiments are shown in Table 4-1. A representative experiment was chosen as the experiment which had mean FITC intensity values closest to the overall average values expressed in Table 4-1. For the representative unstained control experiment, the flow cytometry histogram data are shown in Figure 4-1.

Table 4-1. Flow cytometry data for unstained control experiments (n = 18).

Time (min)	Mean FITC Intensity	% Green	Log (Events/mL)
0	36 ± 38	0.17 ± 0.12	6.13 ± 0.33
60	24 ± 19	0.18 ± 0.19	6.15 ± 0.30
120	21 ± 8	0.26 ± 0.34	6.18 ± 0.30
180	28 ± 20	0.28 ± 0.44	6.20 ± 0.34

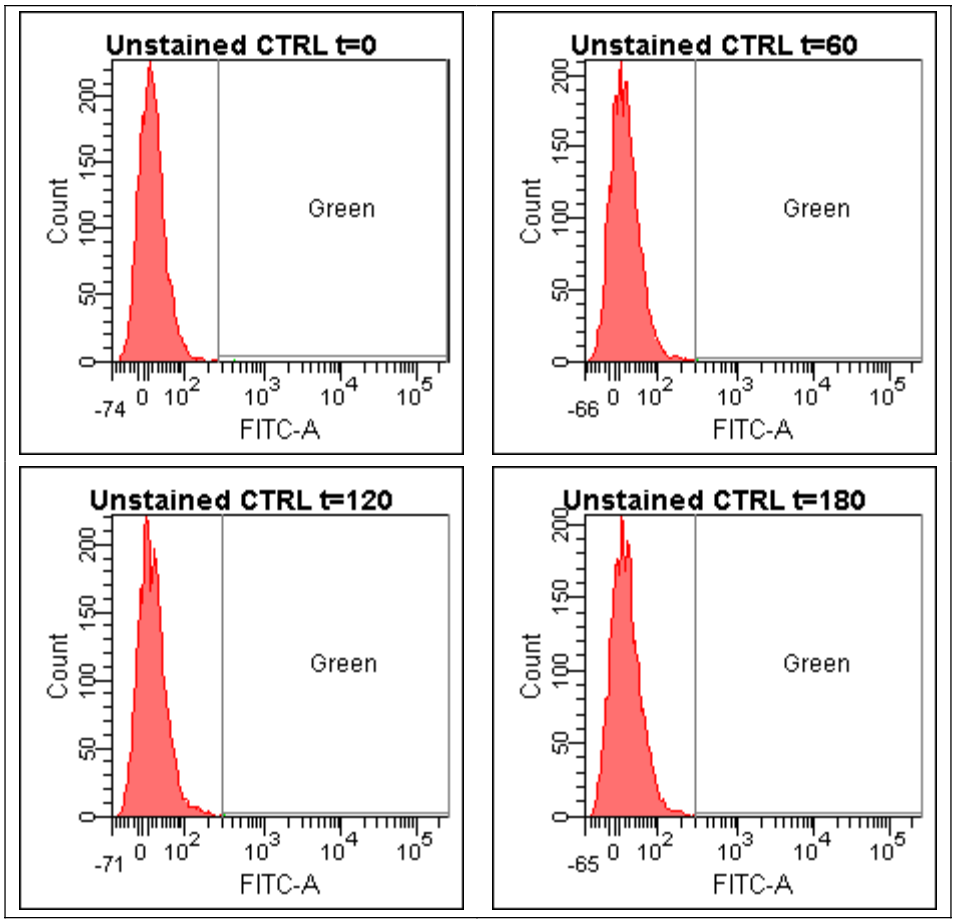


Figure 4-1. Representative flow cytometry histograms of unstained control. Time is in minutes.

Over the course of the 3 h unstained control experiments, the mean FITC intensity for the population of planktonic cells was generally around 30, which was an order of magnitude lower than the "green" threshold that was set at 300. In fact, only about 0.2% of the total cells registered fluorescence intensity greater than the FITC threshold of 300. The number of events/mL did increase slightly over time, suggesting a possible small increase in the number of cells when suspended in sterile PBS.

There were eighteen replicates of the 1 h CAM staining and PBS "wash" phases of the planktonic experiments analyzed with flow cytometry. Samples were taken at t =

0, 20, 40, and 60 min during both CAM staining and PBS wash phases. The data for the CAM staining and PBS wash phases of the experiments are shown in Table 4-2 and Table 4-3, respectively. Representative histogram data for CAM staining and PBS experiments were chosen as those data which most closely resembled the overall average FITC intensity data shown in Table 4-2 and Table 4-3, respectively. Histogram data are shown below for CAM staining (Figure 4-2) and the PBS wash phase (Figure 4-3).

Table 4-2. Flow cytometry data for 1 h CAM staining of planktonic bacteria. (n = 18)

Time (min)	Mean FITC Intensity	% Green	Log (Events/mL)
0	51 ± 19	0.71 ± 0.64	6.13 ± 0.34
20	1674 ± 925	90.7 ± 11.2	6.20 ± 0.32
40	3589 ± 1633	95.5 ± 7.10	6.24 ± 0.29
60	5666 ± 2090	97.1 ± 4.76	6.26 ± 0.30

During the 1 h CAM staining period, the planktonic population of cells began with a mean FITC intensity of 51 (unstained) and ended with a mean FITC intensity of about 5700 (bright green). Approximately 97% of the cells were stained green by CAM and registered fluorescence intensity greater than the FITC threshold of 300. Also, the number of cells increased slightly (0.13-Log) during the 1 h CAM staining period.

The 1 h PBS wash phase of these experiments showed the cells retaining their fluorescence. In fact, the cells seem to increase in their staining intensity, from about 7000 at t = 0, to about 12000 at t = 60 min of PBS washing. There was a slight decrease (0.11-Log) in the number of events/mL, but 98% of the remaining cells had fluorescence intensity above the green threshold.

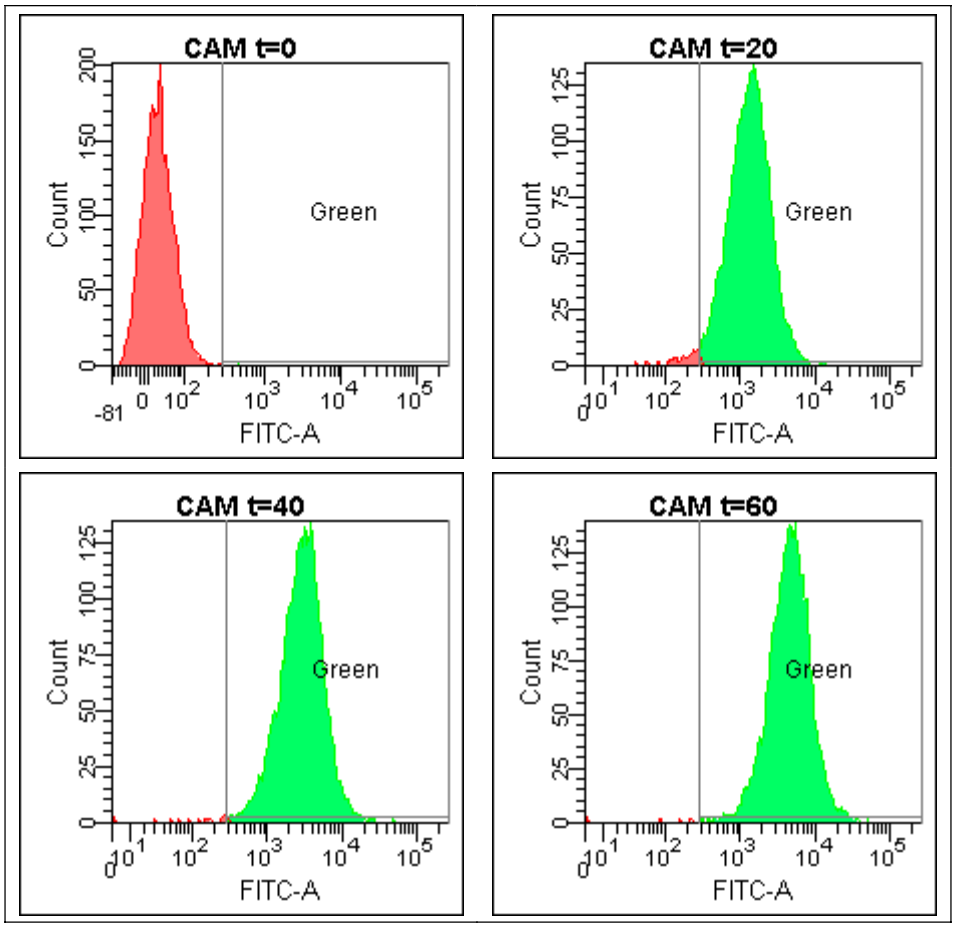


Figure 4-2. Representative flow cytometer histograms for 1 h CAM staining phase. Time is in minutes.

Table 4-3. Flow cytometry data for 1 h PBS wash of planktonic bacteria. (n = 18)

Time (min)	Mean FITC Intensity	% Green	Log (Events/mL)
0	6995 ± 3433	97.1 ± 3.62	5.92 ± 0.37
20	9183 ± 4242	97.5 ± 3.49	5.78 ± 0.39
40	10585 ± 4390	97.7 ± 3.10	5.78 ± 0.34
60	12128 ± 4812	97.9 ± 2.93	5.81 ± 0.38

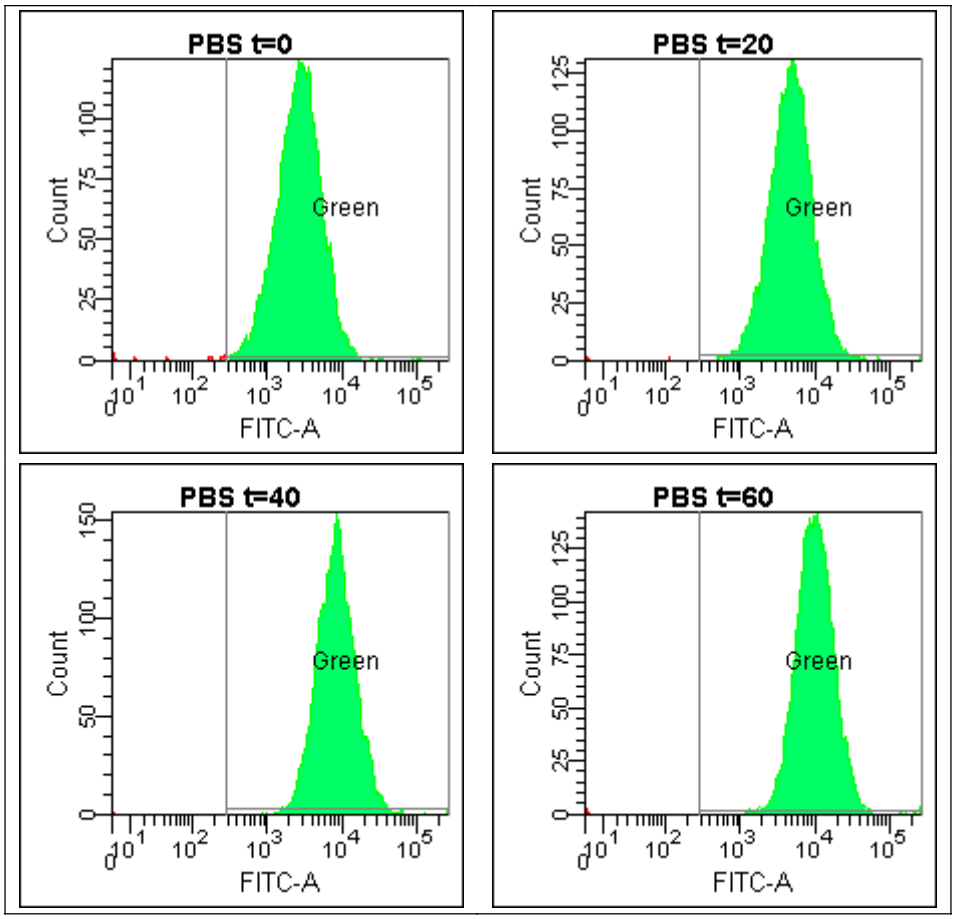


Figure 4-3. Representative flow cytometer histograms for 1 h PBS wash phase. Time is in minutes.

For each antimicrobial agent used in this research project, triplicate experiments were performed using flow cytometry to analyze the effect of the antimicrobial on bacterial cell membrane integrity. During each 1 h treatment phase, samples were collected at t = 0, 5, 10, 15, 20, 40, and 60 min. The mean FITC (green) intensity of the suspended population was collected at each time point. Also at these time points, the percentage of the bacterial cells (events) which registered green fluorescence intensity greater than the threshold of 300 on the FITC scale (% Green) was recorded. As a control for the antimicrobial treatment of planktonic bacteria, an equivalent volume of

PBS was added to the bacterial suspension. Data for the triplicate PBS control experiments can be seen below in Table 4-4. A representative experiment for each treatment was chosen as that which exhibited mean FITC intensity values closest to the overall average FITC intensity values for the three experiments combined. Histogram data from the time points during the representative 1 h PBS control treatment are shown in Figure 4-4.

Table 4-4. Flow cytometer data for 1 h PBS control treatment. (n = 3)

Time (min)	Mean FITC Intensity	% Green	Log (Events/mL)
PBS t=60	14118 ± 1554	99.0 ± 0.66	5.88 ± 0.22
1	15578 ± 4541	98.8 ± 0.47	5.87 ± 0.12
5	16352 ± 4698	98.8 ± 0.53	5.80 ± 0.09
10	16854 ± 4993	98.7 ± 0.49	5.86 ± 0.11
15	16955 ± 4593	98.6 ± 0.72	5.77 ± 0.14
20	17393 ± 4912	98.6 ± 0.67	5.77 ± 0.19
40	18773 ± 5782	99.0 ± 0.20	5.67 ± 0.01
60	19101 ± 4679	98.7 ± 0.55	5.63 ± 0.11

The time point "PBS t=60" is the time immediately before addition of the antimicrobial agent (i.e., t = 0 of the antimicrobial treatment). It took approximately 1 min from the time the antimicrobial agent was added to the cell suspension to the point when the data was collected from the flow cytometer. This 1 min delay was due to the following steps: adding the antimicrobial agent, vortexing the sample briefly, diluting the sample into a flow cytometer test tube, vortexing a second time, and loading the test tube onto the cytometer. Also, the flow cytometer takes up to 20 seconds to collect and record data from one sample.

The control experiments, in which planktonic cells were treated with PBS, showed the cells retaining their fluorescence. During the 1 h PBS control treatment, the mean FITC intensity increased from about 16000 to about 19000. There was a 0.24-Log decrease in events/mL during the control, on average, with approximately 99% of the remaining cells recording florescence intensity above the green threshold.

Data for the triplicate experiments in which planktonic bacteria were treated with Barquat can be seen below in Table 4-5. Representative histogram data was chosen in a similar fashion as described previously, and the histogram plots are shown in Figure 4-5. Planktonic cells treated for 1 h with Barquat showed an initial decrease in FITC fluorescence intensity during the first minute of treatment. The FITC intensity increased during the course of the treatment, ending at a level comparable to that of the value before Barquat was added.

Table 4-5. Flow cytometry data for 1 h treatment with Barquat. (n = 3)

Time (min)	Mean FITC Intensity	% Green	Log (Events/mL)
PBS t = 60	10744 ± 4328	99.4 ± 0.40	5.85 ± 0.73
1	985 ± 378	87.5 ± 8.76	5.58 ± 0.57
5	1053 ± 223	90.7 ± 7.51	5.46 ± 0.69
10	1256 ± 267	92.5 ± 7.12	5.24 ± 0.71
15	1381 ± 98.3	91.5 ± 9.96	4.88 ± 0.70
20	2283 ± 988	92.9 ± 8.29	4.59 ± 0.76
40	3661 ± 517	94.6 ± 5.60	4.41 ± 0.60
60	9417 ± 5408	89.9 ± 3.70	4.17 ± 0.68

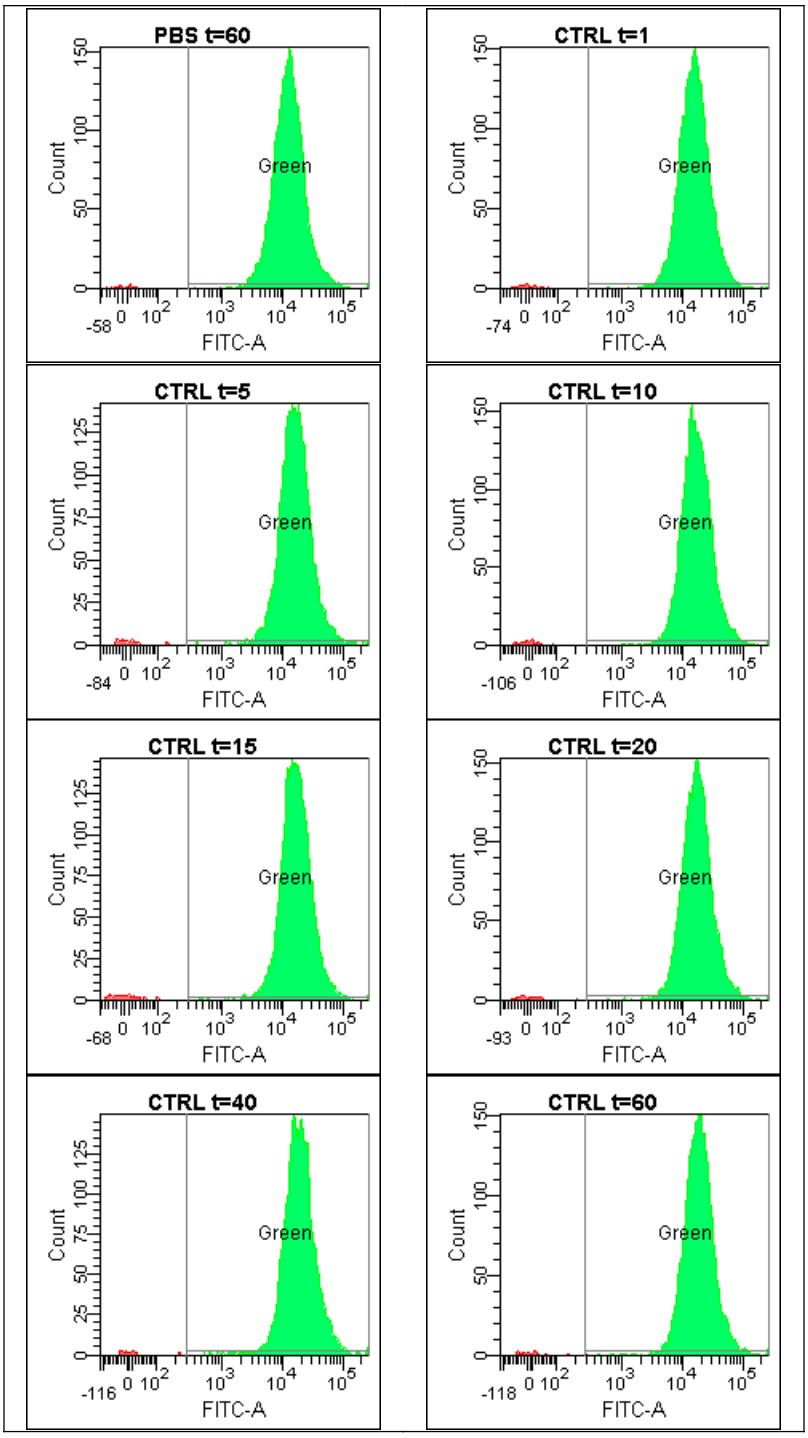


Figure 4-4. Representative flow cytometry histogram data for 1 h PBS control treatment. The first panel shows the final time point of the PBS wash period, immediately prior to the control treatment. Time is in minutes.

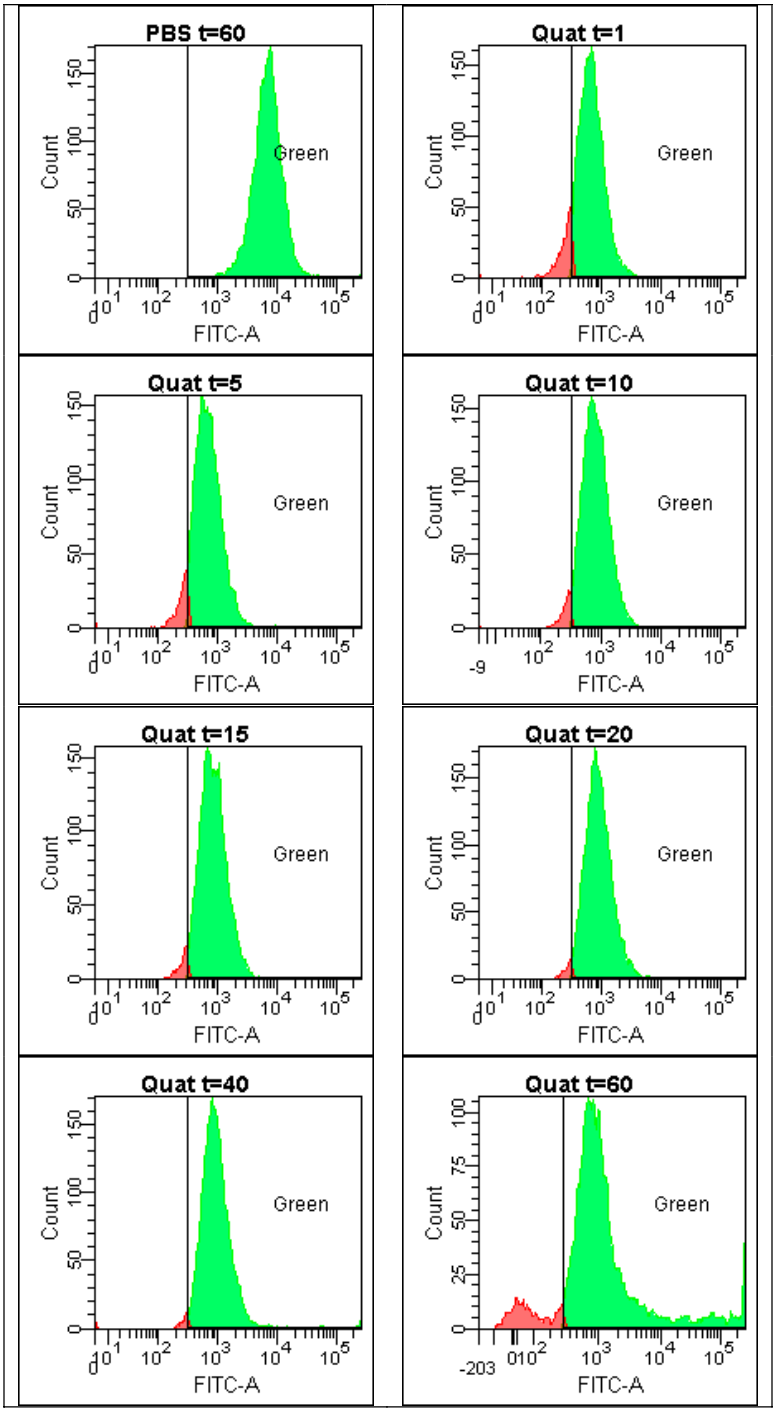


Figure 4-5. Representative flow cytometer histogram data for 1 h Barquat treatment. The top left panel shows the final time point of the PBS wash phase, immediately prior to Barquat treatment. Time is in minutes.

Before the Barquat was added, 99% of all cells were stained green. Immediately after the addition of Barquat, 12% of the cells lost their fluorescence. After the 1 h treatment, the number of events/mL had decreased by 1.68-Log, and 90% of the remaining cells retained their fluorescence.

The data for the triplicate experiments in which planktonic bacteria were treated for 1 h with 50 mg/L chlorine can be seen below in Table 4-6. Representative histogram data was chosen in a similar fashion as described previously, and the histogram plots are shown in Figure 4-6. Mean FITC intensity for the planktonic cell suspension decreased from about 9100 to about 7900 during the 1 h treatment with 50 mg/L chlorine. There was a 0.60-Log reduction in events/mL during the 1 h treatment with 50 mg/L chlorine, and an average of 94.7% of the remaining cells retained their green fluorescence.

Table 4-6. Flow cytometry data for 1 h treatment with 50 mg/L chlorine. (n = 3)

Time (min)	Mean FITC Intensity	% Green	Log (Events/mL)
PBS t = 60	9054 ± 3977	97.1 ± 4.48	5.94 ± 0.42
1	9118 ± 2232	97.9 ± 2.73	5.86 ± 0.52
5	8264 ± 1002	94.7 ± 3.40	5.78 ± 0.45
10	8240 ± 361	95.5 ± 2.10	5.81 ± 0.49
15	8425 ± 703	94.3 ± 3.10	5.63 ± 0.51
20	8504 ± 939	95.2 ± 2.20	5.61 ± 0.39
40	7896 ± 676	94.1 ± 1.42	5.59 ± 0.44
60	7919 ± 922	94.7 ± 0.93	5.34 ± 0.94

Data for the triplicate experiments in which the planktonic cells were treated for 1 h with 10 mg/L chlorine are shown in Table 4-7. Representative histogram data from flow cytometry analyses were chosen in a similar fashion as described previously, and the plots are displayed in Figure 4-8.

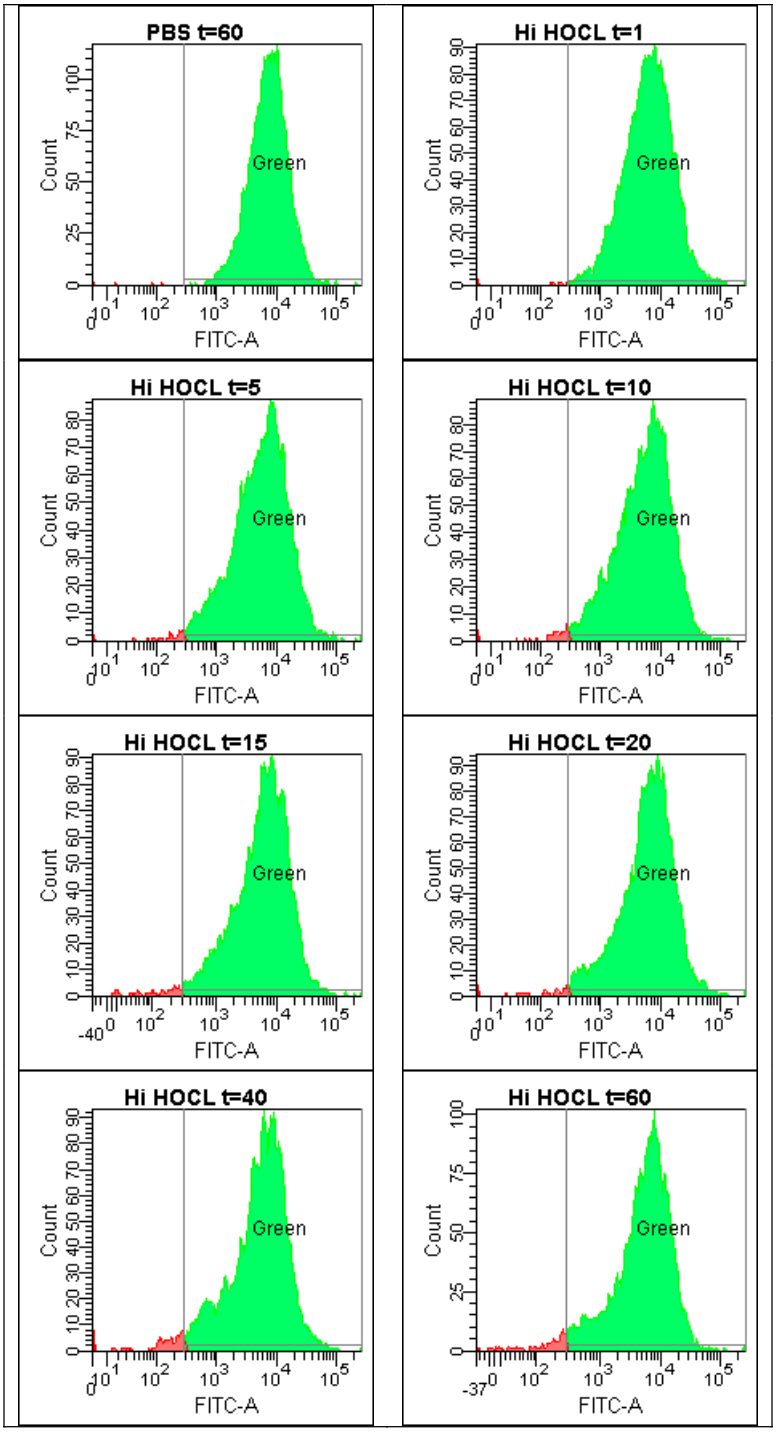


Figure 4-6. Representative histogram data for 1 h treatment with 50 mg/L chlorine. The top left panel shows the final time point of the PBS wash phase, immediately prior to treatment with 50 mg/L chlorine. Time is in minutes.

Table 4-7. Flow cytometry data for 1 h treatment with 10 mg/L chlorine. (n = 3)

Time (min)	Mean FITC Intensity	% Green	Log (Events/mL)
PBS t = 60	11714 ± 5539	96.2 ± 5.02	5.65 ± 0.26
1	15765 ± 5166	96.2 ± 4.95	5.67 ± 0.28
5	15622 ± 5197	95.9 ± 5.72	5.64 ± 0.26
10	15283 ± 4923	96.0 ± 5.37	5.62 ± 0.29
15	15080 ± 5801	93.5 ± 9.87	5.55 ± 0.27
20	15736 ± 5870	95.4 ± 6.41	5.58 ± 0.26
40	16352 ± 7210	93.5 ± 9.79	5.60 ± 0.34
60	16158 ± 6785	91.5 ± 13.2	5.51 ± 0.23

During the 1 h treatment of planktonic cells with 10 mg/L chlorine, the mean FITC staining intensity increased, from about 11700 to about 16200. At the same time, the total number of events/mL decreased slightly, as indicated by the 0.14-Log reduction in events/mL and 91.5% of the remaining cells had retained their green fluorescence.

A chlorine residual test was performed for the lower concentration of chlorine for the planktonic experiments in order to determine the chlorine demand imposed by the presence of *S. epidermidis* bacteria suspended in PBS buffer. A chlorine standard curve for total chlorine concentration was generated using spectrophotometry and can be seen in Figure 4-7 below. The concentrations of total chlorine and free chlorine were determined spectrophotometrically at t = 0, 15, 30, 45, and 60 min during treatment of planktonic cells in PBS, where t = 0 min was the time immediately after the addition of chlorine to the cell suspension. The values of free chlorine and total chlorine during the 10 mg/L chlorine treatment of planktonic cells can be seen in Table 4-8. When 10 mg/L chlorine was added to PBS alone (without bacteria present in solution), the concentration was verified by the same assay.

Table 4-8. Total and free chlorine residual during 1 h treatment of planktonic cells with 10 mg/L chlorine.

Time (min)	Total chlorine (mg/L)	Free chlorine (mg/L)
0	4.07	3.90
15	3.25	0.28
30	3.06	0.25
45	3.59	0.22
60	3.61	0.18

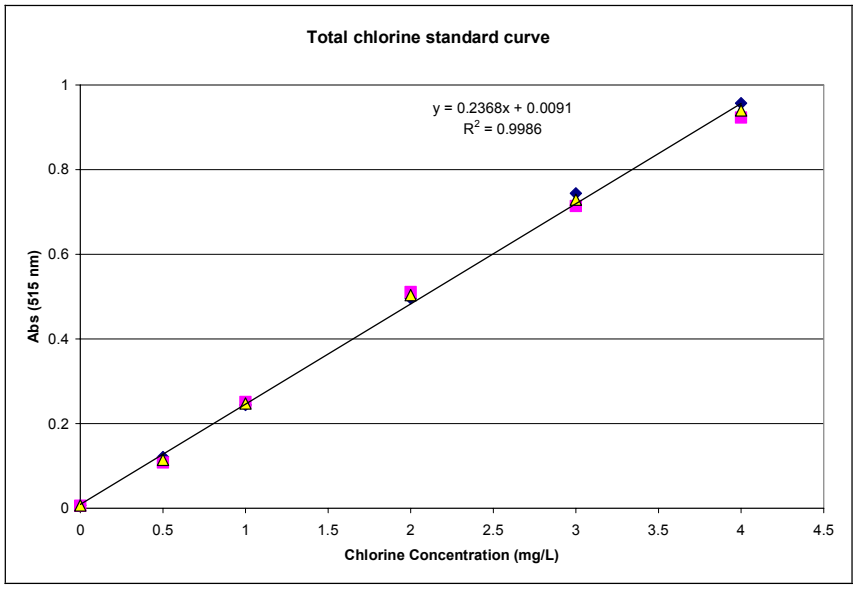


Figure 4-7. Total chlorine standard curve.

Data for the triplicate experiments in which planktonic cells were treated for 1 h with glutaraldehyde are shown in Table 4-9. Representative histogram data from flow cytometry analyses were chosen in a similar fashion as described previously, and the plots are displayed in Figure 4-9. The 1 h glutaraldehyde treatment showed an instant increase in FITC fluorescence intensity, from about 14100 to 18500. During the remaining 1 h of treatment, the FITC intensity of the cell population decreased to about 16100. It appeared that no cells lost their fluorescence, with roughly 98% of the total cell

population retaining its fluorescence throughout the treatment. A 0.10-Log increase in events/mL was observed during the glutaraldehyde treatment.

Data for the triplicate experiments in which planktonic cells were exposed to a 1 h treatment with nisin are shown in Table 4-10. Representative histogram data from flow cytometry analyses were chosen in a similar fashion as described previously, and the plots are displayed in Figure 4-10. The planktonic cells instantaneously lost much of their fluorescence when nisin was introduced, with mean FITC intensity decreasing from 13000 to 8900 in the first minute of treatment. The mean FITC intensity decreased to about 2800 after the 1 h nisin treatment. Only about 39% of the cells retained their green fluorescence after the treatment period. The number of events/mL actually increased initially by 0.38-Log, but stayed constant for the remainder of the treatment.

Table 4-9. Flow cytometry data for 1 h treatment with glutaraldehyde. (n = 3)

Time (min)	Mean FITC Intensity	% Green	Log (Events/mL)
PBS t = 60	14107 ± 5809	98.2 ± 1.86	5.82 ± 0.36
1	18550 ± 10016	98.1 ± 1.50	5.81 ± 0.30
5	17646 ± 9338	98.0 ± 1.69	5.78 ± 0.15
10	18032 ± 9938	98.3 ± 1.78	5.89 ± 0.29
15	18121 ± 9165	98.3 ± 1.99	5.89 ± 0.29
20	17966 ± 9902	97.6 ± 3.24	5.86 ± 0.30
40	16541 ± 8259	98.4 ± 2.14	5.88 ± 0.20
60	16128 ± 8737	98.3 ± 2.40	5.92 ± 0.27

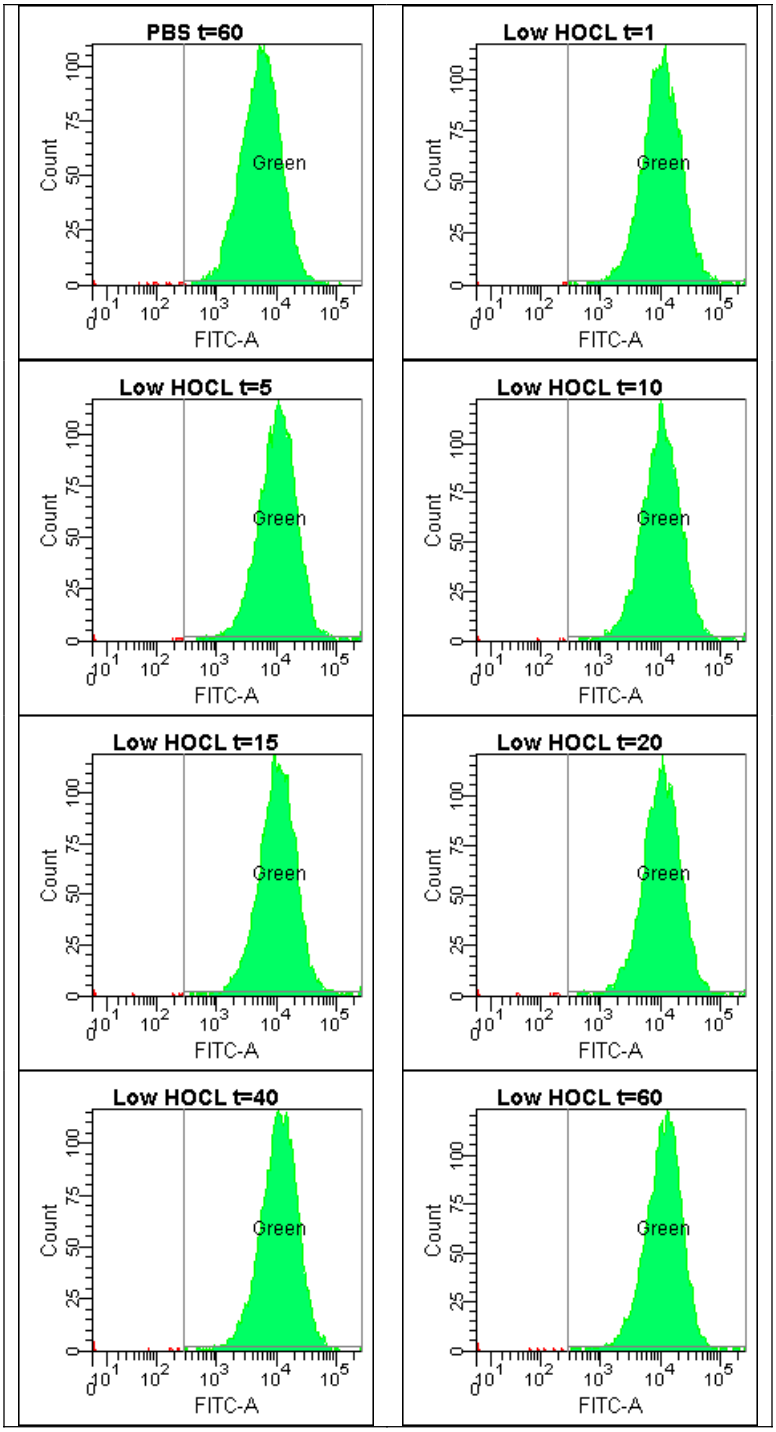


Figure 4-8. Representative histograms of 1 h treatment with 10 mg/L chlorine. The top left panel shows the final time point of the PBS wash phase, immediately prior to treatment with 10 mg/L chlorine. Time is in minutes.

Table 4-10. Flow cytometry data for 1 h treatment with nisin. (n = 3)

Time (min)	Mean FITC Intensity	% Green	Log (Events/mL)
PBS t = 60	13034 ± 8068	97.3 ± 3.51	5.78 ± 0.25
1	8905 ± 9770	66.7 ± 17.8	6.16 ± 0.14
5	6016 ± 8707	59.1 ± 24.2	6.14 ± 0.16
10	5047 ± 7481	55.5 ± 26.4	6.14 ± 0.12
15	4131 ± 6204	51.5 ± 28.1	6.13 ± 0.16
20	3877 ± 5935	49.2 ± 29.5	6.11 ± 0.14
40	3146 ± 4899	43.7 ± 31.2	6.15 ± 0.15
60	2794 ± 4339	38.7 ± 30.4	6.15 ± 0.20

The relative increase or decrease in mean FITC intensity can be determined by normalizing the FITC intensity at each time point during the antimicrobial treatment to the FITC intensity at the end of the PBS wash phase. This relative change in FITC intensity can allow for comparisons between the different antimicrobial treatments. Figure 4-11 shows graphs of relative changes in FITC intensity for each treatment.

A cumulative comparison of the antimicrobial treatments as analyzed with flow cytometry can be seen below in Table 4-11. This table shows the value for t_{50} for each of the treatments, which is the time it took for 50% of the initial mean FITC fluorescence (PBS t=60) to leak out of the cells. If 50% of the fluorescence was lost within the first minute of treatment, a linear interpolation was performed to establish a reasonable estimate for t_{50}. The table also shows changes in events/mL, normalized FITC intensity, and % green cells over the course of the 1 h treatment.

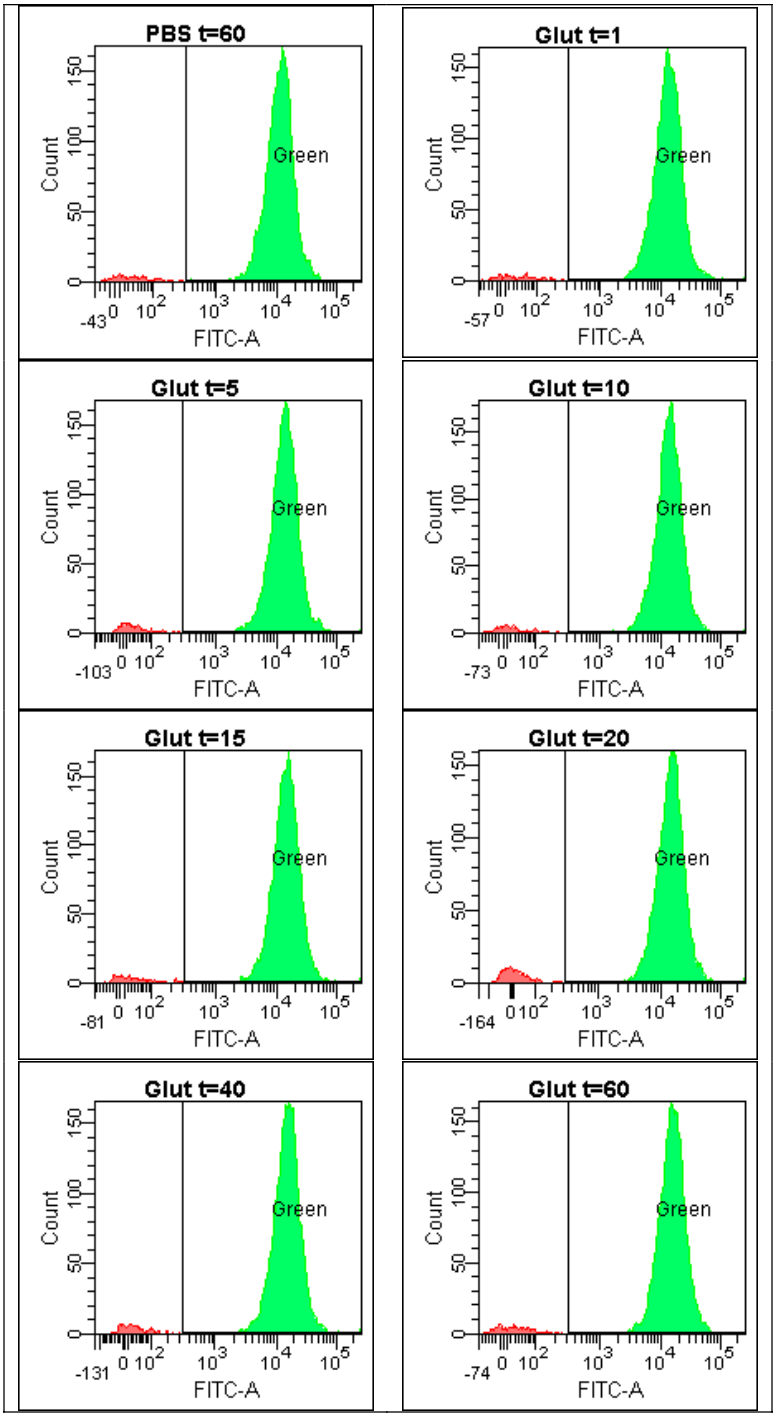


Figure 4-9. Representative histogram data for 1 h glutaraldehyde treatment. The top left panel shows the final time point of the PBS wash phase, immediately prior to glutaraldehyde treatment. Time is in minutes.

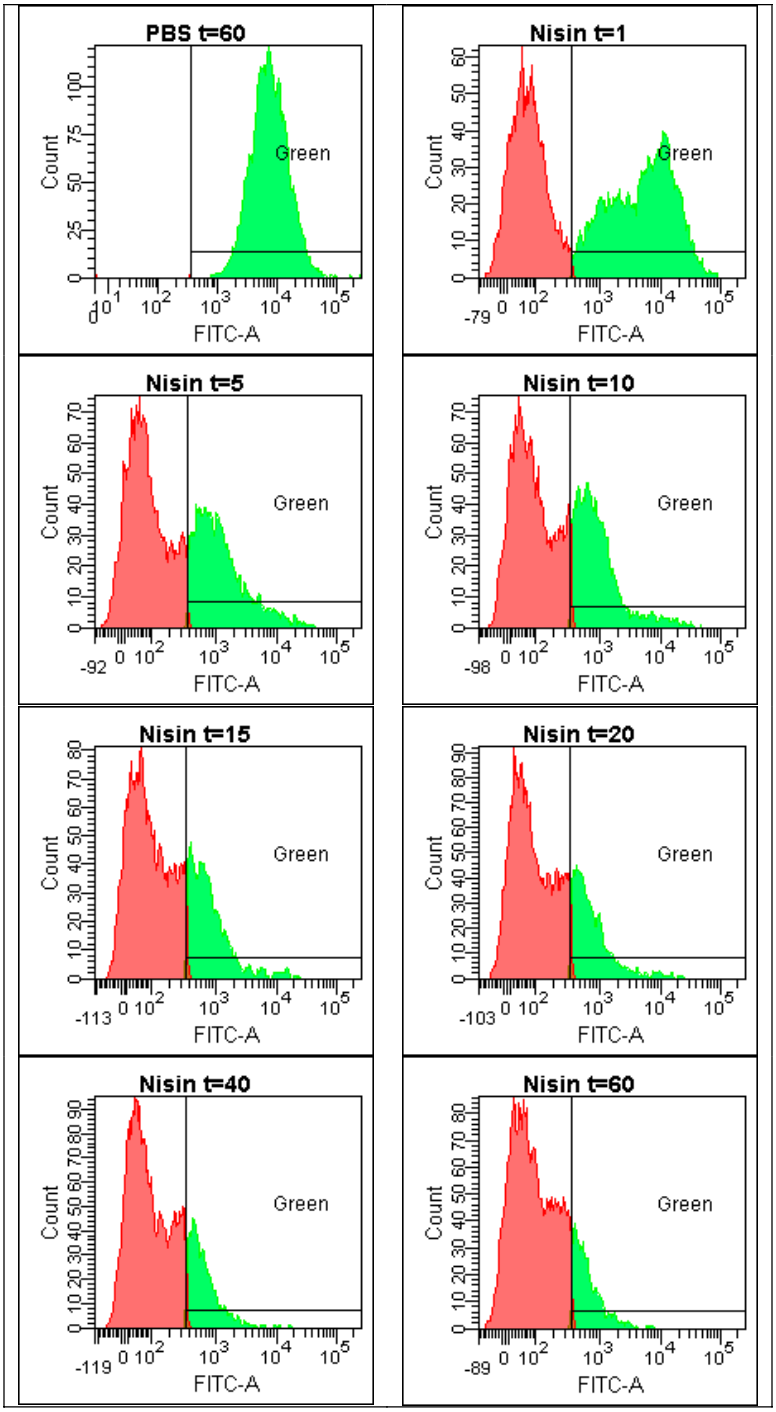


Figure 4-10. Representative histogram data for 1 h treatment with nisin. The top left panel shows the fluorescence intensity at the end of the PBS wash phase, immediately prior to nisin treatment. Time is in minutes.

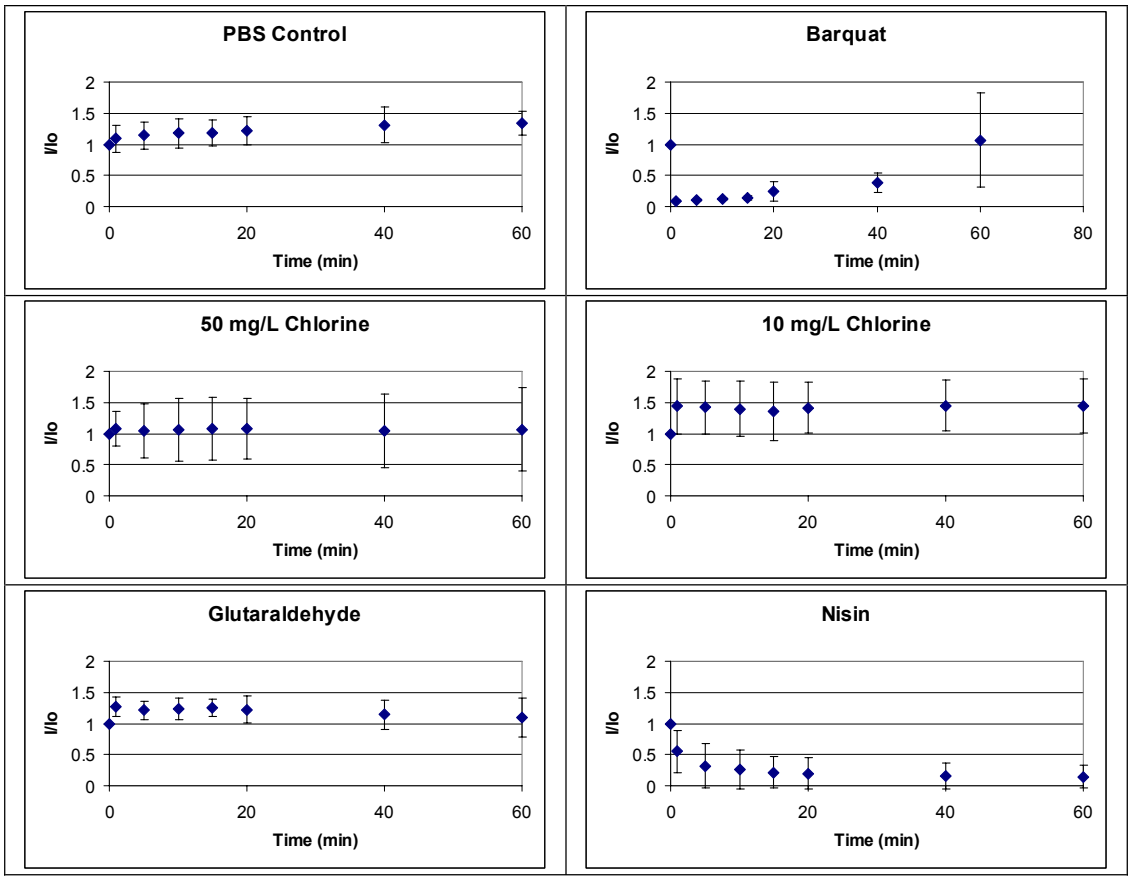


Figure 4-11. Relative change in mean FITC intensity during antimicrobial treatment.

Table 4-11. Comparison of antimicrobial treatments as analyzed with flow cytometry.

Antimicrobial	t_{50} (min)	Δ log(evts/mL)	Δ FITC I/Io	Δ % green
PBS Control	------	-0.25 ± 0.12	+0.34 ± 0.20	-0.33 ± 0.21
Barquat	0.55 ± 0.00	-1.68 ± 0.26	+0.07 ± 0.75	-9.57 ± 3.46
50 mg/L Chlorine	------	-0.60 ± 0.53	+0.07 ± 0.67	-2.33 ± 4.03
10 mg/L Chlorine	------	-0.15 ± 0.05	+0.44 ± 0.44	-4.70 ± 8.14
Glutaraldehyde	------	+0.10 ± 0.17	+0.10 ± 0.31	+0.10 ± 0.70
Nisin	5.55 ± 8.19	+0.37 ± 0.06	-0.86 ± 0.18	-58.6 ± 29.5

Only treatment with Barquat and nisin resulted in a decrease in FITC intensity of at least 50%. The t_{50} values for Barquat and nisin treatments were 0.55 and 5.55 minutes, respectively. There was a decrease in events/mL during the 1 h treatment with Barquat and the two concentrations of chlorine, as well as the PBS control. Barquat treatment

resulted in the greatest log reduction of events/mL, at 1.68, while the log reductions for the control and the high and low concentrations of chlorine were 0.25, 0.60, and 0.15, respectively. Treatment with glutaraldehyde and nisin resulted in 0.10-log and 0.37-log increases in events/mL, respectively. The only treatment which resulted in a decrease in mean FITC intensity during the 1 h treatment was that of nisin, with a relative decrease of 0.86. All treatments except glutaraldehyde resulted in a decrease in the percentage of cells that were fluorescing green. The PBS control showed the smallest decrease in % green cells, at 0.33%, followed by high chlorine, low chlorine, and Barquat, at 2.33, 4.7, and 9.57% decreases, respectively. The greatest change in % green cells was during the 1 h nisin treatment, where 58.6% of the cells lost their fluorescence, on average. A comparison between the changes in events/mL (measured with the flow cytometer) and CFU/mL (measured by plate counts) after the 1 h treatment period is shown in Figure 4-13 for each antimicrobial treatment.

During flow cytometry experiments, as a particle passes through the laser detector, the laser light is scattered in all directions. Light that is scattered axially with respect to the laser beam is called forward scatter (FSC). Light that is scattered perpendicular to the laser beam is called side scatter (SSC). These parameters are related to different properties of the particle or cell that scattered the light. The relative difference in the size of the cells or particles is given by FSC values. The relative difference in the internal complexity or granularity of the cells or particles is given by SSC values. In the case of *S. epidermidis*, SSC denotes the amount of cell clumping.

Scatter plots of FSC vs. SSC were generated for each time point during the flow cytometry experiments.

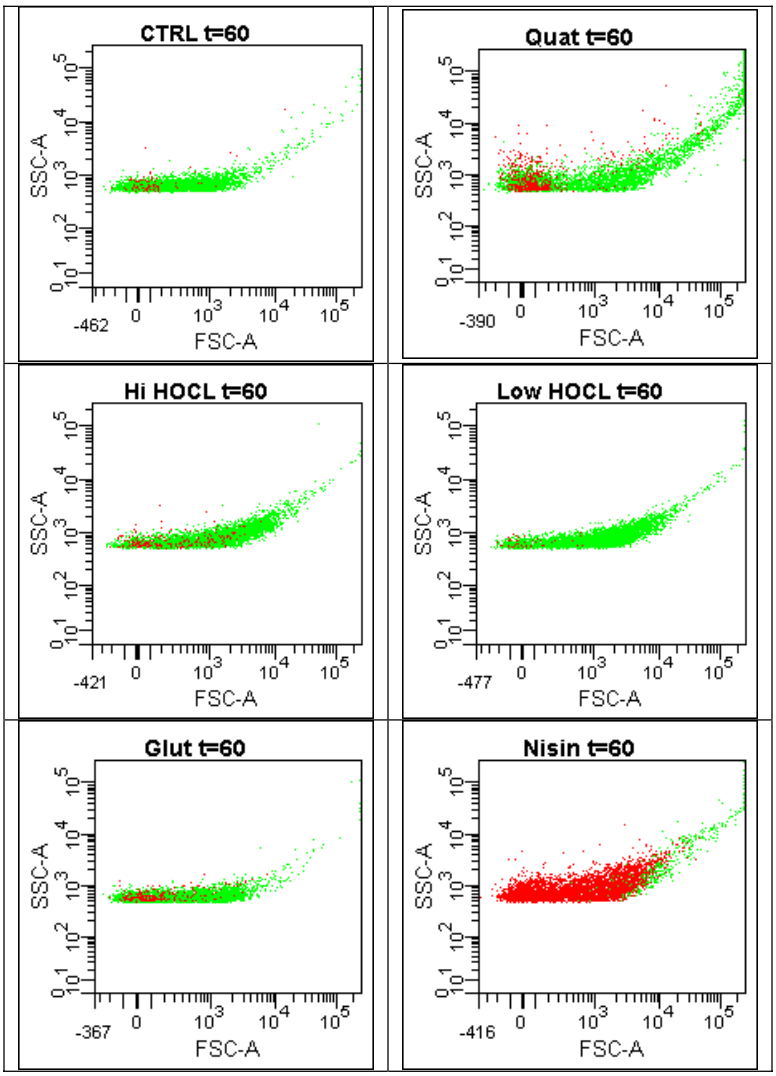


Figure 4-12. FSC vs. SSC scatter plots from the final time point of the representative experiment for each antimicrobial treatment. Red dots represent cells that have lost their fluorescence. Green dots are cells that fluoresce green. Time is in minutes.

For each of the antimicrobial treatments, any loss of fluorescence was focused mainly in the smaller, un-clumped cells. This is demonstrated by the red particles being

concentrated toward smaller values on the FSC vs. SSC scatter plots, as seen in Figure 4-12. The red dots on the scatter plots are cells that had fluorescence intensity below the green threshold, and green dots are cells that had intensity above the threshold. In other words, green dots are stained cells and red dots are cells that have lost their fluorescence. The shapes of the scatter plots are all very similar, but the final time point of the 1 h Barquat treatment suggests significant clumping which is indicated by the increased number of points which registered at higher values on the FSC vs. SSC plot.

Viability Testing

The flow cytometry analyses could not directly offer insight into the viability of the cells that were treated with antimicrobial agents. Rather, these analyses only detected whether those cells maintained enough membrane integrity to retain the fluorescent CAM stain. Therefore, plate counts were performed before and after each 1 h antimicrobial treatment in parallel to the flow cytometry experiments. A sample was also taken from a PBS control, before and after the 1 h antimicrobial treatment, and plate counts were performed on this sample to determine the loss of viable cells due to the filtration step used to rinse the antimicrobial agent from the planktonic cells prior to plating.

For the 21 total PBS control samples taken for viability testing, the loss of viable cells due to filtration was small compared to the log reductions due to antimicrobial exposure. The average log reduction due to filtration was 0.40 ± 0.21 CFU/mL, where CFU stands for colony forming units. Treatment with Barquat showed an average log reduction of 3.61 CFU/mL, and glutaraldehyde treatment yielded an average log reduction in viable cells of 3.83 CFU/mL.

For the chlorine treatments and the nisin treatment, there were no viable cells detectable after the 18-22 h incubation period allotted for CFU formation. However, when the agar plates were allowed to incubate further (up to an additional 36 h), some colonies had formed on the plates. Since there were no CFU present after the initial incubation period, it is inferred that there were fewer than 10 CFU/mL present after the 1 h treatments with chlorine and nisin. This can be assumed, since the detection of 1 CFU in the lowest dilution (10^0 dilution) would equate to 10 CFU/mL. The average log reductions for the high and low concentrations of chlorine were 6.12 and 6.26, respectively, and the average log reduction of viable cells after the 1 h nisin treatment was 5.67. Figure 4-13 shows the events/mL data from the flow cytometer compared to the CFU/mL data from the plate counts, expressed as log reductions for each biocide treatment.

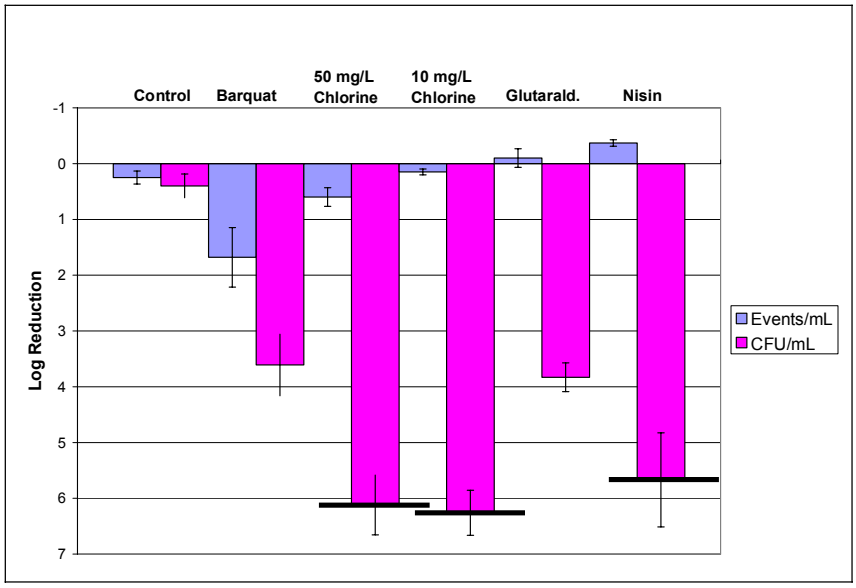


Figure 4-13. Comparison between log reduction in events/mL (flow cytometer) and CFU/mL (plate counts) after 1 h biocide treatment. The heavy black lines represent the detection limit for the chlorine and nisin treatments.

Biofilm

S. epidermidis biofilms grown for 24 h in capillary flow cell reactors were analyzed with time-lapse confocal scanning laser microscopy to evaluate the spatial and temporal effects of the different antimicrobial agents upon the biofilms. The focal plane for these experiments was one which was slightly below the glass ceiling to which the biofilm was attached. Ideally, isolated clusters located within the middle third of the capillary flow cell were analyzed. Oftentimes, there were two clusters which were present in the field of view. Otherwise, biofilm which had accumulated in the outer third of the capillary tubing (i.e., the corners) was analyzed. From this point, these distinct biofilms will be referred to as clusters and corner biofilm.

The first step during these experiments was to "load" the bacterial cells with CAM by statically incubating the biofilm in CAM for 1 h. All of the biofilms stained bright green, as seen in the images from a representative CAM staining phase in Figure 4-14. A total of 25 clusters were analyzed for the CAM staining phase of the biofilm experiments. Average green fluorescence intensity increased from background levels near zero to an average of 50, 64, and 66 at the periphery, medial, and center of the biofilm clusters. A total of 5 corner biofilms were monitored during CAM staining, with average green fluorescence levels increasing from background levels to an average of 11, 20, and 9 at the periphery (biofilm-bulk fluid interface), and depths of 60 and 120 μm, respectively. The average intensity measurements were not normalized during the CAM staining phase of these experiments because normalization was accomplished by dividing

all intensity measurements by the initial intensity measurement, and division by zero is not possible.

The second phase of these experiments was a 1 h PBS buffer wash which rinsed any reacted or unreacted CAM substrate from the bulk fluid and ensured that the presence of green fluorescence was cell-associated. During this phase, most of the biofilm fluorescence increased in all of the regions. The average fluorescence intensity was normalized for each region by dividing the values by the fluorescence intensity at the initial time point for the PBS wash phase. This allowed for a comparison between the relative increases in fluorescence intensity for each region. The relative increases in average fluorescence intensity were 271%, 162%, and 173% for the periphery, medial, and center regions of the 25 biofilm clusters which were analyzed during the 1 h PBS wash phase. The relative increases in average fluorescence intensity for the 5 corner biofilms were 667%, 340%, and 201% for regions at the periphery and at depths of 60 and 120 μm, respectively. A representative PBS wash phase is seen in Figure 4-15.

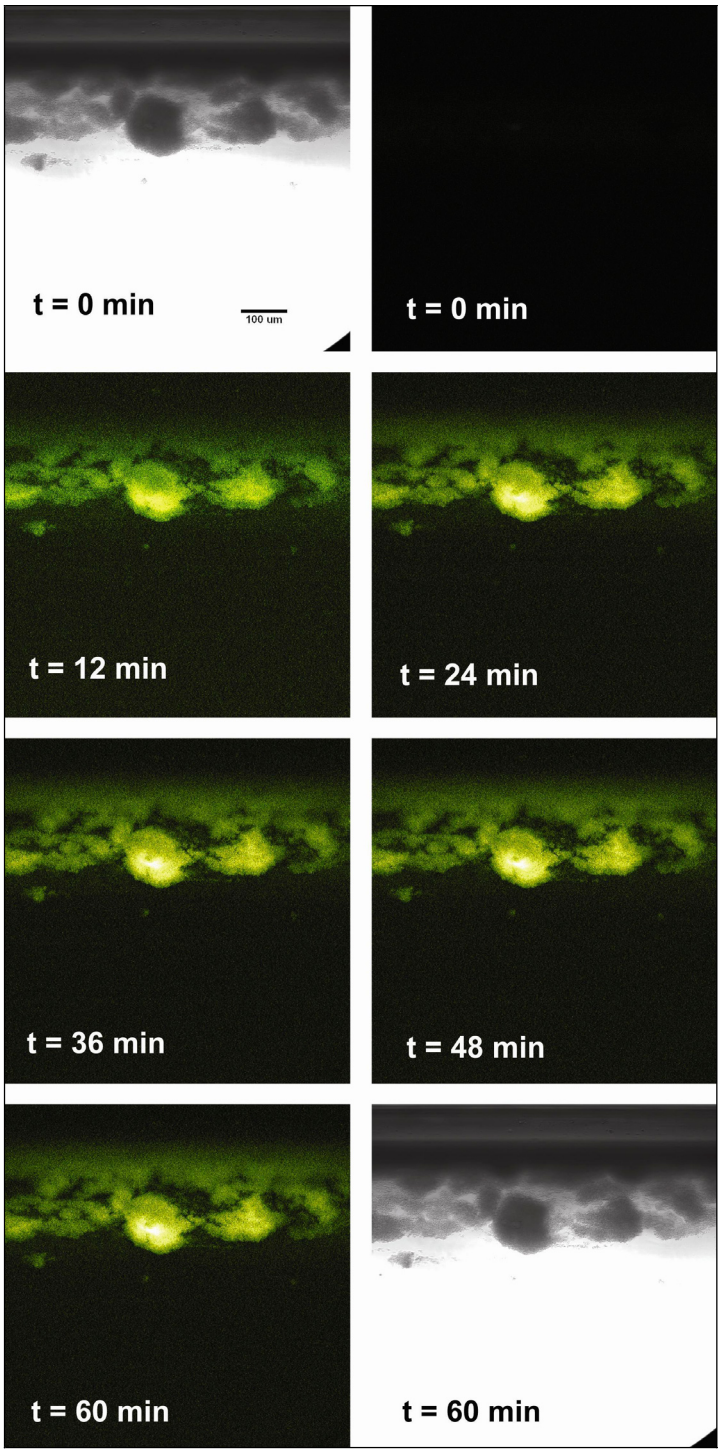


Figure 4-14. CAM staining 1 h time series. The first and last images are transmission-mode images, showing biofilm in grey and bulk fluid in white. All other images are fluorescence images, showing CAM staining.

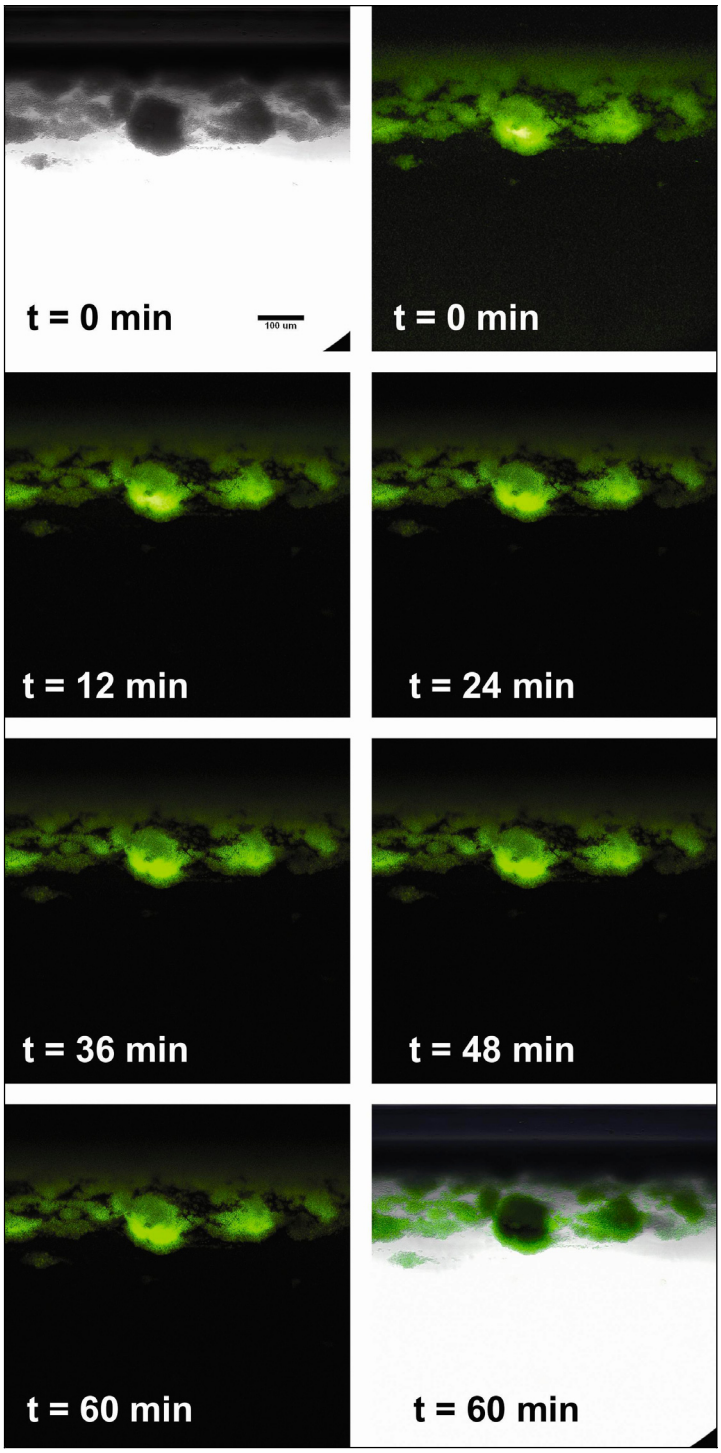


Figure 4-15. Time series images from 1 h PBS wash phase. The first image is in transmission-mode, showing biofilm in grey and bulk fluid in white. Fluorescence images show the retention of CAM in the biofilm. The last picture is a combined image showing the biomass in grey and fluorescence in green.

As a control for the antimicrobial treatments, PBS buffer was pumped through the capillary tubing in which the biofilm was grown for an additional 1 h after the PBS wash phase of the experiments. For PBS control experiments, 5 isolated clusters and 1 corner biofilm were analyzed and the normalized average fluorescence intensities were compared. The average diameter of the biofilm clusters in the PBS control experiments ranged from 166 to 326 μm, with the average diameter of the 5 clusters being 244 μm. For the biofilm clusters, the regions at the periphery retained almost 99% of their initial fluorescence during the 1 h PBS control, while regions at the medial and center of the clusters retained 95% and 94%, respectively. The periphery of the corner biofilm retained 95% of its initial fluorescence during the 1 h PBS control, while only 84% and 83% of the initial fluorescence intensity was retained at depths of 60 and 120 μm. Figure 4-16 shows a representative biofilm cluster during the PBS control treatment, and the image analysis is shown in Figure 4-17.

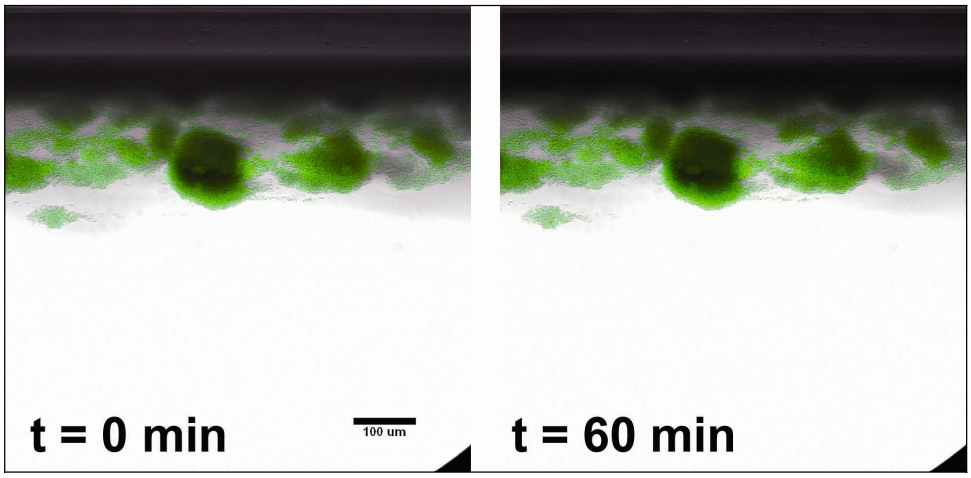


Figure 4-16. Biofilm cluster before and after 1 h PBS control treatment. Transmission-mode images show biofilm in black and bulk fluid in white, and fluorescence images were overlayed which showed the presence of CAM staining.

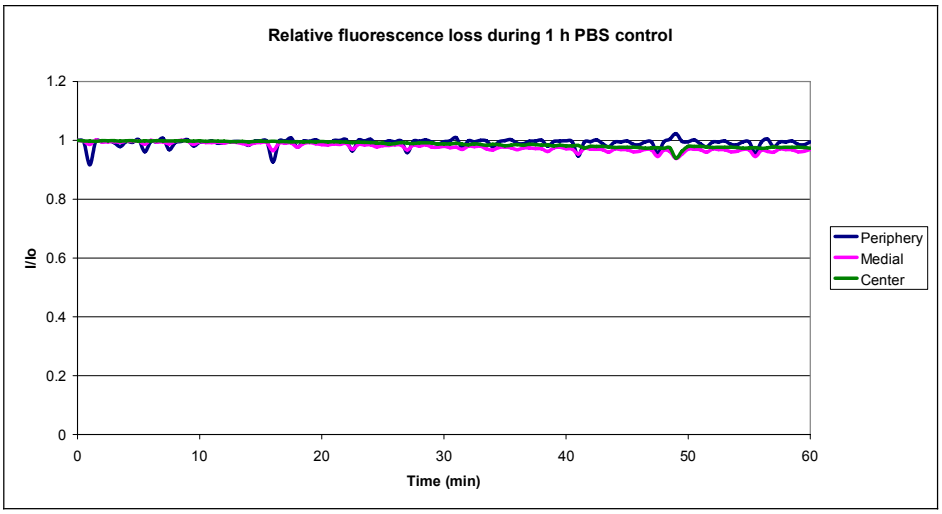


Figure 4-17. Relative fluorescence loss during 1 h PBS control treatment.

Biofilms were treated with Barquat for 1 h and the loss of fluorescence was tracked spatially and temporally. For Barquat treatments, 4 biofilm clusters and 1 corner biofilm were analyzed. The average biofilm cluster diameter ranged from 207 to 305 μm, with an overall average cluster diameter of 258 μm. The periphery of the clusters lost an average of 99% of their initial fluorescence over the course of the 1 h Barquat treatment, while the medial regions and center of the clusters lost an average of 97% and 89% of their initial fluorescence, respectively. The average t_{50} value for the biofilm clusters treated with Barquat was 24.6 minutes. A representative graph of relative fluorescence loss in the three regions within the clusters was chosen as the experiment which had a t_{50} value closest to the overall average t_{50} value for Barquat treatment, as seen in Figure 4-18. Images are seen in Figure 4-19. The corner biofilm lost 98% of its initial fluorescence at the biofilm-bulk fluid interface and lost 99% and 100% of its initial fluorescence at depths of 60 and 120 μm, respectively. The t_{50} value at a depth of 120 μm in the corner biofilm was 21.1 minutes.

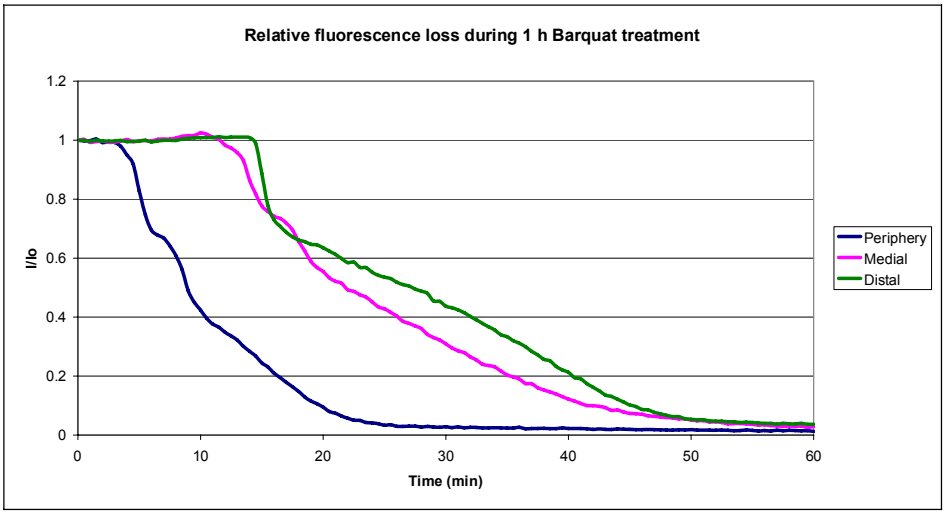


Figure 4-18. Relative fluorescence loss in biofilm clusters during 1 h Barquat treatment for a typical experiment.

During the 1 h Barquat treatment, there were three distinct phases of fluorescence loss within biofilm. This pattern was apparent for both biofilm clusters and corner biofilm alike. Initially after the introduction of Barquat, there was a delay or lag period in which the biofilm retained its original fluorescence. After the lag period, a rapid loss of fluorescence occurred at the peripheral regions of the biofilm. The more inaccessible regions of the biofilm which were located further from the biofilm-bulk fluid interface showed a longer lag period, also followed by a rapid loss of fluorescence. The difference between the periphery and the interior regions of the biofilm arose when these interior regions, both medial and center regions, retained some of their fluorescent cells for a longer period of time than the cells at the periphery of the biofilm. The loss of fluorescence occurred at a slower rate within the biofilm interior than the loss at the biofilm edges.

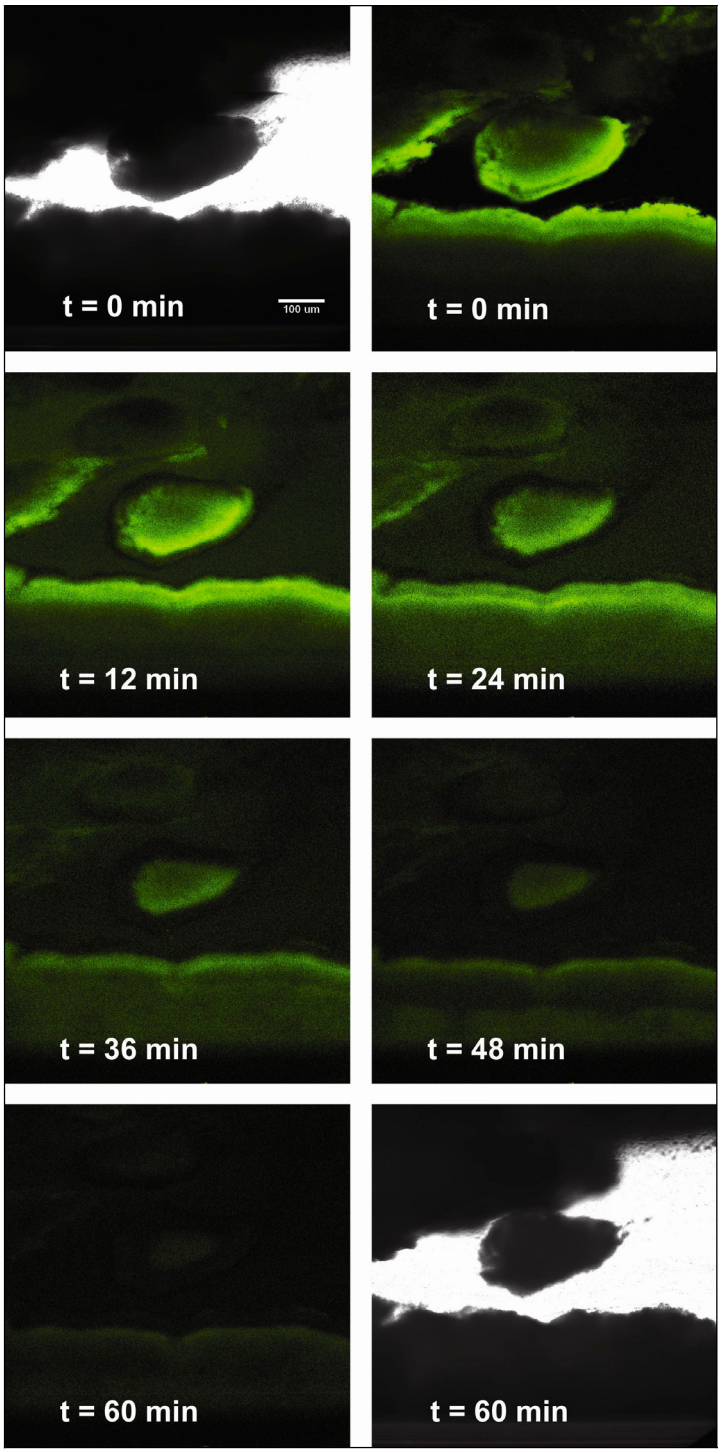


Figure 4-19. Fluorescence loss and biofilm erosion during 1 h Barquat treatment. The final image is the transmission-mode image overlayed with the green fluorescence image in order to show both biomass and the presence of CAM staining after treatment.

Biofilms treated for 1 h with 50 mg/L chlorine exhibited a different response to treatment. There were a total of 6 biofilm clusters analyzed during treatment with 50 mg/L chlorine, with no corner biofilms studied. The biofilm clusters treated with the high concentration of chlorine had average diameters that ranged from 132 to 633 μm, with an average diameter of 398 μm. The periphery and center of the biofilm clusters lost 100% of their initial fluorescence, on average, during the 1 h treatment with 50 mg/L chlorine, while the medial regions of the clusters lost an average of 99% of their fluorescence. The average t_{50} value for the 6 clusters treated with the high concentration of chlorine was 21.4 minutes. The obvious pattern of antimicrobial action exhibited by the high concentration of chlorine involved a balance between reaction and diffusion. The periphery of the clusters lost fluorescence rapidly, but this fluorescence loss occurred in a zone approximately 10 microns wide. This band of fluorescence loss was symmetrical around the cluster exterior. Simultaneously, biomass was eroded, liquefied, and washed downstream. This erosion of biomass allowed for chlorine to penetrate further into the biofilm's interior regions and cause the cells to lose fluorescence. Most of the clusters were completely eroded after the 1 h treatment with 50 mg/L chlorine. A representative graph was chosen as one from the experiment which had a t_{50} value closest to the average t_{50} value, as seen in Figure 4-20. Images from a 50 mg/L treatment of biofilm can be seen in Figure 4-21.

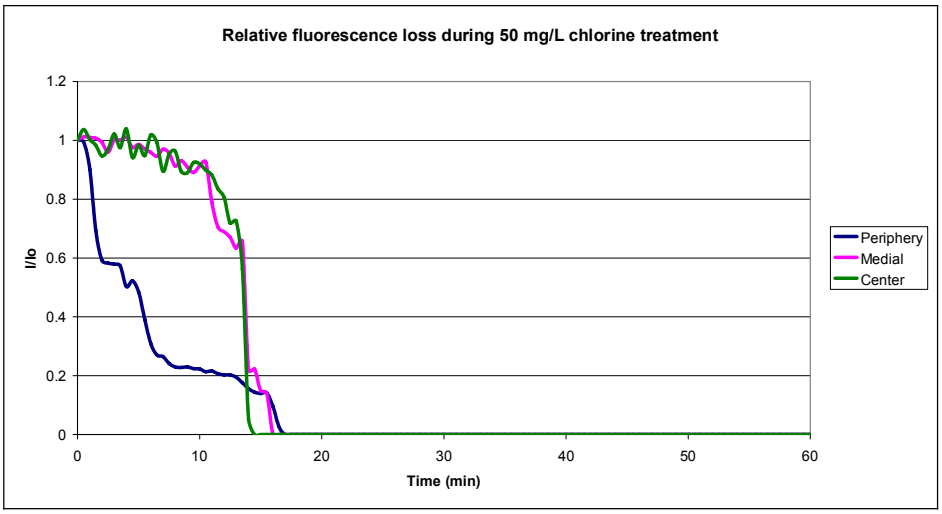


Figure 4-20. Relative fluorescence loss during 1 h treatment with 50 mg/L chlorine.

Biofilms treated with 10 mg/L chlorine showed similar responses as those treated with the higher concentration of chlorine, although biomass erosion was not as pronounced. There were 3 biofilm clusters and 1 corner biofilm treated with 10 mg/L chlorine. The clusters had average diameters that ranged from 191 to 357 μm, with an average of 299 μm. Cells at the periphery of the clusters treated with 10 mg/L chlorine lost an average of 91% of their initial fluorescence during the 1 h treatment, while bacteria in the medial and center of the clusters lost an average of 72% and 75% of their initial fluorescence. The corner biofilm also showed cells at the periphery losing 95% of their initial fluorescence, while cells located at depths of 60 and 120 μm lost 34% and 21% of their initial fluorescence. The average t_{50} value for biofilm clusters treated with 10 mg/L chlorine was 27 minutes, when 50% of the initial fluorescence was reduced. For one of the clusters, there was not a 50% reduction in initial fluorescence intensity, so t_{50} was not established. This was the case for the corner biofilm treated with the low concentration of chlorine as well.

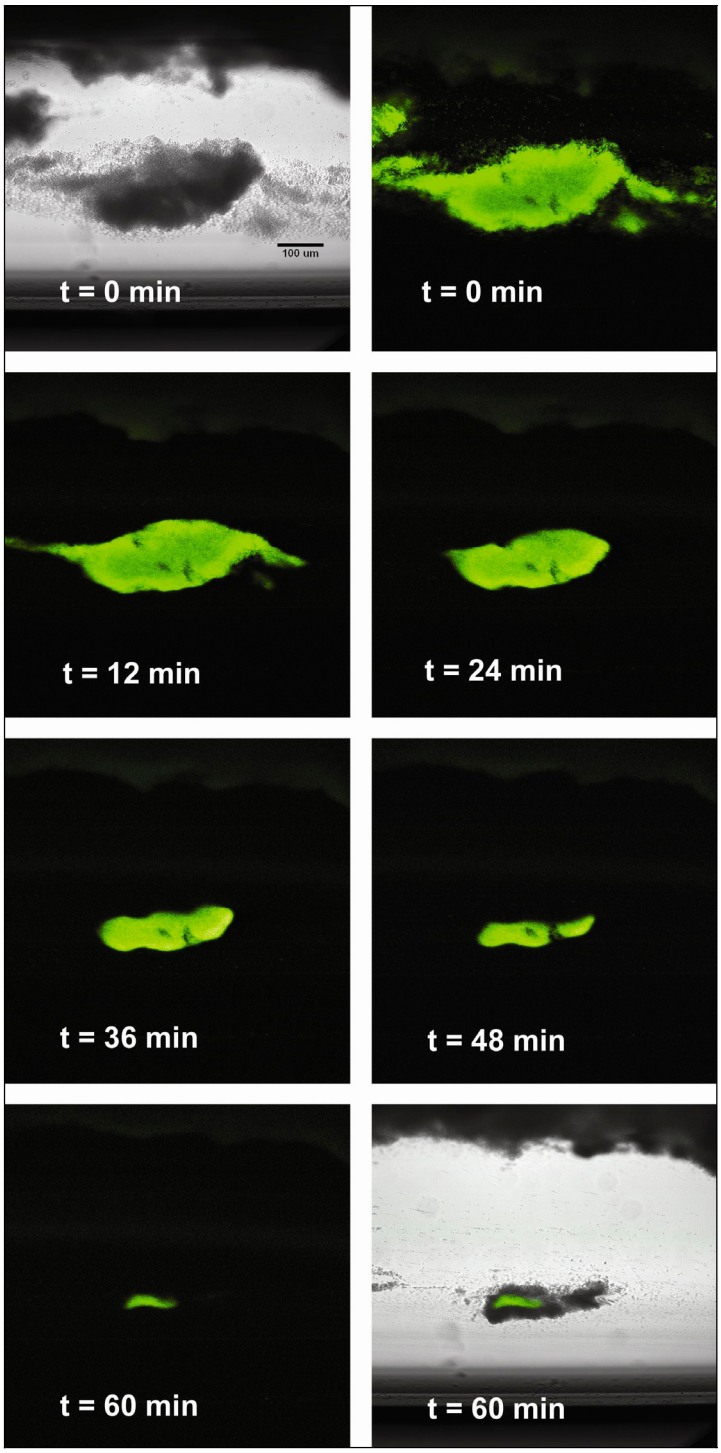


Figure 4-21. Fluorescence loss and biofilm erosion during 1 h treatment with 50 mg/L chlorine. The final image is the transmission-mode image overlayed with the fluorescence image to show both biomass and CAM fluorescence.

The reaction-diffusion interaction was present for the low concentration of chlorine as it acted upon the biofilm. As seen at higher concentrations, chlorine caused the biofilm cells located within a 10 micron band at the exterior of the clusters to lose their fluorescence very rapidly. As cells lost their fluorescence at the periphery of the clusters, biomass was simultaneously eroded which allowed further chlorine penetration. Figure 4-22 shows a representative plot of the relative fluorescence loss during 1 h treatment with 10 mg/L chlorine. Images collected during the treatment can be seen in Figure 4-23.

There were 5 isolated clusters and no corner biofilms analyzed during experiments in which the biofilm was treated for 1 h with glutaraldehyde. The average cluster diameter ranged from 70 to 257 μm, with an overall average cluster diameter of 166 μm. Throughout the 1 h glutaraldehyde treatment, the biofilm cells did not lose as much fluorescence as with previously described treatments. The periphery of the cells lost an average of 21% of its initial fluorescence, while the medial and center of the clusters lost an average of 11% and 16% of their initial fluorescence, respectively. There were no clusters which lost 50% of their initial fluorescence intensity during the 1 h glutaraldehyde treatment, so no t_{50} values were obtained for this antimicrobial agent against biofilms. A representative plot of the relative fluorescence loss at the different regions within the biofilm clusters was chosen as that which had fluorescence losses similar to the overall average loss of fluorescence for glutaraldehyde treatment. This plot can be seen in Figure 4-24, and confocal images can be seen in Figure 4-25.

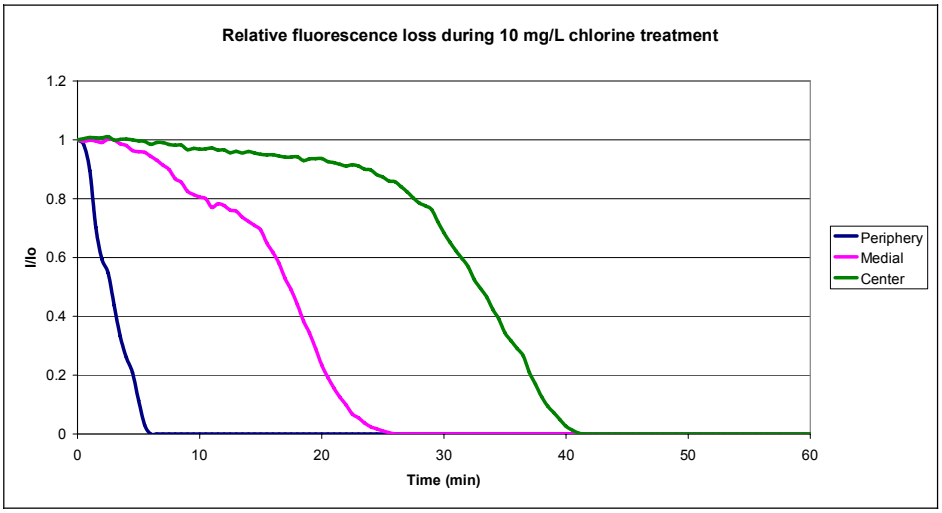


Figure 4-22. Relative fluorescence loss during 1 h treatment with 10 mg/L chlorine.

There were 2 isolated clusters and 2 corner biofilms analyzed during a 1 h treatment with the antimicrobial peptide, nisin. The average cluster diameter ranged from 178 to 260 μm, with an average cluster diameter of 219 μm. The periphery and center of the clusters lost an average of 100% of their initial fluorescence, while the medial regions lost an average of 99% of their initial fluorescence during the 1 h nisin treatment. All regions which were analyzed for the corner biofilms exposed to a 1 h treatment of nisin showed an average loss of 100% of their initial fluorescence. These regions were located at the edge of the biofilm and at depths of 60 and 120 μm. The average t_{50} value for the biofilm clusters treated with nisin was 4.4 minutes, and the average t_{50} value for the corner biofilms was 11.5 minutes. The loss of fluorescence was uniform throughout the isolated clusters during the nisin treatment. Conversely, the corner biofilms showed a penetration delay prior to a decrease in fluorescence, notably for regions that were deeper within the biofilm.

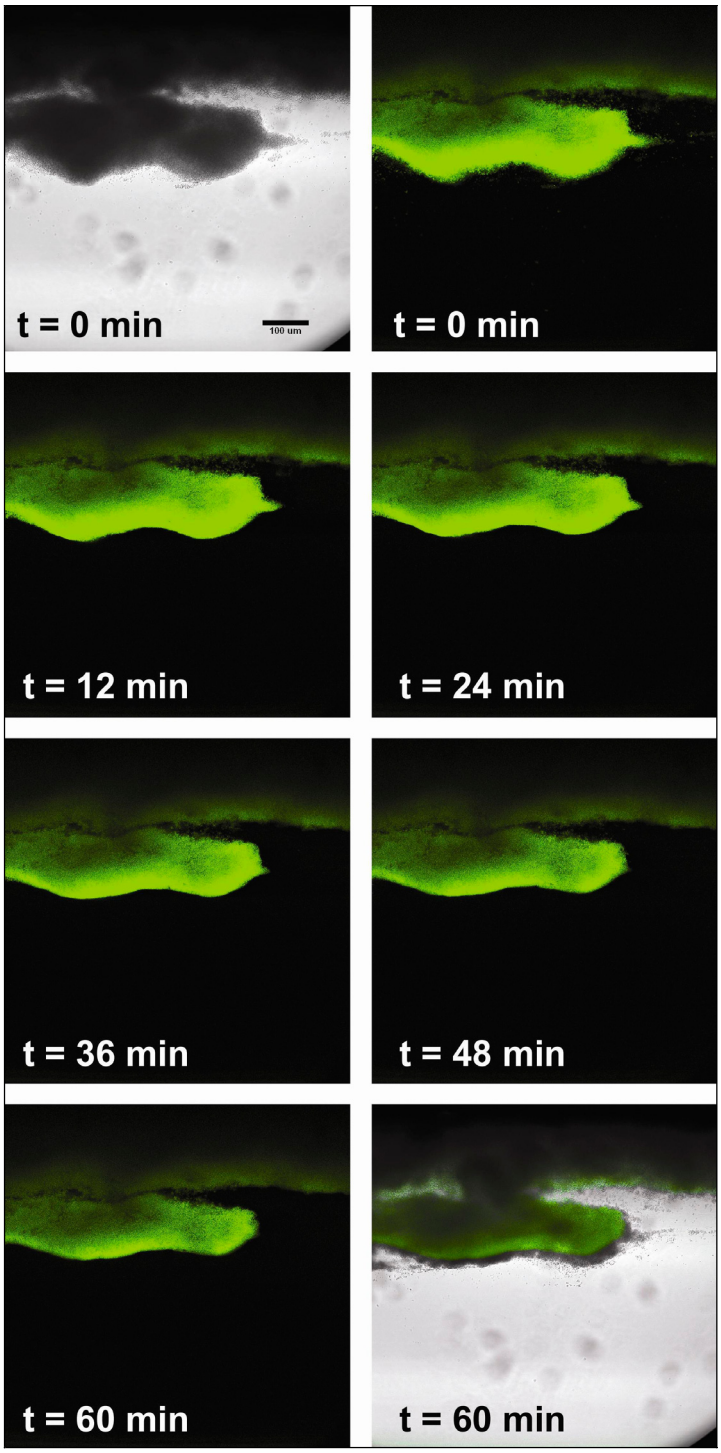


Figure 4-23. Fluorescence loss and biomass erosion during 1 h treatment with 10 mg/L chlorine. The last panel shows both transmission-mode and fluorescence images, overlayed, in order to show both biomass and CAM fluorescence.

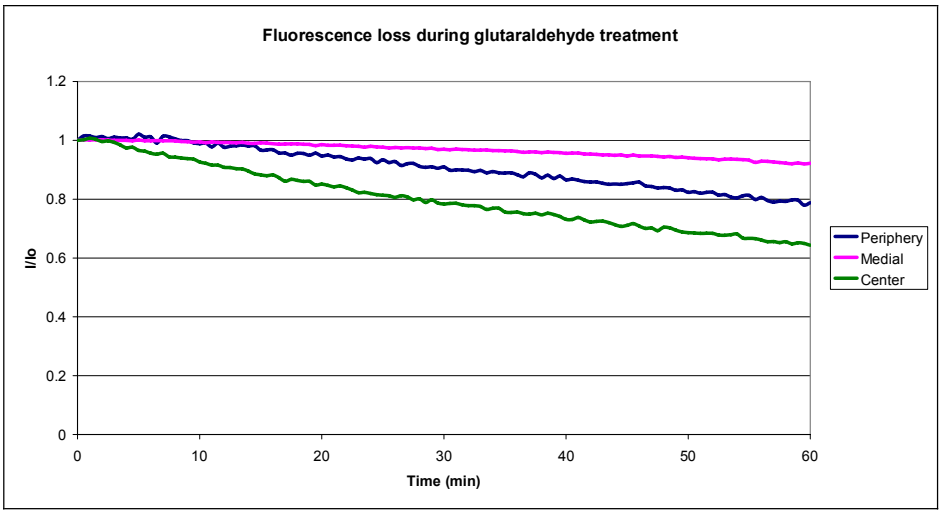


Figure 4-24. Relative fluorescence loss during 1 h glutaraldehyde treatment.

Representative graphs of the relative fluorescence loss during the 1 h nisin treatment of biofilm clusters and corner biofilms are shown in Figure 4-26 and Figure 4-27, respectively. Images of a cluster treated with nisin are seen in Figure 4-28.

During the antimicrobial treatment of capillary biofilms, structural or morphological changes were observed. Some biofilms underwent apparent liquefaction during the treatment, while others were noticeably compressed or shrunken afterward. This shrinkage or erosion was measured for clusters and corner biofilm during treatment. The area covered by biofilm clusters was measured before and after 1 h of antimicrobial treatment. A percentage of biomass loss was calculated for the clusters which were analyzed. For corner biofilms, the biofilm-bulk fluid interface was traced before and after the 1 h of antimicrobial treatment, and the average distance which the biofilm was eroded or retracted was measured. These results are summarized in Table 4-13 and Table 4-15.

After treatment with the different antimicrobial agents, cellular viability could not be discerned directly. Therefore, the redox dye, CTC, was used as a post-treatment viability probe to detect any cellular respiration remaining within the biofilm. For the PBS control, CTC staining yielded bright, red fluorescence throughout the observed cluster. As seen in Figure 4-29, the cluster appeared bright red after the 2 h CTC staining, suggesting the presence of actively respiring cells within the biofilm after the PBS control treatment. The average CTC staining in biofilm clusters after each of the other treatments was normalized by dividing the average fluorescence intensity by the average intensity from the PBS control. This gave a relative comparison of the CTC fluorescence, assuming that the PBS control biofilm was capable of the most respiration. A chart of the relative CTC staining can be seen in Figure 4-30.

The only treated biofilm that exhibited any CTC reduction due to respiring cells was the biofilm treated with glutaraldehyde for 1 h. The average CTC fluorescence in the glutaraldehyde-treated cluster was only 38.6% as bright as the average CTC fluorescence present after the PBS control. There was no CTC reduction after the other treatments.

The summarized results for the average fluorescence loss at different regions within biofilm clusters and corner biofilms can be seen in Table 4-12 and Table 4-14, respectively. The values listed in these tables are of the form mean ± 1 standard deviation.

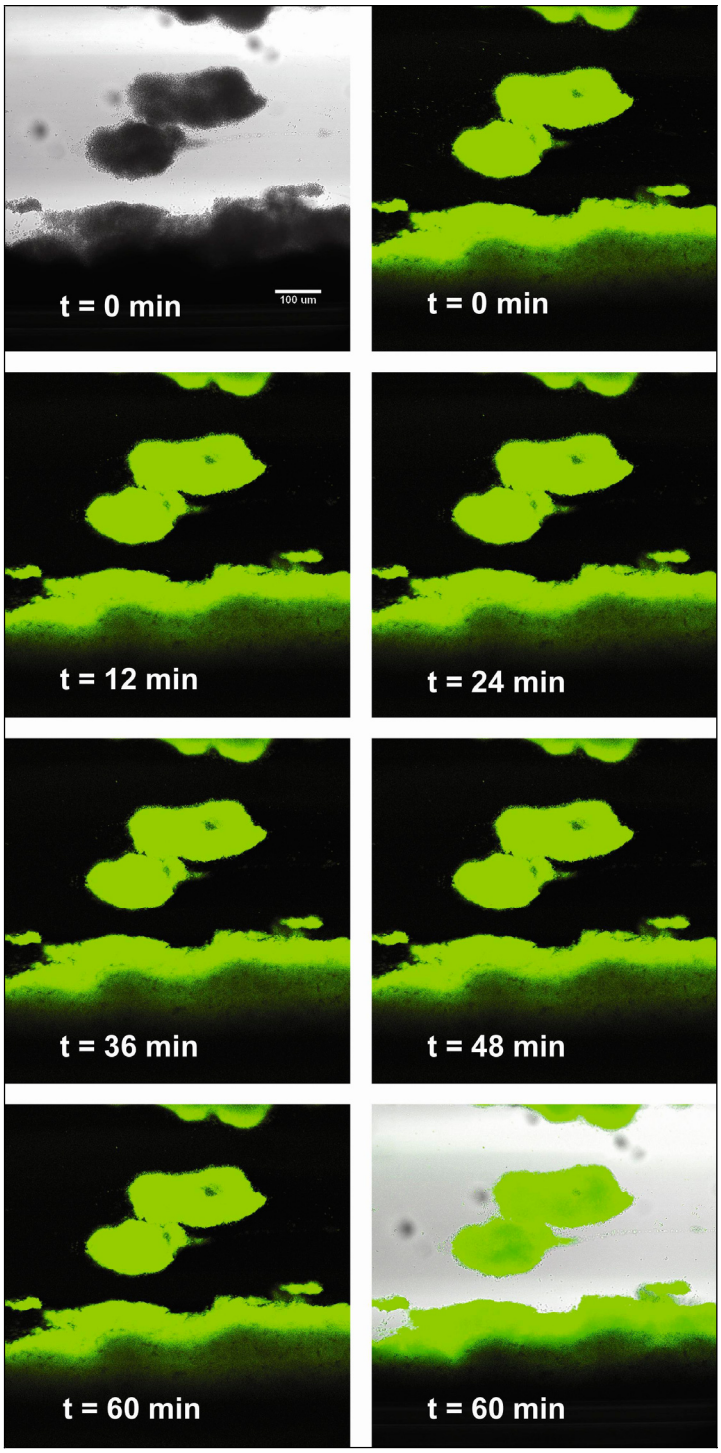


Figure 4-25. Fluorescence loss and biomass erosion during 1 h glutaraldehyde treatment. The final image shows both transmission-mode and fluorescence images, overlayed, in order to display both biomass and CAM fluorescence.

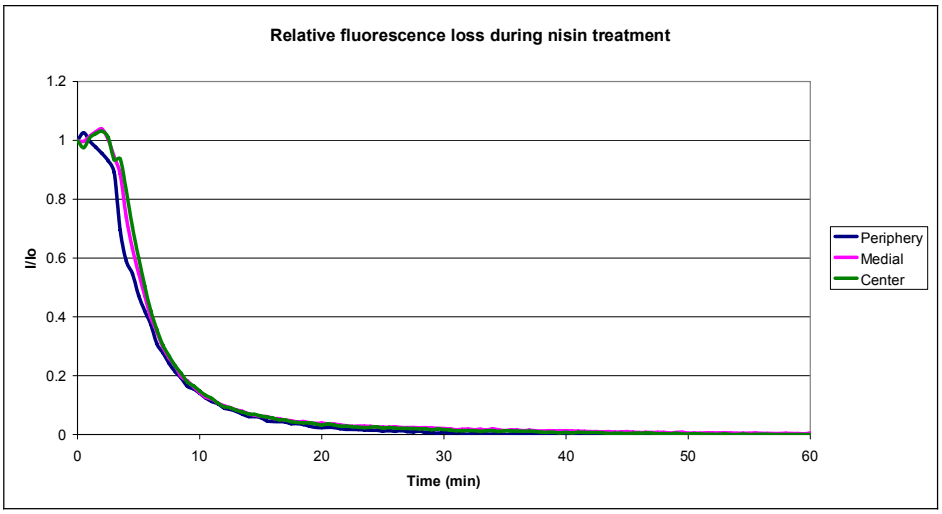


Figure 4-26. Relative fluorescence loss in isolated clusters during 1 h nisin treatment.

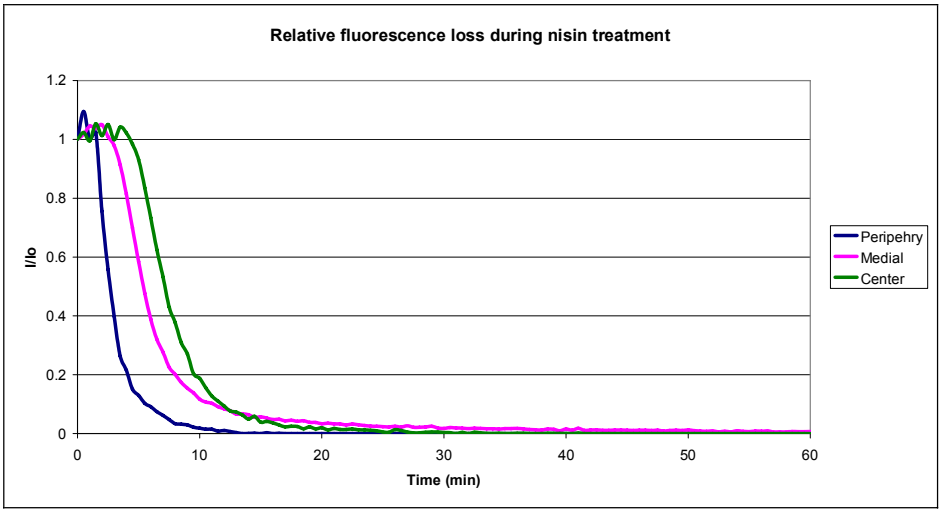


Figure 4-27. Relative fluorescence loss in corner biofilm during 1 h nisin treatment.

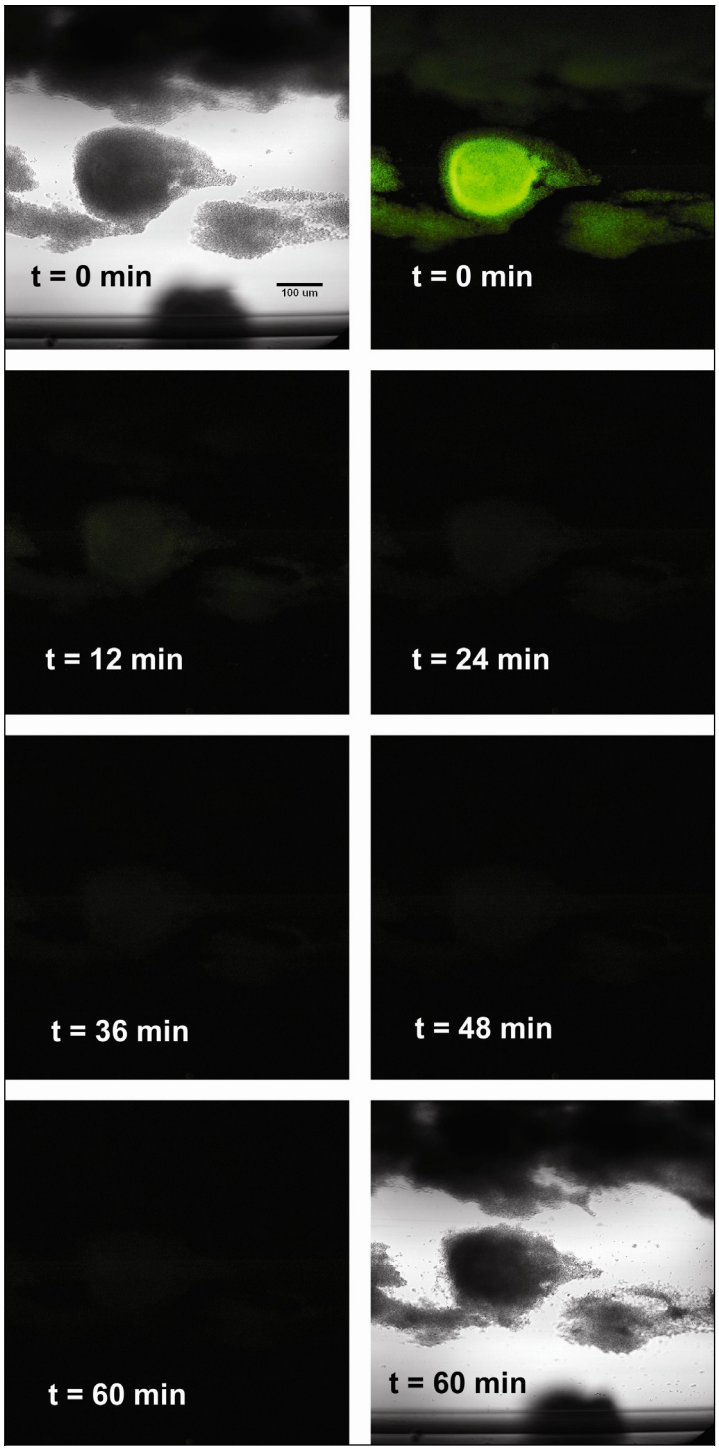


Figure 4-28. Fluorescence loss and biomass erosion during 1 h nisin treatment. The final image shows both transmission-mode and fluorescence images, overlayed, in order to display both biomass and CAM fluorescence.

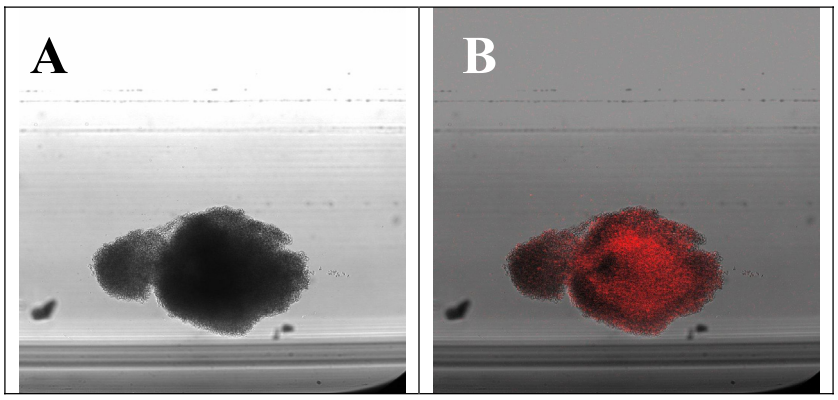


Figure 4-29. PBS control biofilm before (A) and after (B) CTC staining.

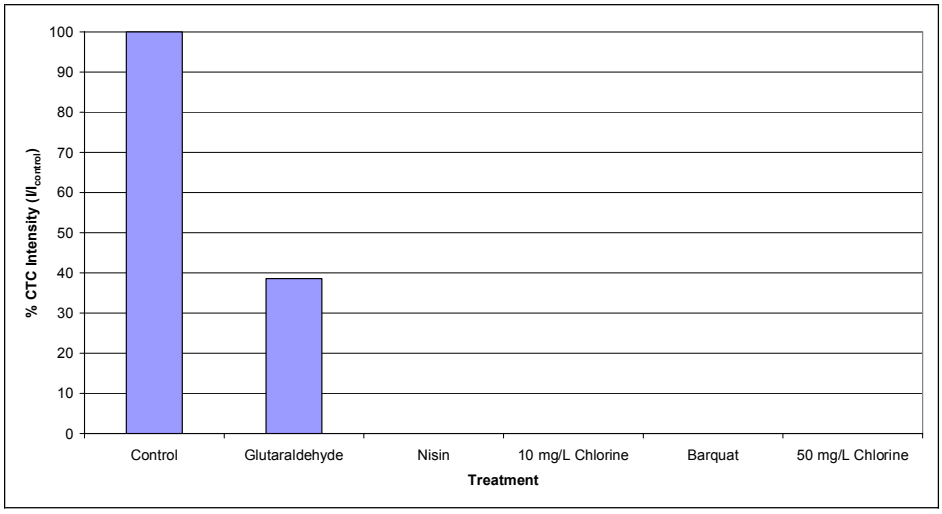


Figure 4-30. Average CTC staining expressed as percentage CTC intensity, relative to PBS control.

Table 4-12. Average CAM fluorescence loss at different regions in biofilm clusters after 1 h treatment.

Antimicrobial	No. of clusters	% fluorescence loss		
		Periphery	Medial	Center
PBS Control	5	1.31 ± 5.52	4.64 ± 3.11	6.54 ± 5.15
Barquat	4	98.8 ± 0.20	97.0 ± 1.37	89.5 ± 15.1
10 mg/L Chlorine	3	91.0 ± 12.4	71.9 ± 47.3	75.2 ± 42.1
50 mg/L Chlorine	6	100 ± 0.00	99.4 ± 1.50	100 ± 0.00
Glutaraldehyde	5	21.5 ± 14.5	11.4 ± 10.3	16.3 ± 17.2
Nisin	2	99.8 ± 0.35	99.4 ± 0.12	99.7 ± 0.41

Table 4-13. Values for t_{50}, changes in area coverage, and percent CTC staining after 1 h treatment of biofilm clusters.

Antimicrobial	No. of clusters	t_{50} (min)	Δ % area	% CTC stain
PBS Control	5	------	+0.33 ± 0.50	100
Barquat	4	24.6 ± 14.7	-9.18 ± 9.61	0.00
10 mg/L Chlorine	3	27.0 ± 8.06	-42.6 ± 34.8	0.00
50 mg/L Chlorine	6	21.3 ± 16.2	-90.4 ± 14.2	0.00
Glutaraldehyde	5	------	+0.90 ± 1.95	38.6
Nisin	2	4.42 ± 1.31	-8.08 ± 9.20	0.00

Table 4-14. Average CAM fluorescence loss at different regions in corner biofilms after 1 h treatment.

Antimicrobial	No. of corner biofilms	% fluorescence loss		
		Periphery	60 μm depth	120 μm depth
PBS Control	1	5.29	16.0	16.9
Barquat	1	97.8	99.0	100
10 mg/L Chlorine	1	95.1	33.4	21.0
50 mg/L Chlorine	0	------	------	------
Glutaraldehyde	0	------	------	------
Nisin	2	100 ± 0.00	99.7 ± 0.48	100 ± 0.00

Table 4-15. Values for t_{50} (at a depth of 120 μm) and distance the edge of the corner biofilm retracted during treatment. Negative numbers in the Δ edge column are indicative of biofilm shrinkage or retraction toward the wall.

Antimicrobial	No. of corner biofilms	t_{50} (min)	Δ edge (μm)
PBS Control	1	------	0.00
Barquat	1	20.1	-14.0 ± 2.47
10 mg/L Chlorine	1	------	-22.6 ± 15.5
50 mg/L Chlorine	0	------	------
Glutaraldehyde	0	------	------
Nisin	2	11.5 ± 3.14	-28.3 ± 14.7

Mathematical Modeling of Antimicrobial Diffusion

The non-reactive diffusion rate of each biocide into a hemisphere of biomass attached to a surface was calculated at different regions within the model cluster. This mathematical modeling of the antimicrobial diffusion was based upon the experimental

data for those treatments. For example, the average cluster radius for the clusters analyzed during the experimental 1 h Barquat treatment was also the cluster radius which was used as an input into the model for that particular biocide treatment. The value of α_{50} was calculated at r/R values of 0.9, 0.5, and 0.1 which corresponded to the periphery, medial, and center regions of the model clusters.

The model biofilm calculations were able to predict the α_{50} values (time it takes for 50% of the bulk fluid biocide concentration to reach different regions of the biofilm via non-reactive diffusion), and those values were compared to the t_{50} values (time it takes for a 50% decrease in initial fluorescence intensity) observed during the 1 h antimicrobial treatment of a biofilm cluster. The average cluster radius for the experiments in which biofilm clusters were treated with Barquat was 129 μm. Therefore, the radius of the model cluster was input as the same value. The α_{50} values for the non-reactive diffusion of Barquat into the periphery, medial, and center regions of the model biofilm cluster were calculated to be 28.1, 19.4, and 1.9 sec, respectively. A plot depicting the non-reactive diffusion of Barquat into the different regions of the model cluster during the first minute of treatment can be seen in Figure 4-31.

The average radii of the clusters treated with 50 mg/L and 10 mg/L chlorine were 199 μm and 150 μm, respectively. The α_{50} values for the non-reactive diffusion of the high concentration of chlorine into the periphery, medial, and center regions of the model cluster were 3.9, 2.7, and 0.6 sec, respectively. The values of α_{50} for the diffusion of the low concentration of chlorine into the same regions were 2.9, 2.0, 0.6 sec, respectively.

Diffusion graphs for the high concentration (Figure 4-32) and low concentration (Figure 4-33) are shown below.

The α_{50} values for the diffusion of glutaraldehyde into a model cluster with a radius of 83.1 μm were 5.4, 3.7, and 0.7 sec at the periphery, medial, and center regions, respectively. This radius was the average cluster radius for those biofilms analyzed experimentally, and the diffusion curves can be seen in Figure 4-34.

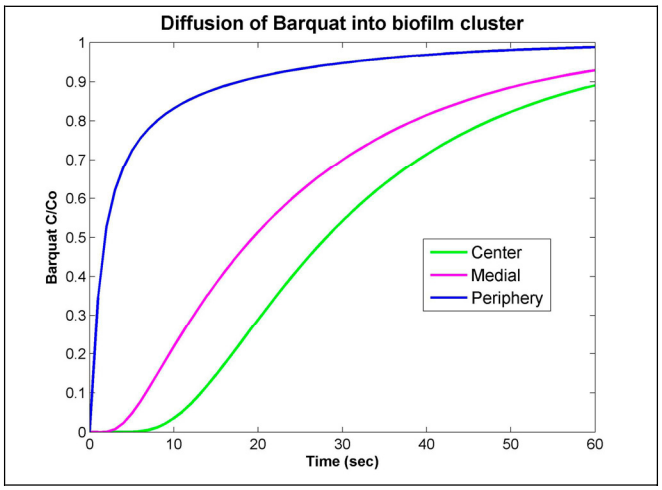


Figure 4-31. Non-reactive diffusion of Barquat into different regions of a model biofilm cluster.

The α_{50} values for nisin diffusion into a biofilm cluster with a radius of 109 μm were calculated to be 45.7, 31.6, and 2.9 sec at the periphery, medial, and center regions. This transient, non-reactive diffusion of nisin into the model cluster can be seen in Figure 4-35.

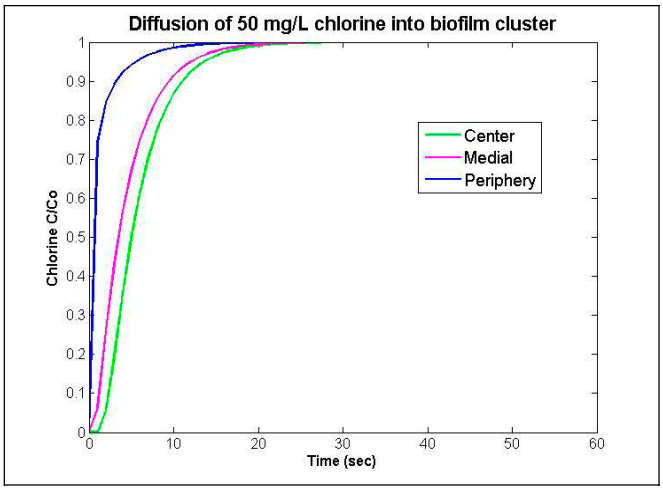


Figure 4-32. Non-reactive diffusion of 50 mg/L chlorine into different regions of a model biofilm cluster.

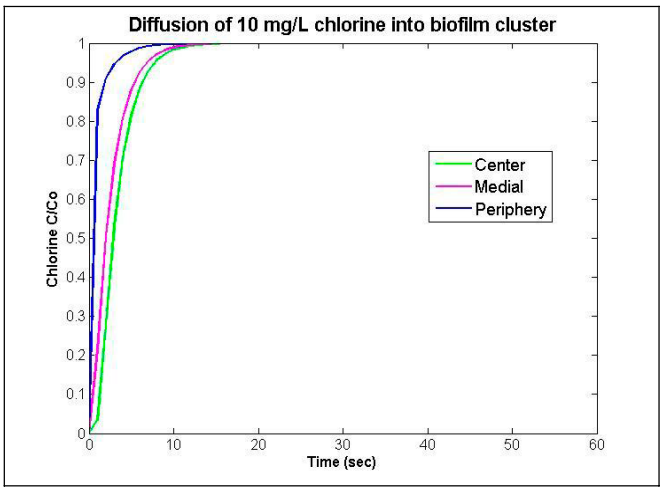


Figure 4-33. Non-reactive diffusion of 10 mg/L chlorine into different regions of a model biofilm cluster.

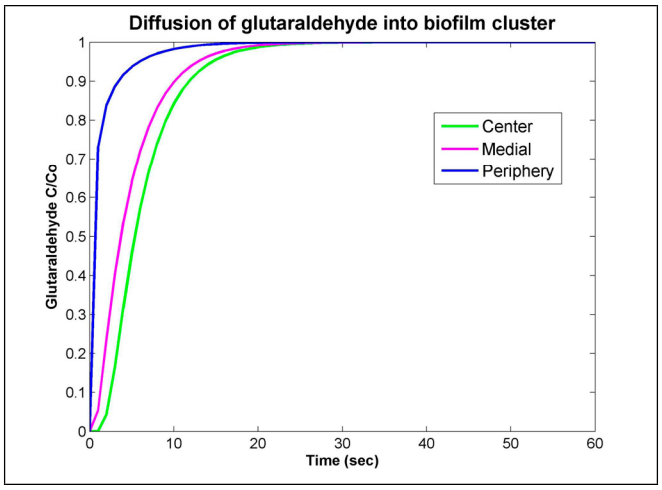


Figure 4-34. Non-reactive diffusion of glutaraldehyde into model cluster.

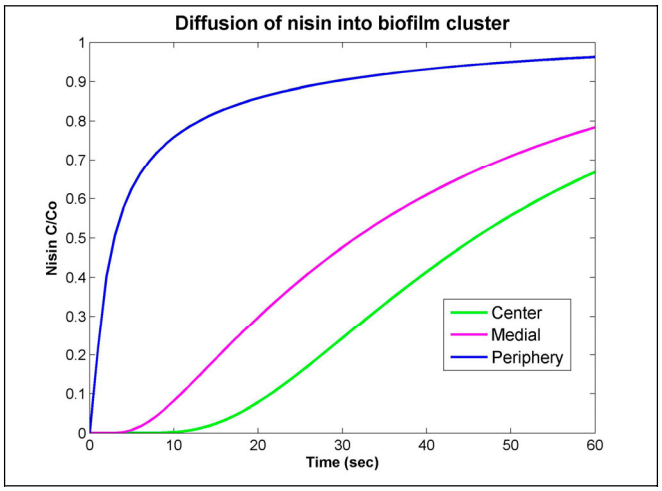


Figure 4-35. Non-reactive diffusion of nisin into model cluster.

A comparison between the t_{50} values which were observed experimentally and the α_{50} values that were calculated mathematically can be seen below in Table 4-16 through Table 4-18.

Table 4-16. Comparison between t_{50} (measured fluorescence loss time) and α_{50} (predicted biocide diffusion time) values at the periphery of biofilm clusters. D_e is the effective diffusion coefficient in biofilm at 23°C.

Antimicrobial	[cm^2 sec^{-1}] D_e x 10^6, 23°C	[μm] Avg. Radius	[min] t_{50}	[min] α_{50}
Barquat	0.81	129	7.17	0.031
50 mg/L chlorine	10.8	199	6.95	0.011
10 mg/L chlorine	10.8	150	4.50	0.010
Glutaraldehyde	1.76	83	------	0.011
Nisin	0.36	109	3.83	0.049

Table 4-17. Comparison between t_{50} (measured fluorescence loss time) and α_{50} (predicted biocide diffusion time) values at the medial region of biofilm clusters. D_e is the effective diffusion coefficient in biofilm at 23°C.

Antimicrobial	[cm^2 sec^{-1}] D_e x 10^6, 23°C	[μm] Avg. Radius	[min] t_{50}	[min] α_{50}
Barquat	0.81	129	19.0	0.324
50 mg/L chlorine	10.8	199	14.0	0.045
10 mg/L chlorine	10.8	150	21.0	0.033
Glutaraldehyde	1.76	83	------	0.062
Nisin	0.36	109	4.33	0.527

Table 4-18. Comparison between t_{50} (measured fluorescence loss time) and α_{50} (predicted biocide diffusion time) values at the center of biofilm clusters. D_e is the effective diffusion coefficient in biofilm at 23°C.

Antimicrobial	[cm^2 sec^{-1}] D_e x 10^6, 23°C	[μm] Avg. Radius	[min] t_{50}	[min] α_{50}
Barquat	0.81	129	28.0	0.469
50 mg/L chlorine	10.8	199	13.7	0.064
10 mg/L chlorine	10.8	150	31.5	0.048
Glutaraldehyde	1.76	83	------	0.090
Nisin	0.36	109	4.42	0.761

CHAPTER 5

DISCUSSION

The results of this research project provide evidence that the antimicrobial agents which were tested against planktonic and biofilm bacteria have different modes of action. The planktonic bacteria appear to have a very diverse distribution of physiological states, giving rise to a wide array of characteristics. For instance, the uptake and retention of the CAM fluorophore yielded a very wide distribution of fluorescence intensities, as measured by the flow cytometer with FITC as the standard green fluorescent dye. Similarly, only a portion of the cells which were initially stained showed a loss of fluorescence during antimicrobial treatment. It has been shown that planktonic bacteria can display a wide array of phenotypic variation when exposed to environmental stresses, which could account for the apparent minimal cell membrane permeabilization during antimicrobial treatment (1) (109) (196). During the 1 h CAM staining phase, the average FITC intensity increased 100-fold and had a wide distribution of intensities, ending with a mean ± SD of 5666 ± 2090 at t = 60 min of staining. This successful loading period implied that the intact CAM passively diffused across the bacterial cell membranes, and was subsequently cleaved by intracellular esterase which caused the calcein to fluoresce and be retained within the cells (52) (66) (190). The average staining intensity then increased during the 1 h PBS wash phase, but again had a wide distribution of staining intensities at 12128 ± 4812 on the FITC scale. This wide distribution of cell staining

suggests that there may be a very diverse set of cell states within each suspended population of cells.

The increase in CAM staining intensity during the 1 h PBS wash phase was a consistent pattern for both planktonic and biofilm bacteria. This wash phase was intended to accomplish two things: 1) rinse any excess reacted or unreacted CAM from the bulk fluid surrounding the cells and 2) ensure that any detectable fluorescence was cell-associated. Since the concentration of CAM in the bulk fluid was drastically decreased during this wash phase, the driving force for CAM uptake was removed, making the increase in fluorescence puzzling. One hypothesis which explains the increase in apparent CAM staining during the PBS wash is that only a portion (probably the most sterically accessible) of the numerous ester linkages are cleaved during the initial CAM staining period. During the PBS wash phase, the ester bonds which are directly attached to the calcein ring structure are cleaved and a significant increase in fluorescence occurs. Another hypothesis is that the presence of excess CAM substrate has a quenching effect upon the fluorescent calcein in the cells, although this is highly unlikely because the reaction which causes CAM to be converted to fluorescent calcein would have to be a reversible reaction. Calcein has been shown to be self-quenching (i.e., the emitted fluorescence is reabsorbed by the fluorophore, reducing the net detectable fluorescence), but this occurs at concentrations much higher (> 20 mM) than those used for this research project (190).

The FSC vs. SSC scatter plots from the planktonic analyses with the flow cytometer also show diverse populations in terms of cellular aggregation. The J-shaped

scatter plot suggests that there is a distribution of cells which range from singular entities to large, clumped masses of many cells. Although the CAM staining and retention within the cells seemed uniformly distributed throughout the different sized cellular agglomerations, the distribution of cell aggregates could contribute to the planktonic cell population's response to antimicrobial treatment.

The PBS control treatment of planktonic bacteria showed a gradual increase in the population's average FITC staining intensity, from about 14000 to 19000 over the course of the 1 h period. There was a decrease in cell density, as indicated by a 0.25-log reduction in events/mL, but 98.7% of the remaining cells had retained their fluorescence. Biofilm clusters exposed to the PBS control lost an average of 4.16% of their initial CAM fluorescence intensity, while corner biofilms lost an average of 12.7% of their initial fluorescence. Neither biofilm clusters nor corner biofilm showed significant changes in areal coverage during the 1 h PBS control.

When compared to the PBS control, the antimicrobial treatment of planktonic cells resulted in varying degrees of cell permeabilization which were detected by the decrease in fluorescent events on the flow cytometer. Barquat treatment showed a very rapid 10-fold decrease in the cell population's average FITC intensity within the first minute of exposure to the biocide, indicated by the entire histogram shifting left (decreasing) by a factor of ten. This rapid fluorescence loss (during the first minute of treatment) was accompanied by a 0.3-Log reduction in events/mL, and 88% of the remaining cells had fluorescence intensity above the green threshold. Interestingly, after the initial decrease in fluorescence, the average FITC intensity for the cell suspension

subsequently increased 10-fold during the 1 h exposure to Barquat, returning to the average FITC intensity of the cells immediately prior to biocide treatment. There was a 1.68-Log reduction in events/mL during the Barquat treatment, and 90% of the remaining cells had fluorescence intensity which registered above the green threshold value.

The FSC vs. SSC data from the Barquat treatment showed the cells that were more susceptible were either individual cells or cell aggregates consisting of very few cells. This suggests that cellular aggregation offers increased protection from Barquat killing. Studies have shown that biofilm emboli which detached as cell clusters consisting of up to 1000 cells were more tolerant to antibiotic attack than dispersed, individual planktonic cells (54). Although there was a decrease in cell density during the Barquat treatment period, 90% of the remaining cell population retained the fluorescent CAM stain which suggests the possibility of a subpopulation of cells that were more tolerant to Barquat treatment.

Two distinct phenomena were observed with the flow cytometry analysis during Barquat treatment of planktonic cells. There was a 1.68-Log reduction in events/mL during the 1 h treatment, but the FSC vs. SSC data suggests that this decrease in cell density could be due to an increase in cellular aggregation. Also, there was the increasing fluorescence intensity (after the initial rapid fluorescence loss) throughout the course of the treatment period. The increase in the population's average FITC intensity during Barquat treatment could be attributed to the presence of fluorescent CAM in the bulk fluid surrounding the cells which was leaked out of the permeabilized cells. The distinction between a fluorescing particle in a non-fluorescent medium and a non-

fluorescent particle in a fluorescent liquid may be difficult to separate with flow cytometry. Another hypothesis for the increasing fluorescence is that the increased cell aggregation yields increased fluorescence, since a single event consisting of many stained cells in a cluster would register a higher fluorescence intensity than a single stained cell. A third explanation of the increase in fluorescence during the 1 h Barquat treatment is that the brightest stained cells do not lyse. If the most dimly stained cells are also those that are susceptible to membrane permeabilization with Barquat, the average fluorescence intensity would inherently increase during the treatment period.

Using plate count data, the average log reduction in viable cells during Barquat treatment of planktonic cells was 3.61, suggesting that 99.98% of the cells were killed. The fluorescence loss and decrease in events/mL during the Barquat treatment do not imply a correlation to the log reduction in viable bacteria as enumerated with plate counts.

Biofilms were only analyzed by fluorescence loss during biocide treatment. Cell viability is often associated with membrane integrity (14) (80) (96), so some correlation between loss of fluorescence and loss of viability can be assumed for the biofilm experiments. For biofilms treated with Barquat, the overall average loss of fluorescence was about 95% in clusters and 99% in corner biofilm. There was no cellular respiration present in biofilms treated with Barquat, as indicated by CTC staining, which also suggests the lack of cell viability.

For every biofilm treated with Barquat, the periphery regions lost their fluorescence very rapidly and the more interior regions of the biofilm retained a portion

of their initial fluorescence for a longer period of time. The interior regions also lost their fluorescence more slowly after the initial rapid decrease in fluorescence loss. This slower rate of fluorescence loss (indicated by the change in slope of the relative fluorescence loss curves) suggests the possible existence of a subpopulation of cells located in the more inaccessible regions of the biofilm which are more tolerant to Barquat challenge.

Barquat treatment of biofilm did result in some cluster shrinkage during the 1 h exposure to the biocide. The biofilm cluster area coverage decreased by an average of 9% and the edge of the corner biofilm retracted an average of 14 μm. This shrinkage might be attributed to the surfactant affecting the stability of the bacterial cell membranes within the biofilm, causing the cells to collapse and thus the shriveling of the biofilm structure. The mode of action of Barquat against bacterial cells involves a general perturbation of cell membranes which causes the leaking of cytoplasmic constituents to the environment, and at high biocide concentrations the cell membranes are completely solubilized (56) (91) (128) (129) (130).

The planktonic t_{50} value for cells treated with Barquat was 0.55 min, while the average biofilm t_{50} value at the center of the clusters was 28 min. The predicted diffusion time, α_{50}, for Barquat into the center of a biofilm cluster was 0.47 min. The discrepancy between the predicted diffusion time and the measured time for fluorescence loss in biofilm can be attributed to the presence of reaction or sorption phenomena occurring with Barquat treatment (90) (148).

Planktonic cells treated with 50 and 10 mg/L chlorine (high and low concentration, respectively) showed an average increase in FITC intensity of 7% and

44%, respectively, during the 1 h treatment period. The high concentration treatment decreased the average number of events/mL by 0.6-Log and the low concentration decreased the average events/mL by 0.15-Log during the 1 h treatment. About 95% and 92% of the remaining cells treated with the high and low concentrations of chlorine, respectively, retained their green fluorescence.

The chlorine residual tests showed that there was 3.6 mg/L of free chlorine present after 1 h of treatment with the low concentration of chlorine. This concentration can be considered sufficient to react with the organic material present in bacterial cells and render them inactive, since the US EPA suggests a minimum free chlorine residual of only 0.2 mg/L in drinking water distribution systems for the control of microbial proliferation (172). The increases in average FITC intensity during the chlorine treatments suggest that the cell membranes were not compromised. The addition of chlorine to an unstained cell suspension did not increase the fluorescence intensity as detected with flow cytometry, so the increase in average FITC intensity cannot be attributed to the presence of chlorine alone.

The FSC vs. SSC scatter plot data suggested that the majority of the planktonic cells which lost fluorescence during the chlorine treatments were either individual cells or smaller cell aggregates. Plate count data showed that there was an average log reduction of 4.12 and 4.26 for the high and low concentrations of chlorine, respectively. This is effectively a reduction of the viable cells by over 99.99% by both concentrations of chlorine. Again, the flow cytometry analyses which show changes (in this case, increases) in cell-associated fluorescence which can be attributed to the loss of cell

membrane integrity do not directly correlate to the cellular viability as ascertained with traditional plate count methods.

The most noticeable spatio-temporal pattern observed during the chlorine treatment of biofilm was the liquefaction of biomass. The cells which were located in a 10 micron zone at the periphery of the cell clusters were readily permeabilized and lost their CAM fluorescence. Simultaneously, the biomass appeared to become liquefied and washed downstream, and this erosion allowed for the chlorine to penetrate further into the clusters. Although the biomass erosion was more prevalent with higher concentrations of chlorine, there was still liquefaction during treatments at the lower concentration. The clusters treated with the high concentration of chlorine decreased in areal coverage by an average of 90%, while those treated with the lower concentration shrunk an average of 43%. The edge of the corner biofilm treated with the low chlorine concentration was eroded an average of 22.6 μm during treatment.

The chlorine penetration seemed to be limited by its high reactivity with the organic material in the biofilm. The relative fluorescence loss curves support the presence of reaction-diffusion interaction during chlorine treatment, as there is a downward curvature of the loss curves which is consistent with simultaneous reaction and diffusion. Other supporting evidence of limited chlorine penetration is the longer t_{50} times measured at the center of the clusters, with average values of 13.7 and 31.5 minutes for the high and low concentrations, respectively. These experimentally determined t_{50} times are much longer than the predicted values for the non-reactive diffusion of chlorine, α_{50}, which were 3.8 sec and 2.9 sec for the high and low concentrations of chlorine,

respectively, when diffusing into biofilm clusters of equal size to those observed in the laboratory.

The sustained erosion which occurred during chlorine treatment of biofilm could be attributed to a chemical disruption of the biofilm matrix in combination with the mechanical removal of the biofilm imposed by the convective flow of the media. Some work has been done on the addition of chemical agents to promote biofilm detachment, with varying results (29) (188). Since this erosive removal was not a phenomenon observed during the other biocide treatments, the chlorine treatment affected the biofilm matrix in a different fashion, most likely by oxidative degradation of the EPS matrix and cell can be attributed to a reduction in extracellular protein (29).

After biofilms were treated with the high concentration of chlorine, there was no biomass present in the capillary tubing which could be stained with CTC to observe cellular respiratory activity. After the low concentration of chlorine was used as a biocide treatment, the corner biofilm showed no CTC reduction, suggesting that there were no actively respiring cells in the biofilm. The lack of CTC staining in biofilm treated with the low concentration of chlorine does not imply the lack of cellular viability, however (104).

Both planktonic and biofilm bacteria treated with glutaraldehyde exhibited a retention of CAM fluorescence throughout the treatment. Planktonic cell density increased an average of 0.10-Log events/mL, and the average FITC intensity increased slightly for the cell population from about 14000 to 16000 during the course of the 1 h glutaraldehyde treatment. The change in cell density during the glutaraldehyde treatment

was different than the 0.25-log reduction in events/mL which was seen during the 1 h PBS control. The increase in average FITC intensity during the control and glutaraldehyde treatments was similar, with the average intensity increasing from 14000 to 19000 for the control. The addition of glutaraldehyde to an unstained cell suspension did not increase the FITC intensity as seen on the flow cytometer, so the increase in FITC intensity during the glutaraldehyde treatment cannot be attributed to the presence of the biocide. Plate counts after glutaraldehyde treatment showed an average log reduction of 3.83, suggesting that over 99.98% of viable bacteria were killed during the 1 h planktonic experiments. This killing would not be discernable if viability was only measured via flow cytometry and the decrease in CAM fluorescence.

Biofilm bacteria exposed to a 1 h glutaraldehyde treatment lost an overall average of 16% of their initial fluorescence, with more fluorescence lost at the periphery of cell clusters. Experimental values for t_{50} could not be determined for planktonic or biofilm bacteria, since 50% of the initial fluorescence did not leak out of the cells during 1 h treatment with glutaraldehyde. The predicted glutaraldehyde α_{50} value for diffusive penetration into the center of a biofilm cluster was 5.4 sec, when non-reacting diffusion is assumed. Glutaraldehyde is often used as a microbiological fixative agent and it works by cross-linking cell membrane-associated proteins (26) (61) (68). This fixing mechanism (as opposed to one which lyses cell membranes) is one explanation for why there is not a significant fluorescence loss when this biocide is used against bacteria.

There was very little change in the areal coverage of biofilm clusters during glutaraldehyde treatment. After the 1 h treatment with this biocide, there was some CTC

staining, which implies the presence of actively respiring cells within the biofilm. The CTC reduction after glutaraldehyde treatment was only about 39% as intense as the staining after the PBS control experiment. Interestingly, at 50 mg/L, glutaraldehyde is considered a germicidal agent for medical and industrial applications (98). Obviously, both the planktonic and biofilm experiments which were carried out during this research project show the presence of viable bacteria after a 1 h treatment of glutaraldehyde at this germicide concentration.

Nisin, an antimicrobial peptide, appeared to be the most effective antimicrobial agent at cell membrane permeabilization. The nisin concentration in this study, 50 mg/L, was much greater than doses which showed efficacy against Gram positive bacteria in previous work (108). The planktonic experiments showed a rapid fluorescence loss in which the average FITC intensity for the cell population decreased by almost half of its original value during the first 5 min of treatment. Over the course of the 1 h treatment, average FITC intensity decreased by 6-fold and the percentage of green cells was reduced by almost 59%. However, the number of events/mL increased by 0.38-Log during nisin treatment. The FSC vs. SSC scatter plot data showed the overwhelming fluorescence loss throughout the planktonic cell suspension, and the only cells that retained any CAM fluorescence were those that were associated with the larger cell aggregates. The planktonic t_{50} value was determined to be 5.5 min.

The viability testing after nisin treatment of planktonic bacteria showed that there were no living cells after the exposure to the biocide. The average log reduction during nisin treatment was 4.67, which is indicative of a decrease of over 99.99% of viable

bacteria. The plate count data do not directly correlate to the flow cytometry data, in that the flow cytometry data suggested that there was a log-increase in events/mL and about 39% of the cells retained their fluorescence (i.e., maintained their cell membrane integrity) after the nisin treatment. One explanation for the increase in the number of events/mL during the nisin treatment could be the disaggregation of clumped cells, although this is purely hypothetical.

All of the biofilms treated with nisin showed an average fluorescence loss of 100% during the 1 h treatment period. This fluorescence loss was very uniform throughout the biofilm clusters, but there was a very slight penetration lag for the corner biofilms that were monitored. The average experimental t_{50} value in biofilm clusters was 4.4 min, which was longer than the predicted α_{50} value of 45.7 sec for the non-reactive diffusion of nisin into the center of a biofilm cluster. Nisin took slightly longer to effectively penetrate 120 μm into corner biofilms, which was indicated by the slightly longer t_{50} value of 11.5 min. The biofilm and planktonic t_{50} values for the nisin treatment very similar, which suggests that the presence of EPS and other matrix material does not inhibit the penetration of nisin into the biofilm, despite its high molecular weight. In other words, nisin appears to be limited by the intrinsic kinetics of killing, not by transport phenomena.

The immediate decrease in cellular fluorescence throughout the entire biofilm when cells are treated with nisin was surprisingly uniform and complete. One explanation for the observation that the cells in the center of the clusters lose their fluorescence at the same rate as the cells at the periphery is that those cells in the interior

regions of the biofilm are more susceptible to nisin treatment. This has been shown experimentally in *Pseudomonas aeruginosa*, where the peripheral regions of the biofilm were more tolerant to attack by antimicrobial agents which targeted cell membranes (60).

There was a definite shrinking of biofilm during nisin treatment, with the clusters shrinking in areal coverage by an average of about 8%. The edges of the corner biofilm retracted an average of 28 μm during nisin treatment. This shrinkage could be attributed to the physical collapsing of bacterial cells during nisin treatment. Nisin acts against gram-positive bacteria in a way that targets the destruction of cell membranes (11) (63) (173) . The structures of bacterial cell membranes are altered due to nisin attack, thus possibly altering the three-dimensional structure of the biofilm. After nisin treatment, no CTC staining was present which suggests that no cells were actively respiring.

There were significant differences between the observed t_{50} values and the predicted α_{50} values for each of the antimicrobial agents used against biofilm in this research project. The spatio-temporal patterns of antimicrobial action were also very different for the individual biocides. Since the mathematical determination of α_{50} values for the treatment of biofilms did not take into account the possibility of a reaction occurring with the biomass, one explanation for the discrepancies between the t_{50} and α_{50} values is that the sorption or reaction of the biocide retards the antimicrobial penetration. This is intuitive if one considers the reaction of a biocide as a consumption term in which the biocide concentration is depleted very rapidly as it diffuses into the biofilm structure, and reaction-diffusion interactions have been described previously (148) (157). The transient penetration of a biocide would also be decreased if the antimicrobial agent was

adsorbing to the components of the biomass while it was diffusing into the cluster. Chemical sorption phenomena have been observed and described for several antibiotics and other antimicrobial agents (90) (148).

The lack of correlation between the flow cytometry cell density data (events/mL) and the CFU/mL calculated via plate counts after the 1 h antimicrobial treatments was puzzling. Enumeration of viable cells via standard plate count methods has been the conventional benchmark for microbiologists concerned with antimicrobial efficacy against any given bacteria. Considering this, the significant decreases in viable cells after the 1 h biocide treatment periods as determined by plate counts suggests effective killing by all of the antimicrobials tested. The changes in fluorescence intensity and cell density as measured with flow cytometry offered no correlation to the plate count data. Therefore, determination of cell viability with flow cytometry techniques which investigate cell membrane permeabilization or changes in cell density may be challenging.

Post-treatment staining of biofilm with CTC is not a gold standard for detection of viable or culturable cells. Research has shown that the reduction of CTC does not necessarily mean the cells are viable, and CTC staining may overestimate the number of cells which are culturable via plate counts (102) (197) . Conversely, the lack of CTC staining does not imply that the cells are unable to be cultured (104). Although the reduction of CTC does indicate the presence of functional cell "machinery," it is often necessary to perform many assays which attempt to detect cell physiologies.

CONCLUSIONS

Flow cytometry offers the distinct advantage of high throughput screening of planktonic cell populations, and can provide researchers with information pertaining to particle sizes, fluorescence, and cellular complexity. As powerful as flow cytometry techniques are, there may still be some limitations when planktonic bacterial populations are analyzed. This research project utilized flow cytometry to detect the loss of CAM fluorescence in planktonic *S. epidermidis* bacteria, which would indicate the permeabilization of the cellular membranes.

Antimicrobial treatment of planktonic bacteria showed varying results when analyzed with flow cytometry. Some treatments demonstrated an increase in average fluorescence intensity over the 1 h biocide exposure (control, Barquat, 10 mg/L chlorine, and glutaraldehyde) while others showed decreasing fluorescence (50 mg/L chlorine and nisin). Increases in cell density were observed for some treatments (glutaraldehyde and nisin), while other treatments illustrated a decrease in cell density (control, Barquat, and both concentrations of chlorine).

Complicating the interpretation of the flow cytometry data was the lack of correlation with the plate count data. All of the treatments resulted in at least a 3-log reduction (Barquat and glutaraldehyde) or 4-log reduction (both chlorine concentrations and nisin) of viable cells which were capable of forming colonies on agar plates. This significant log reduction in viable bacteria was not echoed by the flow cytometry data in any way.

The spatial and temporal patterns of antimicrobial action were very distinct for each of the antimicrobial agents which were investigated against *S. epidermidis* biofilms. Cellular CAM fluorescence loss during the 1 h treatment with Barquat was in an outward-in pattern, with the interior regions of the biofilm retaining some fluorescence for a longer time than the periphery. This pattern could be consistent with the presence of a subpopulation of cells in the more inaccessible regions of biofilm which is more tolerant to Barquat challenge. Barquat treatment did result in a slight shrinkage of biomass after the 1 h treatment period. Biofilms exposed to glutaraldehyde showed very little fluorescence loss throughout the clusters, indicative of a lack of cell permeabilization. Since glutaraldehyde is a cross-linking fixative agent, the absence of cell lysing seems intuitive.

Chlorine treatments of biofilm displayed antimicrobial action which was characterized by reaction-diffusion interaction. Cells located at the periphery of cell clusters were rapidly lysed and CAM fluorescence leaked out, while the simultaneous erosion of biomass allowed for further penetration of the reactive chlorine into the biofilm. Biofilm clusters treated with nisin showed the fastest and most uniform pattern of fluorescence loss amongst the biocides which were tested. Cells at the periphery appeared to be permeabilized and lost their fluorescence at the same time and rate at which cells in the center of the clusters were affected. Also, a slight shrinking of the cell clusters was observed during the 1 h nisin treatment.

Time-lapse CSLM has allowed for the non-invasive, direct imaging of spatial patterns of antimicrobial action in real-time. This technique is novel and was

concurrently tested for its applicability to monitor mixed-species dental biofilm challenged with different antimicrobial agents (166). The detection of cell permeabilization is possible with this method and the utilization of the cell-specific CAM dye. Although the loss of fluorescence t_{50} values are much greater than those predicted mathematically (α_{50}), some of this difference can be accounted for by assuming that reaction or sorption phenomena are present in this system.

Considerations for Future Work

Since the inception of fluorescence microscopic techniques applied to biological systems, the applications and advancements within the field have been unceasing. Confocal microscopy added more insight into biological systems with the advent of time-lapse and three-dimensional observation of heterogeneous structures which are often observed in biofilms. Confocal microscopy has made major advances in the past several years, far past the capabilities of the technologies utilized in this research project. There are confocal microscopes manufactured today which scan the surface of the observed object at an amazing rate of 30 scans/sec! This real-time scan rate allows for the researcher to conduct real-time observations at the same frame rate which movies are played. The acquisition of these technologies for use in biofilm research could mean the opportunity to generate and collect data on the sub-second time scale, which has not been done thus far. For experimental approaches similar to those outlined in this research project, measurements of fluorescence loss rates could be obtained with greater accuracy.

The techniques used in this research, although novel, were limited in the information which was directly observed. In order to determine the diffusive penetration times for the different biocides, and thus deduce experimental diffusion coefficients, assumptions would have to be made about the rate at which cells were permeabilized by the agent. One type of experimental design that could allow for a more direct observation of the antimicrobial diffusion and permeabilization of cell membranes would employ a viability dye which indicated the integrity of cell membranes, such as propidium iodide (PI). The addition of PI to the antimicrobial treatment solution would allow a direct observation of the rate at which cells were permeabilized due to the presence of the antimicrobial agent. This type of experiment has been performed previously, but not in a manner that interrogated the diffusive penetration of antimicrobial agents into a biofilm. Another option to observe antimicrobial agents would be to fluorescently label the biocide itself, although this process (if even feasible) could be cost prohibitive.

The chemical effect upon the mechanical properties and overall three-dimensional structure of the biofilm was an interesting phenomenon which was a theme in this project. There has been work published on the removal effects of different chemical treatments and physiological conditions on biofilm-covered surfaces (29), but it is limited due to the complexity of the factors contributing to biofilm recalcitrance. It has been shown with magnetic resonance microscopy (MRM) that the addition of the biocides used for this research project affected the intrinsic diffusion of carbohydrate molecules within the biofilm structure, effectively altering the chain lengths of the polymers and causing changes in carbohydrate mobility in the matrix (69). One strategy of biofilm

removal is to stiffen the EPS matrix of the biofilm, making the biofilm more brittle, and then applying flow-induced or other mechanical stresses to the biofilm in order to cause major detachment events. This stiffening could be achieved by the addition of chemical chelating agents, which would act in a way to cross-link the proteins and polymer chains of the EPS matrix. The viability of the detached bacteria would have to be closely monitored, though, especially for applications which could have clinical or industrial significance.

Biofilm modeling efforts have become increasingly complex over the past decade, and the diffusion of biocides could be modeled in a very complex manner as well. With the experimental results from this project as evidence, a reaction or sorption term must be added to more closely model the transient diffusion of antimicrobial agents into biofilm. Reaction phenomena occur with many components of biofilm, including EPS and cell constituents. To be more accurate, reaction and diffusion incidents occur on a much different time scale at the single-cell level, in which molecular interactions must be accounted for. Modeling these reaction and diffusion phenomena with more stringent analyses could offer insight into the behaviors observed in biofilm research.

With the clinical significance of biofilm infections at the forefront of this project, the inhibition of bacterial growth and biofilm colonization of medically implantable surfaces is an emerging field. The investigations of bio-compatible surface treatments or coatings which inhibit or alter the growth of biofilms, or increase their susceptibility to antimicrobial attack could lead to increased industrial collaborations and technology transfer. Inevitably, inhibition of biofilm growth is of utmost importance in medicine.

REFERENCES

1. Ali, A., M. H. Rashid, and D. K. R. Karaolis. 2002. High-frequency rugose exopolysaccharide production by *Vibrio cholerae*. Appl Environ Microbiol. 68:5773-5778.

2. Alpkvist, E. and I. Klapper. 2007. A multidimensional multispecies continuum model for heterogeneous biofilm development. Bull Math Biol. 69:765-789.

3. Alpkvist, E. and I. Klapper. 2007. Description of mechanical response including detachment using a novel particle model of biofilm/flow interaction. Wat Sci Technol. 55:265-273.

4. Alpkvist, E., C. Picioreanu, M. C. M. van Loosdrecht, and A. Heyden. 2006. Three-dimensional biofilm model with individual cells and continuum EPS matrix. Biotechnol Bioeng. 94:961-979.

5. Anderl, J. N., M. J. Franklin, and P. S. Stewart. 2000. Role of antibiotic penetration limitation in *Klebsiella pneumoniae* biofilm resistance to ampicillin and ciprofloxacin. Antimicrob Agents Chemother. 44:1818-1824.

6. Anwar, H., T. Vanbiesen, M. Dasgupta, K. Lam, and J. W. Costerton. 1989. Interaction of biofilm bacteria with antibiotics in a novel in vitro chemostat system. Antimicrob Agents Chemother. 33:1824-1826.

7. Archer, G. L. 1978. Antimicrobial susceptibility and selection of resistance among *Staphylococcus epidermidis* isolates recovered from patients with infections of indwelling foreign devices. Antimicrob Agents Chemother. 14:353-359.

8. Atkinson, B., A. W. Busch, and G. S. Dawkins. 1963. Recirculation, reaction kinetics, and effluent quality in a trickling filter flow model. Trans Inst Chem Engrs. 35:1307-1317.

9. Atkinson, B. and I. J. Davies. 1974. The overall rate of substrate uptake (reaction) by microbial films. Part I - A biological rate equation. Trans Inst Chem Engrs. 52:248-259.

10. Auschill, T. M., N. B. Artweiler, L. Netuschil, M. Brecx, E. Reich, and A. Sculean. 2001. Spatial distribution of vital and dead microorganisms in dental biofilms. Arch Oral Biol. 46:471-476.

11. Baba, T. and O. Schneewind. 1998. Instruments of microbial warfare: bacteriocin synthesis, toxicity and immunity. Trend Microbiol. 6:66-71.

12. Banerjee, S. N., T. G. Emori, D. H. Culver, R. P. Gaynes, W. R. Jarvis, T. Horan, J. R. Edwards, J. Tolson, T. Henderson, and W. J. Martone. 1991. Secular trends in nosocomial primary bloodstream infections in the United States, 1980-1989. Am J Med. 6:479-486.

13. Banin, E., K. M. Brady, and E. P. Greenberg. 2006. Chelator-induced dispersal and killing of *Pseudomonas aeruginosa* cells in a biofilm. Appl Environ Microbiol. 72:2064-2069.

14. Banning, N., S. Toze, and B. J. Mee. 2002. *Escherichia coli* survival in groundwater and effluent measured using a combination of propidium iodide and the green fluorescent protein. J Appl Microbiol. 93:69-76.

15. Bender, J. W. and W. T. Hughes. 1980. Fatal *Staphylococcus epidermidis* sepsis following bone marrow transplantation. Johns Hop Med J. 146:13-15.

16. Blouse, L. E., G. D. Latrhop, L. N. Kolonel, and R. M. Brockett. 1978. Epidemiologic features and phage types associated with nosocomial infections caused by *Staphylococcus epidermidis*. Zentralbl Bakteriol [Orig A]. 241:119-135.

17. Boles, B. R., M. Thoendel, and P. K. Singh. 2005. Self-generated diversity produces 'insurance effects' in biofilm communities (vol 101, pg 16630, 2004). Proc Nat Acad Sci USA. 102:955.

18. Borriello, G., E. Werner, F. Roe, A. M. Kim, G. D. Ehrlich, and P. S. Stewart. 2004. Oxygen limitation contributes to antibiotic tolerance of *Pseudomonas aeruginosa* in biofilms. Antimicrob Agents Chemother. 48:2659-2664.

19. Brooun, A., S. H. Liu, and K. Lewis. 2000. A dose-response study of antibiotic resistance in *Pseudomonas aeruginosa* biofilms. Antimicrob Agents Chemother. 44:640-646.

20. Brown, M. R. W., D. G. Allison, and P. Gilbert. 1988. Resistance of bacterial biofilms to antibiotics - A growth-rate related effect. J Antimicrob Chemother. 22:777-780.

21. Callaghan, R. P., S. J. Cohen, and G. T. Stewart. 1961. Septicaemia due to colonization of Spitz-Holter valves by staphylococci. Five cases treated with methicillin. Brit Med J. 1:860-863.

22. Campanac, C., L. Pineau, A. Payard, G. Baziard-Mouysset, and C. Roques. 2002. Interactions between biocide cationic agents and bacterial biofilms. Antimicrob Agents Chemother. 46:1469-1474.

23. Carslaw, H. S. and J. C. Jaeger. 1948. The flow of heat in a sphere and a cone, p. 198-215. *In* Conduction of Heat in Solids. Oxford University Press, London.

24. Chambless, J. D., S. M. Hunt, and P. S. Stewart. 2006. A three-dimensional computer model of four hypothetical mechanisms protecting biofilms from antimicrobials. Appl Environ Microbiol. 72:2005-2013.

25. Chambless, J. D. and P. S. Stewart. 2007. A three-dimensional computer model analysis of three hypothetical biofilm detachment mechanisms. Biotechnol Bioeng. 97:1573-1584.

26. Chambon, M., J. L. Bailly, and H. Peigue-Lafeuille. 1992. Activity of glutaraldehyde at low concentrations against capsid proteins of poliovirus type 1 and echovirus type 25. Appl Environ Microbiol. 58:3517-3521.

27. Cheema, M. S., J. E. Rassing, and C. Marriott. 1986. The diffusion characteristics of antibiotics in mucus glycoprotein gels. J Pharm Pharmacol. Supp 38.

28. Chen, X. and P. S. Stewart. 1996. Chlorine penetration into artificial biofilm is limited by a reaction-diffusion interaction. Environ Sci Tech. 30:2078-2083.

29. Chen, X. and P. S. Stewart. 2000. Biofilm removal caused by chemical treatments. Wat Res. 34:4229-4233.

30. Cochran, W. L., G. A. McFeters, and P. S. Stewart. 2000. Reduced susceptibility of thin *Pseudomonas aeruginosa* biofilms to hydrogen peroxide and monochloramine. J Appl Microbiol. 88:22-30.

31. Cogan, N. G. Hybrid numerical treatment of two-fluid problems with passive interfaces. 2006. Ref Type: Unpublished Work

32. Colasanti, R. L. 1992. Cellular automata models of microbial colonies. Binary. 4:191-193.

33. Costerton, J. W., K. J. Cheng, G. G. Geesey, T. I. Ladd, J. C. Nickel, M. Dasgupta, and T. J. Marrie. 1987. Bacterial biofilms in nature and disease. Ann Rev Microbiol. 41:435-464.

34. Costerton, J. W., G. G. Geesey, and K. J. Cheng. 1978. How bacteria stick. Sci Am. 238:86-95.

35. Costerton, J. W., Z. Lewandowski, D. E. Caldwell, D. R. Korber, and H. M. Lappin-Scott. 1995. Microbial biofilms. Ann Rev Microbiol. 49:711-745.

36. Costerton, J. W. and P. S. Stewart. 2001. Battling biofilms - The war is against bacterial colonies that cause some of the most tenacious infections known. The weapon is knowledge of the enemy's communication system. Sci Am. 285:74-81.

37. Costerton, J. W., P. S. Stewart, and E. P. Greenberg. 1999. Bacterial biofilms: A common cause of persistent infections. (Cover story). Science. 284:1318.

38. Dalton, H. M. and P. E. March. 1998. Molecular genetics of bacterial attachment and biofouling. Curr Opin Biotech. 9:252-255.

39. Darouiche, R. O., A. Dhir, A. J. Miller, G. C. Landon, I. I. Raad, and D. M. Musher. 1994. Vancomycin penetration into biofilm covering infected prostheses and effect on bacteria. J Infect Dis. 170:720-723.

40. Das, J. R., M. Bhakoo, M. V. Jones, and P. Gilbert. 1998. Changes in the biocide susceptibility of *Staphylococcus epidermidis* and *Escherichia coli* cells associated with rapid attachment to plastic surfaces. J Appl Microbiol. 84:852-858.

41. deBeer, D., P. Stoodley, and Z. Lewandowski. 1997. Measurement of local diffusion coefficients in biofilms by microinjection and confocal microscopy. Biotechnol Bioeng. 53:151-158.

42. deBeer, D., P. Stoodley, F. Roe, and Z. Lewandowski. 1994. Effects of biofilm structures on oxygen distribution and mass-transport. Biotechnol Bioeng. 43:1131-1138.

43. Diaper, J. P. and C. Edwards. 1994. The use of fluorogenic esters to detect viable bacteria by flow cytometry. J Appl Bacteriol. 77:221-228.

44. Dibdin, G. H. 1992. A finite-difference computer model of solute diffusion in bacterial films with simultaneous metabolism and chemical reaction. Bioinformatics. 8:489-500.

45. Dillon, R., L. Fauci, A. Fogelson, and D. Gaver III. 1996. Modeling biofilm processes using the immersed boundary method. J Comp Phys. 129:57-73.

46. Dismukes, W. E., A. W. Karchmer, M. J. Buckley, W. G. Austen, and M. N. Swartz. 1973. Prosthetic valve endocarditis: Analysis of 38 Cases. Circulation. 48:365-377.

47. Dockery, J. and J. Keener. 2001. A mathematical model for quorum sensing in *Pseudomonas aeruginosa*. Bull Math Biol 63:95-116.

48. Dockery, J. and I. Klapper. 2001. Finger formation in biofilm layers. SIAM J Appl Math. 62:853.

49. Dodd, H. M. and M. J. Gasson. 1994. Bacteriocins of lactic acid bacteria, p. 211-251. *In* M. J. Gasson and W. M. deVos (eds.), Genetics and Biotechnology of Lactic Acid Bacteria. Blackie Academic and Professional.

50. Domingo, P. and A. Fontanet. 2001. Management of complications associated with totally implantable ports in patients with AIDS. AIDS Patient Care & STDs 15:7-13.

51. Dunne, W. M., E. O. Mason, and S. L. Kaplan. 1993. Diffusion of rifampin and vancomycin through a *Staphylococcus epidermidis* biofilm. Antimicrob Agents Chemother. 37:2522-2526.

52. Essodaigui, M., H. J. Broxterman, and A. Garnier-Suillerot. 1998. Kinetic analysis of calcein and calcein-acetoxymethyl ester efflux mediated by the multidrug resistance protein and P-glycoprotein. Biochem. 37:2243-2250.

53. Flora, J. R. V., M. T. Suidan, P. Biswas, and G. D. Sayles. 1993. Modeling substrate transport into biofilms - Role of multiple ions and pH effects. J Environ Eng-ASCE. 119:908-930.

54. Fux, C. A., S. Wilson, and P. Stoodley. 2004. Detachment characteristics and oxacillin resistance of *Staphylococcus aureus* biofilm emboli in an in vitro catheter infection model. J Bacteriol. 186:4486-4491.

55. Gilbert, P. and M. R. W. Brown. 1995. Mechanisms of the protection of bacterial biofilms from antimicrobial agents, p. 118-130. *In* H. M. Lappin-Scott and J. W. Costerton (eds.), Microbial Biofilms. Cambridge University Press, Cambridge.

56. Gilbert, P. and L. E. Moore. 2005. Cationic antiseptics: diversity of action under a common epithet. J Appl Microbiol. 99:703-715.

57. Gordon, C. A., N. A. Hodges, and C. Marriott. 1988. Antibiotic interaction and diffusion through alginate and exopolysaccharide of cystic fibrosis-derived *Pseudomonas aeruginosa*. J Antimicrob Chemother. 22:667-674.

58. Goto, T., Y. Nakame, M. Nishida, and Y. Ohi. 1999. In vitro bactericidal activities of beta-lactamases, amikacin, and fluoroquinolones against *Pseudomonas aeruginosa* biofilm in artificial urine. Urology. 53:1058-1062.

59. Gotz, F. 2002. Staphylococcus and biofilms. Mol Microbiol. 43:1367-1378.

60. Haagensen, J. A. J., M. Klausen, R. K. Ernst, S. I. Miller, A. Folkesson, T. Tolker-Nielsen, and S. Molin. 2007. Differentiation and distribution of colistin- and sodium dodecyl sulfate-tolerant cells in *Pseudomonas aeruginosa* biofilms. J Bacteriol. 189:28-37.

61. Habeeb, A. J. and R. Hiramoto. 1968. Reaction of proteins with glutaraldehyde. Arch Biochem Biophys. 126:16-26.

62. Hammond, G. W. and H. G. Stiver. 1975. Combination antibiotic therapy in an outbreak of prosthetic endocarditis caused by *Staphylococcus epidermidis*. Can Med Assoc J. 118:524-530.

63. Hancock, R. E. W. and D. S. Chapple. 1999. Peptide antibiotics. Antimicrob Agents Chemother. 43:1317-1323.

64. Herigstad, B., M. Hamilton, and J. Heersink. 2001. How to optimize the drop plate method for enumerating bacteria. J Microbiol Meth. 44:121-129.

65. Hermanowicz, S. W. 1998. A model of two-dimensional biofilm morphology. Wat Sci Technol. 37:219-222.

66. Hollo, Z., L. Homolya, C. W. Davis, and B. Sarkadi. 1994. Calcein accumulation as a fluorometric functional assay of the multidrug transporter. Biochim Biophys Acta. 1191:384-388.

67. Holt, R. 1969. The classification of staphylococci from colonized ventriculo-atrial shunts. J Clin Pathol. 22:475-482.

68. Hopwood, D. 1972. Theoretical and practical aspects of glutaraldehyde fixation. Histochem J. 4:267-303.

69. Hornemann, J. A., Codd, S. L., Lysova, A. A., Seymour, J. D., and Stewart, P. S. Magnetic resonance microscopy study of biofilm EPS. 2007. Ref Type: Unpublished Work

70. Horvath, A. L. 1985. Handbook of aqueous electrolyte solutions. John Wiley, New York.

71. Hoyle, B. D. and J. W. Costerton. 1991. Bacterial resistance to antibiotics: the role of biofilms. Prog Drug Res. 37:91-105.

72. Huang, C. T., F. P. Yu, G. A. McFeters, and P. S. Stewart. 1995. Nonuniform spatial patterns of respiratory activity within biofilms during disinfection. Appl Environ Microbiol. 61:2252-2256.

73. Hunt, S. M., M. A. Hamilton, J. T. Sears, G. Harkin, and J. Reno. 2003. A computer investigation of chemically mediated detachment in bacterial biofilms. Microbiol. 149:1155-1163.

74. Hunt, S. M., E. M. Werner, B. Huang, M. A. Hamilton, and P. S. Stewart. 2004. Hypothesis for the role of nutrient starvation in biofilm detachment. Appl Environ Microbiol. 70:7418-7425.

75. Invitrogen-Molecular Probes. Acetoxymethyl (AM) and acetate esters. Product information sheet. 2004. Ref Type: Pamphlet

76. Jack, R. W., J. R. Tagg, and B. Ray. 1995. Bacteriocins of gram-positive bacteria. Microbiol Mol Biol Rev. 59:171-200.

77. Jefferson, K. K., D. A. Goldmann, and G. B. Pier. 2005. Use of confocal microscopy to analyze the rate of vancomycin penetration through *Staphylococcus aureus* biofilms. Antimicrob Agents Chemother. 49:2467-2473.

78. Jones, D., H. V. Kojouharov, D. Le, and H. Smith. 2003. The Freter model: A simple model of biofilm formation. J Math Biol. 47:137-152.

79. Kaneko, Y., M. Thoendel, O. Olakanmi, B. E. Britigan, and P. K. Singh. 2007. The transition metal gallium disrupts *Pseudomonas aeruginosa* iron metabolism and has antimicrobial and antibiofilm activity. J Clin Invest. 117:877-888.

80. Keer, J. T. and L. Birch. 2003. Molecular methods for the assessment of bacterial viability. J Microbiol Meth. 53:175-183.

81. Keren, I., N. Kaldalu, A. Spoering, Y. P. Wang, and K. Lewis. 2004. Persister cells and tolerance to antimicrobials. FEMS Microbiol Lett. 230:13-18.

82. Kirisits, M. J. and M. R. Parsek. 2006. Does Pseudomonas aeruginosa use intercellular signalling to build biofilm communities? Cell Microbiol. 8:1841-1849.

83. Kissel, J. C., P. L. McCarty, and R. L. Street. 1984. Numerical simulation of mixed-culture biofilm. J Environ Eng. 110:393-411.

84. Klapper, I., C. J. Rupp, R. Cargo, B. Purvedorj, and P. Stoodley. 2002. Viscoelastic fluid description of bacterial biofilm material properties. Biotechnol Bioeng. 80:289-296.

85. Klausen, M., A. Aaes-Jorgensen, S. Molin, and T. Tolker-Nielsen. 2003. Involvement of bacterial migration in the development of complex multicellular structures in *Pseudomonas aeruginosa* biofilms. Mol Microbiol 50:61.

86. Korber, D. R., J. R. Lawrence, B. Sutton, and D. E. Caldwell. 1989. Effect of laminar flow velocity on the kinetics of surface recolonization by Mot+ and Mot– *Pseudomonas fluorescens*. Microb Ecol. 18:1-19.

87. Kreft, J. U., G. Booth, and J. W. Wimpenny. 1998. BacSim, a simulator for individual-based modelling of bacterial colony growth. Microbiol. 144:3275-3287.

88. Kreft, J. U., C. Picioreanu, J. W. T. Wimpenny, and M. C. M. van Loosdrecht. 2001. Individual-based modelling of biofilms. Microbiol. 147:2897-2912.

89. Kreft, J. U. and J. W. Wimpenny. 2001. Effect of EPS on biofilm structure and function as revealed by an individual-based model of biofilm growth. Wat Sci Technol. 43:135-141.

90. Kumon, H., K. Tomochika, T. Matunaga, M. Ogawa, and H. Ohmori. 1994. A sandwich gun method for the penetration assay of antimicrobial agents through Pseudomonas exopolysaccharides. Microbiol Immun. 38:615-619.

91. Lambert, P. A. and S. M. Hammond. 1973. Potassium fluxes, first indications of membrane damage in micro-organisms. Biochem Biophys Acta. 54:796-799.

92. Lawrence, J. R., D. R. Korber, B. D. Hoyle, J. W. Costerton, and D. E. Caldwell. 1991. Optical sectioning of microbial biofilms. J Bacteriol. 173:6558-6567.

93. Lawrence, J. R., G. D. W. Swerhone, G. G. Leppard, T. Araki, X. Zhang, M. M. West, and A. P. Hitchcock. 2003. Scanning transmission x-ray, laser scanning, and transmission electron microscopy mapping of the exopolymeric matrix of microbial biofilms. Appl Environ Microbiol. 69:5543-5554.

94. Lewis, K. 2001. Riddle of biofilm resistance. Antimicrob Agents Chemother. 45:999-1007.

95. Lewis, K. 2005. Persister cells and the riddle of biofilm survival. Biochemistry-Moscow. 70:267.

96. Lowder, M., A. Unge, N. Maraha, J. K. Jansson, J. Swiggett, and J. D. Oliver. 2000. Effect of starvation and the viable-but-nonculturable state on green fluorescent protein (GFP) fluorescence in GFP-tagged *Pseudomonas fluorescens* A506. Appl Environ Microbiol. 66:3160-3165.

97. Mah, T. F. C. and G. A. O'Toole. 2001. Mechanisms of biofilm resistance to antimicrobial agents. Trend Microbiol. 9:34-39.

98. Mahon, C. R. and G. Manuselis. 2000. Textbook of Diagnostic Microbiology, p. 31. Saunders.

99. Marples, R. R., R. Hone, C. M. Notley, J. F. Richardson, and J. A. Crees-Morris. 1978. Investigation of coagulase-negative staphylococci from infections in surgical patients. Zentralbl Bakteriol [Orig A]. 241:140-156.

100. Mccann, K. S. 2000. The diversity-stability debate. Nature. 405:228-233.

101. McCoy, W. F., J. D. Bryers, J. Robbins, and J. W. Costerton. 1981. Observations of fouling biofilm formation. Can J Microbiol. 27:910-917.

102. McFeters, G. A., B. H. Pyle, J. T. Lisle, and S. C. Broadaway. 1999. Rapid direct methods for enumeration of specific, active bacteria in water and biofilms. Symp Ser Soc Appl Microbiol. 85:193S-200S.

103. Minsky, M. 1988. Memoir on inventing the confocal microscope. Scanning. 10:128-138.

104. Morin, P. and A. K. Camper. 1997. Attachment and fate of carbon fines in simulated drinking water distribution system biofilms. Wat Res. 31:399-410.

105. Moyed, H. S. and K. P. Bertrand. 1983. HipA, A newly recognized gene of *Escherichia coli* K-12 that affects frequency of persistence after inhibition of murein synthesis. J Bacteriol. 155:768-775.

106. Nilsson, P., A. Olofsson, M. Fagerlind, T. Fagerstrom, S. Rice, S. Kjelleberg, and P. Steinberg. 2001. Kinetics of the AHL regulatory system in a model biofilm system: How many bacteria constitute a quorum? J Mol Biol. 309:631-640.

107. O'Gara, J. P. and H. I. L. A. Humphreys. 2001. *Staphylococcus epidermidis* biofilms: importance and implications. J Med Microbiol. 50:582-587.

108. Otto, M., A. Peschel, and F. Gotz. 1998. Producer self-protection against the lantibiotic epidermin by the ABC transporter EpiFEG of *Staphylococcus epidermidis* Tu3298. FEMS Microbiol Lett. 166:203-211.

109. Parsek, M. R. and P. K. Singh. 2003. Bacterial biofilms: An emerging link to disease pathogenesis. Ann Rev Microbiol. 57:677-701.

110. PATTERSON, F. P. and C. S. Brown. 1972. The McKee-Farrar total hip replacement: Preliminary results and complications of 368 operations performed in five general hospitals. J Bone Joint Surg Am. 54:257-275.

111. Pescod, M. B. and J. V. Nair. 1972. Biological disc filtration for tropical waste treatment. Experimental studies. Wat Res. 6:1509-1523.

112. Picioreanu, C., J. U. Kreft, M. Klausen, J. A. Haagensen, T. Tolker-Nielsen, and S. Molin. 2007. Microbial motility involvement in biofilm structure formation--a 3D modelling study. Wat Sci Technol. 55:337-343.

113. Picioreanu, C., M. C. M. van Loosdrecht, and J. J. Heijnen. 1998. A new combined differential-discrete cellular automaton approach for biofilm modeling: Application for growth in gel beads. Biotechnol Bioeng. 57:718-731.

114. Picioreanu, C., M. C. M. van Loosdrecht, and J. J. Heijnen. 1998. Mathematical modeling of biofilm structure with a hybrid differential-discrete cellular automaton approach. Biotechnol Bioeng. 58:101-116.

115. Picioreanu, C., M. C. M. van Loosdrecht, and J. J. Heijnen. 1999. Discrete-differential modelling of biofilm structure. Wat Sci Technol. 39:115-122.

116. Picioreanu, C., M. C. M. van Loosdrecht, and J. J. Heijnen. 2001. Two-dimensional model of biofilm detachment caused by internal stress from liquid flow. Biotechnol Bioeng. 72:205-218.

117. Polson, A. 1950. Some aspects of diffusion in solution and a definition of a colloidal particle. J Phys Chem. 54:649-652.

118. Pyle, B. H., S. C. Broadaway, and G. A. McFeters. 1995. Factors affecting the determination of respiratory activity on the basis of cyanoditolyl tetrazolium chloride reduction with membrane filtration. Appl Environ Microbiol. 61:4304-4309.

119. Raad, I., A. Alrahwan, and K. Rolston. 1998. *Staphylococcus epidermidis*: Emerging resistance and need for alternative agents. Clin Infect Dis. 26:1182-1187.

120. Rani, S. A., B. Pitts, H. Beyenal, R. A. Veluchamy, Z. Lewandowski, W. M. Davison, K. Buckingham-Meyer, and P. S. Stewart. 2007. Spatial patterns of DNA replication, protein synthesis, and oxygen concentration within bacterial biofilms reveal diverse physiological states. J Bacteriol. 189:4223-4233.

121. Rani, S. A., B. Pitts, and P. S. Stewart. 2005. Rapid diffusion of fluorescent tracers into *Staphylococcus epidermidis* biofilms visualized by time lapse microscopy. Antimicrob Agents Chemother. 49:728-732.

122. Retsema, J. A., L. A. Brennan, and A. E. Girard. 1991. Effects of environmental factors on the in vitro potency of azithromycin. Euro J Clin Microbiol Infect Dis. 10:834-842.

123. Roberts, M. E. and P. S. Stewart. 2004. Modeling antibiotic tolerance in biofilms by accounting for nutrient limitation. Antimicrob Agents Chemother. 48:48-52.

124. Rodriguez, G. G., D. Phipps, K. Ishiguro, and H. F. Ridgway. 1992. Use of a fluorescent redox probe for direct visualization of actively respiring bacteria. Appl Environ Microbiol. 58:1801-1808.

125. Rupp, C. J., C. A. Fux, and P. Stoodley. 2005. Viscoelasticity of *Staphylococcus aureus* biofilms in response to fluid shear allows resistance to detachment and facilitates rolling migration. Appl Environ Microbiol. 71:2175-2178.

126. Sahl, H. G., R. W. Jack, and G. Bierbaum. 1995. Biosynthesis and biological activities of lantibiotics with unique post-translational modifications. Euro J Biochem. 230:827-853.

127. Salih, H. R., L. Husfeld, and D. Adam. 2000. Simultaneous cytofluorometric measurement of phagocytosis, burst production and killing of human phagocytes using *Candida albicans* and *Staphylococcus aureus* as target organisms. Clin Microbiol Infect. 6:251-258.

128. Salt, W. G. and D. Wiseman. 1970. The relation between the uptake of cetyltrimethylammonium bromide by *Escherichia coli* and its effects on cell growth and viability. J Pharm Pharmacol. 22:261-264.

129. Salton, M. R. J. 1951. The adsorption of cetyltrimethylammonium bromide by bacteria, its action in releasing cellular constituents and its bactericidal effects. J Gen Microbiol. 5:391-404.

130. Salton, M. R. J. 1968. Lytic agents, cell permeability, and monolayer penetrability. J Gen Physiol. 52:227-252.

131. Sauer, K., A. K. Camper, G. D. Ehrlich, J. W. Costerton, and D. G. Davies. 2002. *Pseudomonas aeruginosa* displays multiple phenotypes during development as a biofilm. J Bacteriol. 184:1140-1154.

132. Schaberg, D. R., D. H. Culver, and R. P. Gaynes. 1991. Major trends in the microbial etiology of nosocomial infection. Am J Med. 91:S72-S75.

133. Schaule, G., H. C. Flemming, and H. F. Ridgway. 1993. Use of 5-cyano-2,3-ditolyl tetrazolium chloride for quantifying planktonic and sessile respiring bacteria in drinking water. Appl Environ Microbiol. 59:3850-3857.

134. Schimke, R. T., P. H. Black, V. H. Mark, and M. N. Swartz. 1961. Indolent *Staphylococcus albus* or *aureus* bacteremia after ventriculoatriostomy. Role of foreign body in its initiation and perpetuation. New Eng J Med. 264:264-270.

135. Schoenbaum, S. C., P. Gardner, and J. Shillito. 2007. Infections of cerebrospinal fluid shunts: epidemiology, clinical manifestations, and therapy. J Infect Dis. 131:543-552.

136. Semwogerere, D. and E. R. Weeks. 2005. Confocal Microscopy, *In* Encyclopedia of Biomaterials and Biomedical Engineering. Taylor & Francis.

137. Severin, E., J. Stellmach, and H.-M. Nachtigal. 1985. Fluorimetric assay of redox activity in cells. Analytica Chimica Acta. 170:341-346.

138. Shapiro, H. 2003. Practical Flow Cytometry, p. 46.

139. Smith, J. J. and G. A. McFeters. 1996. Effects of substrates and phosphate on INT (2-(4-iodophenyl)-3-(4-nitrophenyl)-5-phenyl tetrazolium chloride) and CTC (5-cyano-2,3-ditolyl tetrazolium chloride) reduction in *Escherichia coli*. J Appl Bacteriol. 80:209-215.

140. Soomro, A. H., T. Masud, and K. Anwaar. 2002. Role of lactic acid bacteria (LAB) in food preservation and human health - A review. Pak J Nutrit. 1:20-24.

141. Speller, D. C. E. and R. G. Mitchell. 1973. Coagulase-negative staphylococci causing endocarditis after cardiac surgery. J Clin Pathol. 26:517-522.

142. Spoering, A. L. and K. Lewis. 2001. Biofilms and planktonic cells of *Pseudomonas aeruginosa* have similar resistance to killing by antimicrobials. J Bacteriol. 183:6746-6751.

143. Stellmach, J. 1984. Fluorescent redox dyes. Histochem Cell Biol. 80:137-143.

144. Stellmach, J. and E. Severin. 1987. A fluorescent redox dye. Influence of several substrates and electron carriers on the tetrazolium salt-formazan reaction of Ehrlich ascites tumour cells. Histochem J. 19:21-26.

145. Sternberg, C., B. B. Christensen, T. Johansen, A. T. Nielsen, J. B. Andersen, M. Givskov, and S. Molin. 1999. Distribution of bacterial growth activity in flow-chamber biofilms. Appl Environ Microbiol. 65:4108-4117.

146. Stevens, K. A., B. W. Sheldon, N. A. Klapes, and T. R. Klaenhammer. 1991. Nisin treatment for inactivation of Salmonella species and other gram-negative bacteria. Appl Environ Microbiol. 57:3613-3615.

147. Stewart, P. S. 1994. Biofilm accumulation model that predicts antibiotic resistance of *Pseudomonas aeruginosa* biofilms. Antimicrob Agents Chemother. 38:1052-1058.

148. Stewart, P. S. 1996. Theoretical aspects of antibiotic diffusion into microbial biofilms. Antimicrob Agents Chemother. 40:2517-2522.

149. Stewart, P. S. 1998. A review of experimental measurements of effective diffusive permeabilities and effective diffusion coefficients in biofilms. Biotechnol Bioeng. 59:261-272.

150. Stewart, P. S. 2002. Mechanisms of antibiotic resistance in bacterial biofilms. Intl J Med Microbiol. 292:107-113.

151. Stewart, P. S. 2003. Diffusion in biofilms. J Bacteriol. 185:1485-1491.

152. Stewart, P. S. and J. W. Costerton. 2001. Antibiotic resistance of bacteria in biofilms. Lancet. 358:135-138.

153. Stewart, P. S., L. Grab, and J. A. Diemer. 1998. Analysis of biocide transport limitation in an artificial biofilm system. J Appl Microbiol. 85:495-500.

154. Stewart, P. S., T. Griebe, R. Srinivasan, C. I. Chen, F. P. Yu, D. deBeer, and G. A. McFeters. 1994. Comparison of respiratory activity and culturability during monochloramine disinfection of binary population biofilms. Appl Environ Microbiol. 60:1690-1692.

155. Stewart, P. S., M. A. Hamilton, B. R. Goldstein, and B. T. Schneider. 1996. Modeling biocide action against biofilms. Biotechnol Bioeng. 49:445-455.

156. Stewart, P. S., G. A. McFeters, and C. T. Huang. 2000. Biofilm control by antimicrobial agents, p. 373-405. *In* J. D. Bryers (ed.), Biofilms II: Process Analysis and Applications. Wiley-Liss, Inc.

157. Stewart, P. S. and J. B. Raquepas. 1995. Implications of reaction-diffusion theory for the disinfection of microbial biofilms by reactive antimicrobial agents. Chem Eng Sci. 50:3099-3104.

158. Stickler, D. 1999. Biofilms. Curr Opin Microbiol. 2:270-275.

159. Stoodley, P., R. Cargo, C. J. Rupp, S. Wilson, and I. Klapper. 2002. Biofilm material properties as related to shear-induced deformation and detachment phenomena. J Ind Microbiol Biotech. 29:361-367.

160. Stoodley, P., D. deBeer, and Z. Lewandowski. 1994. Liquid flow in biofilm systems. Appl Environ Microbiol. 60:2711-2716.

161. Stoodley, P., Z. Lewandowski, J. D. Boyle, and H. M. Lappin-Scott. 1999. Structural deformation of bacterial biofilms caused by short-term fluctuations in fluid shear: An in situ investigation of biofilm rheology. Biotechnol Bioeng. 65:83-92.

162. Stoodley, P., K. Sauer, D. G. Davies, and J. W. Costerton. 2002. Biofilms as complex differentiated communities. Ann Rev Microbiol. 56:187-209.

163. Sufya, N., D. G. Allison, and P. Gilbert. 2003. Clonal variation in maximum specific growth rate and susceptibility towards antimicrobials. J Appl Microbiol. 95:1261-1267.

164. Tacconelli, E., M. Tumbarello, M. Pittiruti, F. Leone, M. B. Lucia, R. Cauda, and L. Ortona. 1997. Central venous catheter-related sepsis in a cohort of 366 hospitalised patients. Euro J Clin Microbiol Infect Dis. 16:203-209.

165. Tack, K. J. and L. D. Sabath. 1985. Increased minimum inhibitory concentrations with anaerobiasis for tobramycin, gentamicin, and amikacin, compared to latamoxef, piperacillin, chloramphenicol, and clindamycin. Chemotherapy. 31:204-210.

166. Takenaka, S., H. M. Trivedi, A. Corbin, B. Pitts, and P. S. Stewart. 2008. Direct visualization of spatial and temporal patterns of antimicrobial action within model oral biofilms. Appl Environ Microbiol.

167. Tilman, D., D. Wedin, and J. Knops. 1996. Productivity and sustainability influenced by biodiversity in grassland ecosystems. Nature. 379:718-720.

168. Tolker-Nielsen, T., U. C. Brinch, P. C. Ragas, J. B. Andersen, C. S. Jacobsen, and S. Molin. 2000. Development and dynamics of Pseudomonas sp. biofilms. J Bacteriol. 182:6482-6489.

169. Towler, B. W., A. Cunningham, P. Stoodley, and L. McKittrick. 2007. A model of fluid-biofilm interaction using a Burger material law. Biotechnol Bioeng. 96:259-271.

170. Tuomanen, E., R. Cozens, W. Tosch, O. Zak, and A. Tomasz. 1986. The rate of killing of *Escherichia coli* by beta-lactam antibiotics is strictly proportional to the rate of bacterial-growth. J Gen Microbiol. 132:1297-1304.

171. Tyn, M. T. and T. W. Gusek. 1990. Prediction of diffusion coefficients of proteins. Biotechnol Bioeng. 35:327-338.

172. US Environmental Protection Agency. 1999. Microbial and disinfection byproduct rules simultaneous compliance guidance manual.

173. van Belkum, M. J., J. Kok, G. Venema, H. Holo, I. F. Nes, W. N. Konings, and T. Abee. 1991. The bacteriocin lactococcin A specifically increases permeability of lactococcal cytoplasmic membranes in a voltage-independent, protein-mediated manner. J Bacteriol. 173:7934-7941.

174. Venglarcik, J. S., L. L. Blair, and L. M. Dunkle. 1983. pH-dependent oxacillin tolerance of *Staphylococcus aureus*. Antimicrob Agents Chemother. 23:232-235.

175. von Eiff, C., C. Heilmann, M. Herrmann, and G. Peters. 1999. Basic aspects of the pathogenesis of staphylococcal polymer-associated infections. Infection. 27:S7-S10.

176. Vuong, C. and M. Otto. 2002. *Staphylococcus epidermidis* infections. Microb Infect. 4:481-489.

177. Walters, M. C., F. Roe, A. Bugnicourt, M. J. Franklin, and P. S. Stewart. 2003. Contributions of antibiotic penetration, oxygen limitation, and low metabolic activity to tolerance of *Pseudomonas aeruginosa* biofilms to ciprofloxacin and tobramycin. Antimicrob Agents Chemother. 47:317-323.

178. Wanner, O. and W. Gujer. 1985. Competition in biofilms. Wat Sci Technol. 17:27-44.

179. Wanner, O. and W. Gujer. 1986. A multispecies biofilm model. Biotechnol Bioeng. 28:314-328.

180. Wentland, E. J., P. S. Stewart, C. T. Huang, and G. A. McFeters. 1996. Spatial variations in growth rate within *Klebsiella pneumoniae* colonies and biofilm. Biotechnol Prog. 12:316-321.

181. Werner, E., F. Roe, A. Bugnicourt, M. J. Franklin, A. Heydorn, S. Molin, B. Pitts, and P. S. Stewart. 2004. Stratified growth in *Pseudomonas aeruginosa* biofilms. Appl Environ Microbiol. 70:6188-6196.

182. Williams, I., W. A. Venables, D. Lloyd, F. Paul, and I. Critchley. 1997. The effects of adherence to silicone surfaces on antibiotic susceptibility in *Staphylococcus aureus*. Microbiol-UK. 143:2407-2413.

183. Wilson, P. D. 1977. Joint replacement. South Med J. 70:55-60.

184. Wilson, P. D., Jr., H. C. Amstutz, A. Czerniecki, E. A. Salvati, and D. G. Mendes. 1972. Total hip replacement with fixation by acrylic cement: A preliminary study of 100 consecutive Mckee-Farrar prosthetic replacements. J Bone Joint Surg Am. 54:207-221.

185. Wilson, P. D., E. A. Salvati, P. Aglietti, and L. J. Kutner. 1973. The problem of infection in endoprosthetic surgery of the hip joint. Clin Ortho Rel Res. 96:213-221.

186. Wimpenny, J. W. T. and R. Colasanti. 1997. A unifying hypothesis for the structure of microbial biofilms based on cellular automaton models. FEMS Microbiol Ecol. 22:1-16.

187. Wimpenny, J. W. T. and S. L. Kinniment. 1995. Biochemical reactions and the establishment of gradients within biofilms, p. 99-117. *In* H. M. Lappin-Scott and J. W. Costerton (eds.), Microbial Biofilms. Cambridge University Press, Cambridge.

188. Xavier, J. B., C. Picioreanu, S. A. Rani, M. C. M. van Loosdrecht, and P. S. Stewart. 2005. Biofilm-control strategies based on enzymic disruption of the extracellular polymeric substance matrix - a modelling study. Microbiol. 151:3817-3832.

189. Xavier, J. D. B., C. Picioreanu, and M. C. M. van Loosdrecht. 2005. A general description of detachment for multidimensional modelling of biofilms. Biotechnol Bioeng. 91:651-669.

190. Xiong, Y. Q., K. Mukhopadhyay, M. R. Yeaman, J. Adler-Moore, and A. S. Bayer. 2005. Functional interrelationships between cell membrane and cell wall in antimicrobial peptide-mediated killing of *Staphylococcus aureus*. Antimicrob Agents Chemother. 49:3114-3121.

191. Xu, K. D., G. A. McFeters, and P. S. Stewart. 2000. Biofilm resistance to antimicrobial agents. Microbiol. 146:547-549.

192. Xu, K. D., P. S. Stewart, F. Xia, C. T. Huang, and G. A. McFeters. 1998. Spatial physiological heterogeneity in *Pseudomonas aeruginosa* biofilm is determined by oxygen availability. Appl Environ Microbiol. 64:4035-4039.

193. Yachi, S. and M. Loreau. 1999. Biodiversity and ecosystem productivity in a fluctuating environment: The insurance hypothesis. Proc Nat Acad Sci USA. 96:1463-1468.

194. Yarwood, J. M., D. J. Bartels, E. M. Volper, and E. P. Greenberg. 2004. Quorum sensing in *Staphylococcus aureus* biofilms. J Bacteriol. 186:1838-1850.

195. Yeaman, M. R. and N. Y. Yount. 2003. Mechanisms of antimicrobial peptide action and resistance. Pharmacol Rev. 55:27-55.

196. Yildiz, F. H. and G. K. Schoolnik. 1999. *Vibrio cholerae* O1 El Tor: Identification of a gene cluster required for the rugose colony type, exopolysaccharide production, chlorine resistance, and biofilm formation. Proc Nat Acad Sci USA. 96:4028-4033.

197. Yu, F. P. and G. A. McFeters. 1994. Physiological responses of bacteria in biofilms to disinfection. Appl Environ Microbiol. 60:2462-2466.

198. Zahller, J. and P. S. Stewart. 2002. Transmission electron microscopic study of antibiotic action on *Klebsiella pneumoniae* biofilm. Antimicrob Agents Chemother. 46:2679-2683.

199. Zheng, Z. L. and P. S. Stewart. 2002. Penetration of rifampin through *Staphylococcus epidermidis* biofilms. Antimicrob Agents Chemother. 46:900-903.

200. Zobell, C. E. and D. Q. Anderson. 1936. Observations on the multiplication of bacteria in different volumes of stored sea water and the influence of oxygen tension and solid surfaces. Biol Bull. 71:324-342.